Politecnico di Milano
Department of Energy
Doctoral Programme in Energetics

Waste atomic separation and raw material recovery by application of plasma technology

Doctoral Dissertation of:
Guido Parissenti

Supervisor:
Prof. Alfonso Niro

Tutor:
Prof. Alfonso Niro

The Chair of the Doctoral Program:
Prof. Carlo Bottani

2014 – XXIV Cycle

Abstract

The possibility of obtaining raw materials as pure elements starting from multiple not refined sources, such as wastes, minerals and other sort of low grade materials, is theoretically achievable by using plasma means. The concept has been proposed in the past, for very specific applications, in very different fields ranging from nuclear physics to space science. The process implies the ionization of the source materials and the separation of its constituents by electromagnetic means in a single production step, with the advantage of shortening the overall production chain respect to traditional production processes, at the expenses of a high quantity of electric energy. In this work the problem is analyzed in the special case of silicon production starting from silica, which traditional production method involves many production steps and the usage of large quantities of energy, water and chemicals. The possibility to directly separate silica into its constituents in a single passage would provide benefits in terms of energy consumption, logistics and environmental impact. The problem is initially set to evaluate synergies with previous technologies, and the preliminary set up of a demonstrator plant is proposed with its main constituents. A numerical model is then developed to analyze the process, allowing to perform a more detailed design of the device. The proposed approach is then globally evaluated from the energetic point of view, and its sustainability is compared with traditional production processes. Results show the feasibility of the approach, but also an overall energy consumption unfortunately higher than the traditional production process. Nevertheless the overall environmental impact is limited to the electric energy demand, with

no chemicals involved in the process. Areas of optimization are identified, which may lead to substantial improvements in the energy consumption.

La possibilità di ottenere materie prime sotto forma di elementi puri a partire da una moltitudine di fonti non raffinate, quali ed esempio rifiuti, minerali e altre forme di materiali grezzi, e teoricamente fattibile usanto tecnologie al plasma. Il concetto è stato proposto in passato, per applicazioni molto specifiche, in campi molto differenti tra loro che vanno dalla fisica nucleare alle scienze spaziali. Il processo implica la ionizzazione del materiale di partenza e la separazione dei suoi elementi costitutivi tramite mezzi elettromagnetici in un unico passaggio, con il vantaggio di accorciare l'intera catena di produzione rispetto ai processi produttivi tradizionali, al prezzo di una grande quantità di energia elettrica. In questo lavoro il problema è analizzato nel caso speciale della produzione di silicio a partire da silice, il cui metodo di produzione tradizionale è composto da diversi passaggi di produzione e richiede l'uso di grandi quantità di energia, acqua e prodotti chimici. Il problema è inizialmente definito in modo da valutare sinergie con tecnologie proposte in passato, ed è proposto in via preliminare il concetto di un impianto dimostratore e dei suoi costituenti. Un modello numerico è quindi sviluppato per analizzare il processo, permettendo di eseguire un dimensionamento più dettagliato. L'approccio proposto è quindi valutato dal punto di vista energetico nella sua globalità, e la sua sostenibilità è confrontata con quella di metodi di produzione tradizionali. I risultati dimostrano la fattibilità dell'approccio, ma purtroppo anche un consumo energetico complessivo più elevato del processo produttivo tradizionale. In ogni caso l'impatto ambientale complessivo risulta limitato alla richiesta di energia elettrica, con nessun prodotto chimico coinvolto nel processo. Aree di ottimizzazione, capaci di portare portare miglioramenti sostanziali nella richiesta di energia, sono identificate.

Summary

This research is the results of the last years spent in Politecnico di Milano as a PhD candidate. During this time I had the chance to experiment on myself what research really is, meaning dead ends, lack of data, perseverance and procrastination, sudden boosts (few) and long overthinking on showstoppers (many), unexpected results and, sometimes, the proof that you were wrong. It is indeed a very formative process.

The topic of this research had to be found in a very old idea of mine, which furthermore came from an old sci-fi short story about a new kind of photocopier, able to reproduce not only the printing, but every atom of the paper itself. Instead of an ink reservoir, this machine had a tank with a mixture of the most common elements, allowing to reproduce correctly some things and incorrectly others, if the required elements were missing. The replicator was obviously later used to reproduce not only sheets but also objects and living things, with different results and conclusions. A question raised in me: how could that mixture of elements, some gaseous, some solid, appear? I imagined it as a sort of "magma", but sooner I started thinking how that magma, in which all the elements are freely available without bondings to be positioned at the right place in space, could be obtained. Could a process capable of obtaining pure elements ready to be used, starting from any kind of material, exist? I realized I was asking myself about the final recycling process, in which the perfect separation of every element composing the original object provides pure materials to be used again to produce new things. The holy grail of recycling (despite maybe a strong

energy usage).
This idea remained in my head for many years, during which time I first discovered physics (I did say it remained in my head for many many years), then the mass spectrometry and then plasma physics, during my MSc work. I realized that a possibility for this object to exist may not be null, and then I proposed it as the topic of my PhD research.

As implicitly anticipated, the research is founded on the main idea that the working model of the mass spectrometry can be used to separate non negligible amount of materials. Of the many concepts of the mass spectrometry, the one considered is actually the first to be discovered: due to the Lorentz law, in a uniform and constant magnetic field two particles will rotate with a different radius if they have the same charge and inlet speed, but they differ by the mass.
In this perspective the idea is simple: to design a device, based on the mass spectrometry working model, capable of producing a very high throughput, separating a reasonable quantity of material in a unit of time. Starting from here it is really easy to understand the complications: a certain amount of mass, at least equal to the desired throughput, shall be converted into charged particles. This is somewhat feasible with gases, less so with liquid and solids. This amount of ions shall be processed, and the output material, meaning the pure elements, shall be collected. Each operation requires its own amount of energy.

The research aimed at identifying the characteristics of each step of the process, in order to globally verify its feasibility in terms of requirements and performances. This thesis describes a preliminary design for the device and identifies the criticalities, assumptions and calculations.

Chapter 1 introduces to the motivation and importance of this work, the concept and the research objectives

After consideration of the complexity inherent in the involvement of so many chemical elements, the initial and boundary conditions were simplified to provide a better understanding of the overall process. Chapter 2 provides insight into this problem simplification and the related implications.

Chapter 3 describes the numerical calculation supporting the design choices.

Chapter 4 provides the first the final device description, with its feasibility evaluation.

Chapter 5 list all the conclusion, the open points and possible outcome of this work.

Acknowledgements

Se la pazienza potesse assumere sembianze umane, andrebbero a lei la maggior parte dei miei ringraziamenti. Sono fermamente convinto, infatti, di aver esaurito la pazienza di più di una persona durante il mio dottorato, e mi sembra perciò doveroso sottolineare questa qualità in chi mi appresto a ringraziare.

La medaglia d'Oro va ovviamente al mio Relatore Prof. Alfonso Niro. Non riesco proprio a capacitarmi di come egli mi abbia supportato così tanto e di come si sia dimostrato così tollerante sull'andamento del mio lavoro e dei miei frequenti ritardi. Al suo posto io mi sarei sbattutto fuori dall'ufficio più e più volte. Al contrario egli è stato sempre presente, persino di domenica o alle 2 del mattino, spronandomi a proseguire anche nei momenti più critici. Grazie.

Una menzione speciale va a tutti i professori del Dipartimento di Energia del Politecnico di Milano, ed in particolare a Mattero Passoni e Vincenzo Dossena, che sono stati sempre disponibili a trovare dei compromessi per venire incontro alle mie esigenze logistiche, specialmente riguardo a corsi, esami, revisioni e presentazioni.

Durante il mio lavoro di ricerca ho dovuto affrontare diverse difficoltà e vicoli ciechi, ma ho avuto la fortuna di potermi interfacciare con professionalità che mi hanno dato un aiuto veramente essenziale. Desidero ringraziare quindi tutti i ragazzi dell'università di Padova, e in particolare

Marco e Franco, per il loro supporto su ogni aspetto relativo alla fisica dei plasmi. Grazie anche al Prof. Perini del Politecnico di Milano per l'aiuto nella trattazione di campi magnetici.

Grazie a tutti i ragazzi dell'ufficio dottorandi: Damiano, Lino, Luigi ("lo chef"), Luca. Mille grazie a Susanna e la sua iperattività, per pensare a me ogni volta che qualche pazza ed entusiasmante idea le passa per la testa.

Andrea Simonetto, desidero avvertirti che il tuo lavoro non finisce con la mia discussione. Ti disturberò ancora ed ancora per confrontarmi con te su idee al limite della fattibilità (senza probabilmente darti retta, come al solito) e per chiederti di trovarmi altre decine di articoli. Mille grazie e scusa in anticipo. In ogni caso sappi che non mi farò problemi.

A great thanks to Ashley and Ashley's patience. Thanks for sharing your PhD feelings and experience, thanks for the emails in which you show your passion in anything you do, ranging from work to tango, and many thanks to your patience for the proofreading of my thesis (again).

Vorrei ringraziare poi i miei colleghi, alcuni per avermi sempre spronato e avermi permesso di far fronte agli impegni di dottorato, in particolare Mario, altri solo per aver detto "Non posso credere che ti stai per dottorare, stavi già facendo il dottorato quando ti ho conosciuto. Niente sarà più come prima". Grazie a Raff, Fra, Fede, Martins, Ste, Mattia, Liliana, Primo e Franz. Mille grazie ad Alessandro per essere non solo un ex collega assolutamente professionale, un ex vicino di casa che tutti vorrebbero, ma soprattutto un vero amico.

Grazie ai miei ex coinquilini, Maurizio e Giova, per il tempo passato assieme, per le volte che siamo usciti di casa e per le volte che abbiamo avuto difficoltà a ritornarvi. Non intendo aggiungere altri dettagli.
Vorrei in realtà ringraziare moltissima gente che durante questi anni, pur non avendo nulla a che fare con il mio dottorato, ha contribuito a farmi sentire a casa dovunque io fossi. Non posso elencarli tutti, sono talmente tanti che pur ricordando ognuno di loro rischierei di dimenticarmene qui qualcuno, cosa che non voglio. Vorrei invece citare quelli che oltre ad aver condiviso con me i momenti felici e spensierati sono stati anche presenti quando le cose non andavano del tutto per il verso giusto: grazie a Serena, Cecilia, Giorgio, Graziano e Valentina.

Vorrei infine ringraziare le persone speciali della mia vita.
Grazie ai miei genitori ed a mia sorella. Grazie per il vostro ottimismo e per supportarmi sempre in qualsiasi cosa io faccia, grazie per chiedermi se ho bisogno un aiuto, grazie altre volte per trattenervi dal fare domande.
Giulia, grazie per la tua pazienza e pure per la tua impazienza. Grazie per supportarmi e soprattutto per sopportarmi, per metterti le cuffie mentre guardi un film mentre io studio, per andare al lavoro con le occhiaie perché io sono rimasto alzato a lavorare e tu non sei riuscita a dormire, e per una infinità di altre piccole e grandi cose che fai e per le quali non ti ringrazio mai abbastanza. Grazie per esserti messa in gioco, e per quello che ci aspetta.

Guido

Contents

List of Figures

List of Tables

CHAPTER 1

Introduction

1.1 Motivation

Our society's economical model, in terms of the western way of living based on consumerism, is presently no longer sustainable. The present goods production rate requires a constant supply of raw materials, which results in a continuous draining of the Earth's fossil resources (meaning every resource ever stored, e.g. hydrocarbons, water, minerals) and in the total consumption of the Earth's yearly available renewable resources in usually 7-8 months after the beginning of the year [1].

Attempts are being made to improve our environmental responsibility. Ecological lifestyles, improved production processes and better waste management are some examples of policies introduced to reduce our environmental impact. Unfortunately wastes are still one of the most devastating results of human activities because of its twofold drawback: on one side they represent a reduction of available raw material for goods production, and on the other side they occupy space and mass, polluting natural resources, and creating additional costs for proper disposal.
The obvious best solution to get rid of the waste problem is not to produce wastes, improving reusability and reducing packages. Unfortunately this

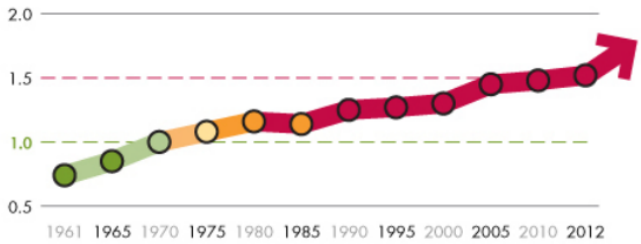

Figure 1.1: *Earth Overshoot Day along the years. On the y axis the "number of Earths" in terms of renewable resources that we used at the end of each year. Source: [1].*

solution can only be gradually implemented, and the problem remains for the already produced wastes, which are mainly managed in three ways:

- **Disposal** in dumps
- **Destruction**, often with energy production (i.e. incinerators)
- **Recycling**, where semifinished material is recovered, but further treatment is required before manufacturing of new goods

Of the three methods the first is the one with the largest drawbacks. The second is an attempt to recover at least the energy contained in the waste at the expense of destroying any possibility to reuse the material. The third is the more environmentally friendly option, because the energy required to produce goods starting from recycled material is many times lower that starting from raw materials.
Despite recycling, mixed wastes which cannot be separated, special wastes, and ashes from incinerators still represent a tremendous potential source of raw material that cannot be exploited but shall inevitably be disposed in dumps.

In this frame the present research takes place. An attempt is made to provide an alternative method to recover raw materials from otherwise non-recyclable wastes, with the additional benefit of reducing land usage and pollution due to disposal in dumps.

1.2 The idea behind high mass flow plasma separation

How could the material recovery take place, considering the intrinsic variety of substances mixed at the most intimate level? The proposed idea

relies on the concept of mass spectrometry, developed in its first version in 1912 by Nobel Prize winner J. J. Thompson.

1.2.1 The mass spectrometer working model

The mass spectrometer is a chemical analysis device that measures the mass-to-charge ratio and abundance of ions in the gas phase. It works by ionizing chemical compounds to generate charged molecules or molecule fragments and measuring their mass-to-charge ratios.

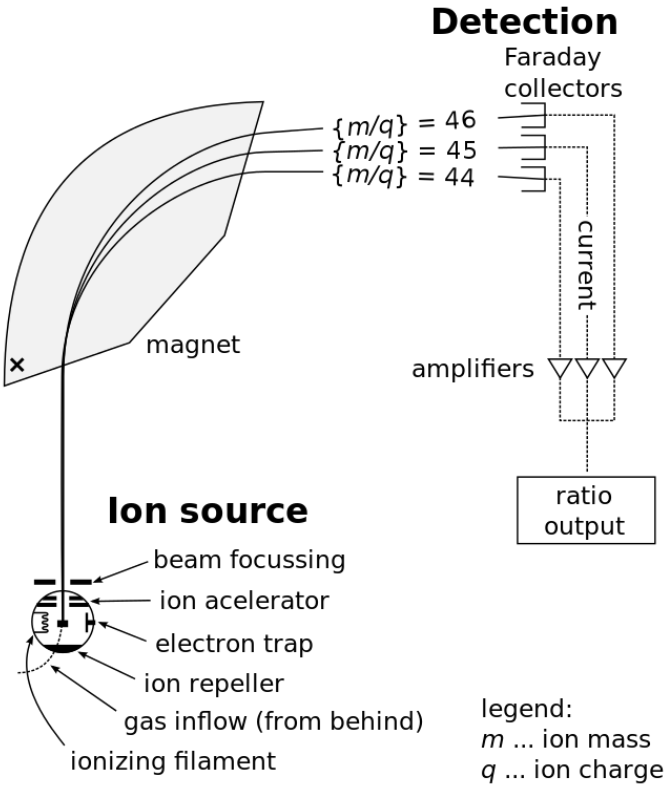

Figure 1.2: *Mass spectrometer schematic*

In general, a mass spectrometer consists of three main components: an ion source, a mass analyzer, and a detector. The ionizer converts a portion of the sample into ions. There is a wide variety of ionization techniques, depending on the phase (solid, liquid, gas) of the sample and the efficiency of various ionization mechanisms for the unknown species. An extraction system removes ions from the sample, which are then injected through the

mass analyzer and onto the detector. The differences in the masses of the fragments allows the mass analyzer to sort the ions by their mass-to-charge ratio. The detector measures the value of an indicator quantity and thus provides data for calculating the abundances of each ion present.

The equations governing the dynamics of charged particles subjected to EM fields in vacuum are the following

$$\mathbf{F} = q\,(\mathbf{E} + \mathbf{v} \times \mathbf{B}) \tag{1.1}$$

$$\mathbf{F} = m\mathbf{a} \tag{1.2}$$

which results in the following relation for ions:

$$\left(\frac{m}{q}\right)\mathbf{a} = \mathbf{E} + \mathbf{v} \times \mathbf{B} \tag{1.3}$$

In the case of a constant and uniform magnetic field B, as in the first embodiment of the device ever developed, the acceleration a is a centripetal acceleration which bends the trajectory of the particle, maintaining constant its perpendicular velocity v, with a radius which is equal to the cyclotron radius r_c

$$r_c = \frac{mv}{qB} \tag{1.4}$$

1.2.2 The concept

Starting from the working model of §1.2.1, an apparatus capable of separating a large amount of any material composed by a large variety of elements shall resemble the main parts of a mass spectrometer, but with the consideration that a much bigger throughput shall be required for the separation operation to be convenient and able to be performed in a reasonable amount of time.

The operation of the device can be imagined in the following way:

- the material to be processed is raised to a plasma state to allow manipulation by electromagnetic means;
- the plasma is then accelerated and subjected to a magnetic field able to separate the different elements according to the mass/charge ratio;

- the flux of different element is then collected and retrieved at special collector locations.

The proposed device is therefore composed of three parts:

1. a source stage where the material containing the metals of interest is heated until vaporization and ionization, to a plasma level state, is attained;
2. an intermediate stage where ionization is maintained ionized and the plasma is accelerated by electromagnetic or electrostatic fields;
3. a separation stage where a static magnetic field separates the ion species composing the plasma are separated one from each other, or separates a particular ion from unwanted species. This section includes the collectors.

A graphical representation of the concept is shown in Figure 1.3.

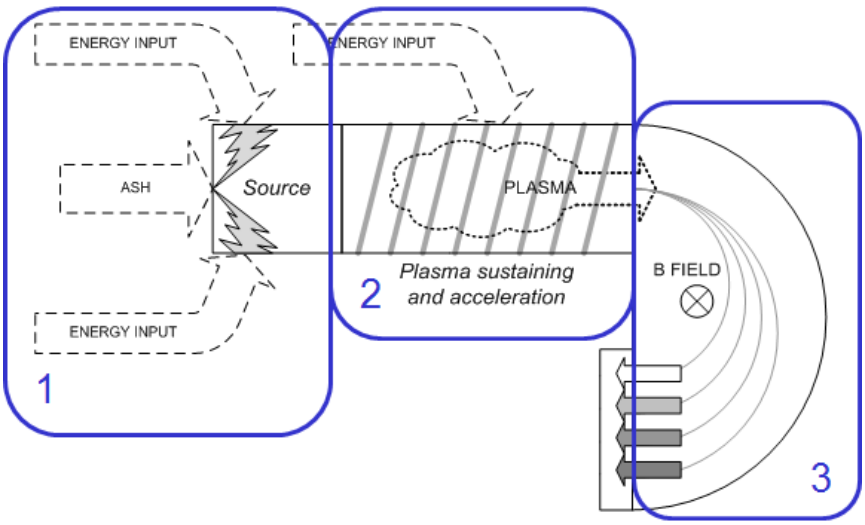

Figure 1.3: *Graphical representation of the demonstrator concept*

The working model of the device resemble those of the Calutron, as described in §1.2.3.

1.2.3 Plasma Raw Material Recovery in literature

Plasma raw material recovery refers to the possibility of obtaining raw materials as pure elements starting from multiple unrefined sources such as

wastes, minerals and other low grade materials. The concept has been proposed, for very specific applications and never in a general form, in very different fields ranging from nuclear physics to space science. Plasma raw material recovery involves ionization of the source material and separation of its constituents by electromagnetic means.

Technologies to separate atoms of different atomic weight using an interaction of electric and magnetic fields were developed during WW2 to produce material required for the first nuclear bombs. Some of these methods are intrinsically inadequate for high mass flow rates or require so much energy that their use outside nuclear programs is impracticable. Other methods have been developed outside the nuclear community for different purposes, but they focused on interesting aspects of the separation of oxides that can be easily applied to increase the raw material recovery yield. The most representative concepts are listed below.

1.2.3.1 Calutron

Massively used during WW2 to produce the ^{235}U for the Hiroshima bomb, developed by Ernest O. Lawrence [2], who got the Nobel prize for the invention of the cyclotron accelerator, the Calutron uses the same working model of a mass spectrometer, separating particles with different charge-to-mass ratio by passing them through a constant **B** field and producing different cyclotron radius and therefore different trajectories. To perform the separation the input material has to be preliminarily ionized and then accelerated to a minimum useful velocity. A first equation used by Lawrence is the simple energy balance between the potential energy provided by an accelerating electric field and the kinetic energy owned by the ions after the acceleration:

$$\frac{1}{2}mv^2 = q\Delta V \tag{1.5}$$

At this point the cyclotron radius or Larmor radius equation, Eq. 1.4, is used:

$$r_c = \frac{mv}{qB} \qquad \text{(1.4 revisited)}$$

In both equations v is the velocity perpendicular to the magnetic field B. If single ionization is assumed for all the particles, with constant v and B, ion mass is directly proportional to the Larmor radius.

Calutron technology is able to produce a high enrichment yield (requiring a lower number of devices in cascade for isotope separation) but is considered to be energetically expensive. The achievable throughput of

Calutron technology is limited by a stream instability that arises as the density of the purely-positive output beam increases. A background neutral gas is injected and ionized upon interaction with the ion beam producing electrons that help keep the beam focused, but the density of the beam, and therefore the throughput of the device, remains limited [3].
Despite this drawback, if used with different elements rather than isotopes of the same atomic species, the separation is more effective due to the higher radius difference that can be achieved with the same magnetic field: the more the collectors are separated, the highest is the purity of the collected elements. For this reason this technology has been preliminarily considered for the development of the demonstrator depicted in §1.2.2. The device would work by modifying the original concept, substituting the electron beam used to vaporize and ionize the material with a plasma source and a further ionization stage. A good choice would be to select a plasma source capable of operating with a quasi-neutral plasma flow, solving the intrinsic volume charge limitation, avoiding the necessity of a background gas and increasing the efficiency [4]. This choice is also compatible with a number of technological configuration with crossed E and B field different from the Lawrence approach [4–6].

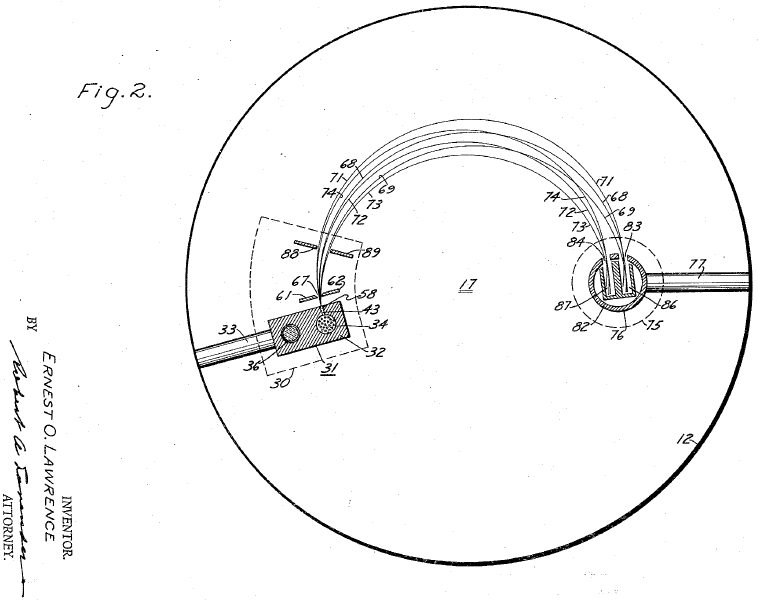

Figure 1.4: *The calutron as depicted by Lawrence. Source: [2].*

1.2.3.2 Selective Ionization

Developed by NASA in the '80s [7, 8], selective ionization was theorized to be mainly used in space exploration and oxygen recovery from In Situ materials found on extraterrestrial planetary bodies. The concept is very close to the initial stage of the Calutron system. The material (such as lunar regolith) is heated to vaporization and thermal ionization. At this point to understand the physics of the problem we can refer to Fig.2.3 in which the ionization potential of the most abundant elements of the Earth's crust is plotted versus temperature. It can be seen that at about 10000 K metals achieve between 40% and 70% ionization ratio, while oxygen achieves less than 2% (see §3.2.3.5 for ionization ratio definition). The Selective Ionization idea is therefore to pass this plasma through an electrostatic field to capture at the cathode the positively charged metal ions, while letting the neutral oxygen continue flowing downstream into a collection system.

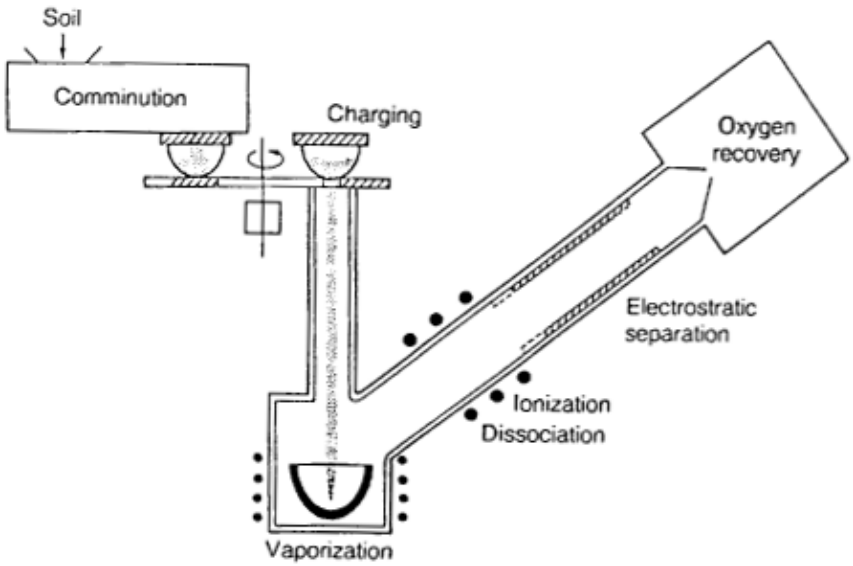

Figure 1.5: *Selective Ionization concept. Source: [8].*

As can be understood the objective of the Selective Ionization is complementary to the recovery of raw material from unrefined source. In the first case the goal is oxygen recovery and the metals are seen as a secondary output, while in the second case the goal is separation of the oxides into the constituent atomic species and the oxygen represents the secondary output which cannot be easily collected due to its gaseous state at temperatures above 90 K.

1.2.3.3 Archimedes plasma mass separation

The designers of the Archimedes (a proprietary name) concept refer to it as a *plasma mass separator* with the purpose of separating atomic plant waste oxide mixtures ion by ion into two groups: light (not radioactive) and heavy (radioactive) particles. It actually acts as a mass filter, because is not able to separate all the elements one by one or to isolate a single ion, but rather it divides ions with an atomic weight above a certain cut-off value from ions with an atomic weight below that value, as can be seen in Fig. 1.6.

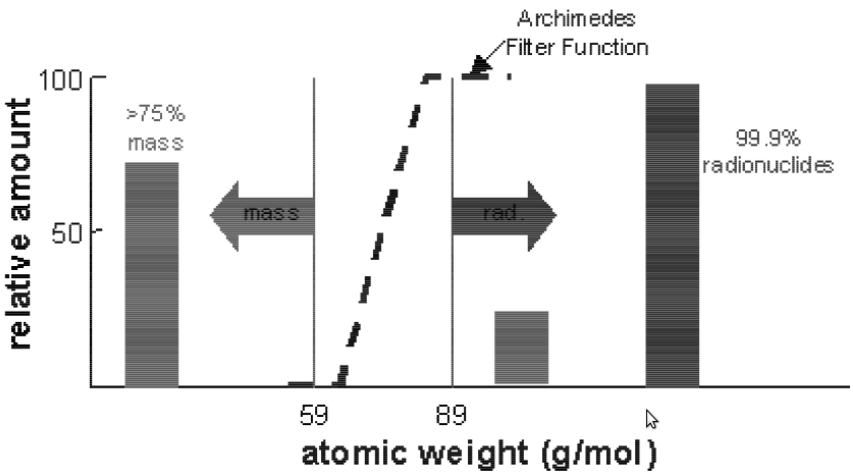

Figure 1.6: *Archimedes Filter function in gap between high atomic weight and low atomic weight (non radioactive) waste. Source: [9].*

The process comprises three main stages: a) the melting of the input mixture with a plasma torch to 500 °C; b) the injection and vaporization of the molten mixture thanks to another plasma torch at 5000 °C into the center of the cylindrical filter unit vacuum vessel; c) the ionization and manipulation of the vapor by EM fields inside the filter unit. In the last step heavy particles are swept radially at the center of the filter and are collected on the cylindrical wall, while light particles are transported toward the bases of the cylinder where they are collected [10]. The basic mechanism used by this device is the Larmor radius: inside the filter a longitudinal magnetic field is present, and the particles injected at the center start rotating along the magnetic field lines with a cyclotron radius which is proportional to the ion mass according to Eq. 1.4. The high atomic weight ions have a large Larmor radius and collide with the cylinder wall where they are collected and removed, while the low atomic weight ions travel towards the end of the cylinder where they are also collected [11].

1.2.3.4 Plasma Separation Uranium Enrichment

The plasma separation process (PSP) is an isotope separation techniques that makes use of advancing technologies in superconducting magnets and plasma physics [12]. In this process, the principle of ion cyclotron resonance (ICR) is used to selectively energize the isotope of interest. The source is either a plate of solid material which is vaporized by bombardment of energetic ions (sputtering), or a crucible in which the material is heated to vaporization. A microwave antenna located in front of the source energizes free electrons which collide with neutral atoms sputtering off the plate, or vaporizing from the crucible, producing a plasma.
The plasma is subjected to a uniform magnetic field along the axis of a cylindrical vacuum chamber as the plasma flows from source to collector. The magnetic field is produced by a superconducting magnet located around the outside of the chamber. The high-strength magnetic field produces helical ion trajectories, with lighter ions spiraling faster and having a higher ion cyclotron frequency than heavier ions. As the ions move toward the collector, they pass through an electric field produced by an excitation coil oscillating at the same frequency as the ion cyclotron frequency of the isotope ions of interest. This causes the helical orbit of these ions to increase in radius while having minimal effect on the orbit of the other particles. The plasma flows through a collector of closely spaced, parallel plates. The large-orbit ions are more likely to deposit on the plates, while the remaining plasma accumulates on an end face of the collector (see Fig. 1.7).

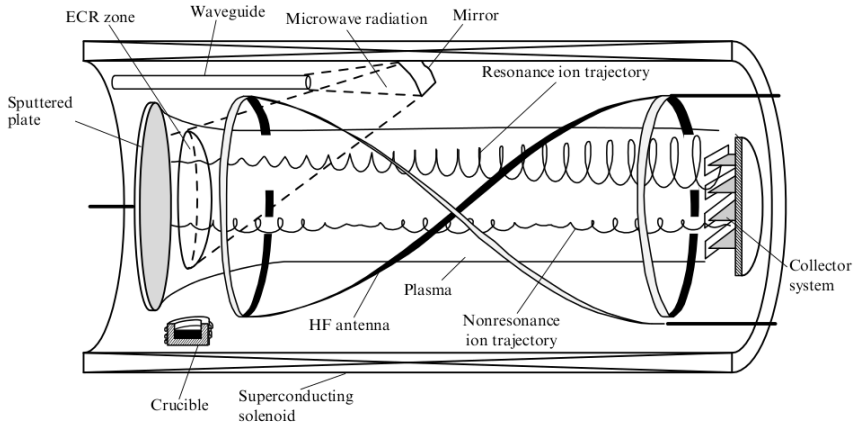

Figure 1.7: *Schematic of the ICR separation. Source: [12].*

The PSP process offers several advantages:

- a relatively high throughput (several dozens kilograms yearly) is possible due to the quasi-neutrality of the plasma;
- moderate to high enrichment is possible in a single pass;
- nearly any metallic-like element can be directly processed and recovered with the PSP without the requirement of a gas phase [13].

The only countries known to have had serious PSP experimental programs are the United States and France from the '70s to the '90s for uranium separation, but the programs suffered slowdowns and stops due to the evolution of apparently more readily available techniques.

1.3 Objective and project goals

Merging the motivation described above and the concept initially identified to be investigated, the general objective of this research is found to be the following:

> **To perform a feasibility study of a demonstrator plant able to recover raw materials from a variety of sources (e.g. waste materials, special and urban wastes and mining raw materials), by using ionizing and selecting processes of the different atomic species enabled by static and variable EM fields.**

This general objective shall be expanded and divided into sub-objectives or goals that clarify the problem from different points of view. The feasibility of such a device can actually depend on many different factors, in particular its technological feasibility and, if granted, its economical feasibility. In other words the objective can be technically achievable but, if the operating cost and hence the cost of the final product greatly exceed the possibility to economically sustain the venture, the feasibility is still not granted. The goals of the present research are therefore the following:

Technological feasibility

Technological issues may be limited not only by the underlying physics, but also by difficulties during design due to the problem complexity, and both of these aspect shall be addressed. The main difficulties that are clearly visible at first are:

- General wastes includes a large variety of oxides, many of them with a high boiling point: how can one create a plasma from them?
- If a suitable plasma creation technique is identified, the feasibility analysis requires a numerical investigation involving all sort of elements and reactions: can numerical models be representative of such a complex process?
- The desired output is an assessment of separation performance as a function of power input, so an economical feasibility study is also needed.

Verification of assumptions

During demonstrator design, assumption and simplifications may be necessary. At a later stage a verification of the correctness of these assumption shall be performed.

Economical sustainability

The energy consumption of the proposed process shall be compared with present production methods to evaluate sustainability.

These goals had a strong impact on the progression of the research. Assumptions and simplifications were applied to the original problem permitting the investigation to be performed in the timespan of a PhD, as explained in Chapter 2. The above goals, opportunely scaled to the simplified problem resulting from the simplification, shall be held to the same verification requirements that applied to the original goals.

CHAPTER 2

Focusing: problem specialization

The previous chapter concluded with the need for simplification of the research objectives to adapt the problem under investigation to the time scale of a PhD. In addition to simplification, the problem must also be clearly identified to allow a solution via mathematical analytical approach.

2.1 Technological constraints

A feasibility study, and therefore a preliminary design, of the device under investigation, must also cover any required analyses. Numerical investigations can be essential in understanding if the relevant underlying physical processes allows the achievement of the project goals. Such numerical analysis would most likely involve a plasma simulation, used to investigate the behavior of elements as they react and ionize due to the inbound energy.

In this perspective, the objective of §1.3 is an attractive idea, but consideration of general waste as input material will result in an **overwhelming** number of elements and reactions in the numerical simulation. Not only

would execution of the numerical code be unmaneageable, the identification of all the reactions involved in the process would likely in and of itself exceed the timeframe of a PhD project.

A downscaling of the problem is therefore necessary. It is proposed to start from a partially refined material, still representative of the complex compounds that can be found in waste, but reducing the number of components and reactions. The material chosen is **silica**, and therefore the process under investigation in this work is the **production of pure silicon starting from silica**.

The objective of the project therefore becomes:

> **To perform a feasibility study of a demonstrator plant able to recover pure silicon from silica, by using ionization and selection for the different atomic species enabled by static and variable EM fields.**

Figure 2.1: *(Left) Silicon powder; (Right) A pure silicon rod*

The motivations for choosing this process are:

- Silicon is fundamental for modern semiconductor industry;
- Silicon is abundant in the Earth's crust;
- Silicon has a high energy production cost for high purity product;
- There are many possible sources of starting material (see §2.2.1):
  - Silica from mining
  - Incinerator ashes
  - Electronic waste

This choice lead to a subsequent important technical difficulty: silicon dioxide SiO_2 is a high boiling point oxide with the following characteristics:

Melting point 1700-2000 K

Boiling point ~3100 K @ 1 bar

Because of these characteristics it is the base material for high temperature, heat, fire, flame resistant and thermal insulating products. Consideration of the silica-silicon production process, while challenging, has the advantage of substantially qualifying the process. Once the process has been validated with SiO_2, which has one of the highest boiling point among all the refractory oxides, it is virtually valid for any compound and mixed waste containing also oxides. The drawback is that **such oxide shall be brought to the plasma state, therefore a suitable device able to perform this operation with a high throughput must be identified**. Attempts in this direction were already provided by Meubus and Huckzo [14–16] who successfully detected the decomposition of oxides in plasma with the deposition of composing metal.

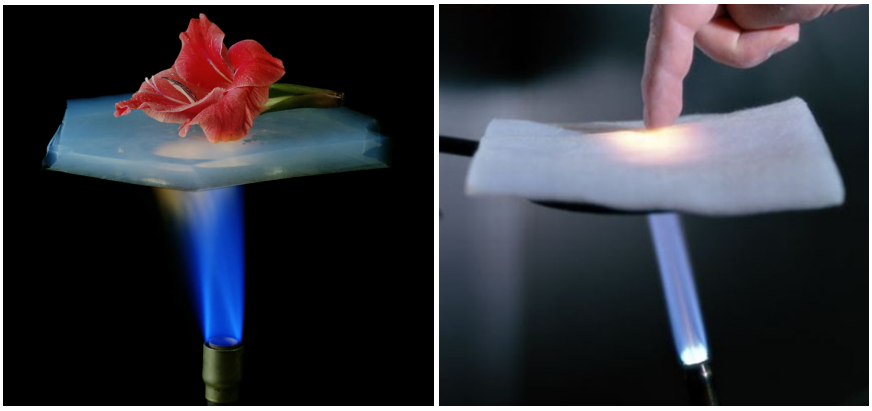

Figure 2.2: *Aerogel insulation capability. Aerogel is a silica porous ultralight material derived from a gel, in which the liquid component of the gel has been replaced with a gas. The result is a solid with extremely low density and very low thermal conductivity.*

NOTE: in the initial process selection phase, Aluminum production was also evaluated, as its present production processes is also very energy intensive and composed of multiple passages. Nevertheless due to its importance in the electronics industry and the fact that it is a high temperature oxide,

the silicon production process has been considered more representative for this research.

2.2 Process sustainability

Considering the downscaling, the goal of verifying the process sustainability is now shifted toward the silica-silicon production process. The new goal becomes **to verify if the overall energy cost per unit mass of silicon can be competitive with present production processes**.

2.2.1 Present silicon production process

The high grade silicon process for microchip production starts from quartz with the application of carbon to produce, through a number of additional operations, the required final product. Starting from the analysis of Williams et al. [17] we can summarize the production process of Si ingots for wafer production with the following steps:

$$\begin{aligned} SiO_2 \xrightarrow{C} Si \xrightarrow{Cl_2} HSiCl_3 \rightarrow \\ \xrightarrow{H_2} \text{hyper-pure Si +(HCl)} \rightarrow \text{single-cristal Si} \rightarrow \text{Si wafer} \end{aligned} \tag{2.1}$$

The starting point is the reduction of quartz (mineral SiO_2) with a carbon source such as coal or charcoal in an electric furnace. The resulting "raw" silicon is typically 98.5 – 99.0% pure and must be purified further to meet the demands of semiconductor fabrication. Typical applications of "raw" silicon include iron alloys and production of silicone compounds.

Powdered raw silicon is reacted with chlorine to yield a mix of trichlorosilane ($HSiCl_3$) and silicon tetrachloride ($SiCl_4$), which can be conveniently purified via distillation. The resulting trichlorosilane is at least 99.9% pure

Stage	Electrical energy input/kg silicon out	Silicon yield (%)
quartz + carbon → silicon	13 kWh	90
silicon → trichlorosilane	50 kWh	90
trichlorosilane → polysilicon	250 kWh	42
polysilicon → single crystal ingot	250 kWh	50
single-crystal ingot → silicon wafer	240 kWh	56
process chain to produce wafer	2130 kWh	9.5

Table 2.1: *Energy usage in silicon wafers production steps. Source: [17].*

with metallic impurities in the several parts per billion (ppb). In the most commonly used Siemens process, trichlorosilane is reacted with H_2 to yield pure elemental silicon via chemical vapor deposition, the result of which is 99.9999% pure (metals<0.4 ppb). This hyperpure silicon is referred to as polysilicon in the industry. Molten polysilicon is drawn into single-crystal ingots via Czochralski or Floating Zone methods, which are sliced into wafers. Wafers are polished and cleaned via Chemical Mechanical Polishing. The electric energy cost for each stage is shown in Tab. 2.1.

The energy cost for production of raw silicon (98.5 – 99% pure) in the first process step is low compared with the energy required to purify the silicon to high grade product (99.9999% pure). The total energy required, much higher than the sum of the energy requirements of the individual stages, is explained by the silicon losses along the process chain that require about 9.4 kg of raw silicon to produce 1 kg of silicon wafer. Tab. 2.1 can be better understood with the breakdown of the energy production cost of the wafer production process shown in Tab. 2.2:

kWh/kg	Yield[%]	Input mass[kg]	Energy [kWh]
13	90	9.4	123
50	90	8.5	425
250	42	3.6	893
250	50	1.8	446
240	56	1	240
		Total	**2127**

Table 2.2: *Breakdown of energy production cost to produce 1 kg of silicon wafer*

For a total cost of 2130 kWh/kg = 7668 MJ/kg of produced silicon wafer. If, from this table, we remove the energy cost to produce the silicon wafer and we stop at the crystal ingot step, the overall cost is provided in Tab. 2.3.

kWh/kg	Yield[%]	Input mass[kg]	Energy [kWh]
13	90	5.3	69
50	90	4.8	238
250	42	2.0	500
250	50	1	250
240	56	0	0
		Total	**1057**

Table 2.3: *Breakdown of energy production cost to produce 1 kg of silicon monocristalline ingot*

Considering the different yields of each phase we arrive to the final result of 1057 kWh or 3805 MJ. It is with this value that the results of this research can be meaningfully compared.

Other than the pure energy consumption comparison, consideration shall be given to other costs of the process, in particular the strong environmental impact. Silicon production requires many steps, which include transportation, fossil fuels, chemicals and water usage [17] but these sources of pollution are very difficult to evaluate.

2.2.2 Silicon sources

Other than obtaining silicon from raw silica, such as from caves or mines, it is possible to identify alternative sources that may provide an advantage in terms of purity of the starting material or in terms of sustainability. Caves or mines are impacting from the point of view of the landscape and of the energy used to extract the material. Wastes, general or special, are often a good source of silica, due to its characteristics of being one of the most abundant element on the Earth's crust.

2.2.2.1 Silicon extraction from incinerator ashes

Waste-to-Energy (WtE) plants, widely used worldwide, incinerate solid urban waste to reduce landfill mass and produce electricity. Although these plants are a source of pollution and encourage disposal as opposed to recyling or reutilization, their bi-products (heavy and fly ashes) do contain a variety of elements, predominantly silica. The other components range from calcium and aluminum to heavy metals like zinc, lead and cadmium. The composition of a typical sample of incinerator by-products, or fly ash, is shown in Tab. 2.4.

Compound	Percentage [%]	Compound	Percentage [%]
SiO2	39.1	K2O	2.3
CaO	15	SO	6.9
Al2O3	13.6	Cl	2.4
Na2O	5.5	CO-	0.71
Fe3O4	3.2	Zn	0.84
TiO2	2.8	Pb	0.4
MgO	2.7	Cd	0.014

Table 2.4: *Typical fly ash composition. Source: [18]*

Considering the above percentages, it is theoretically possible to obtain

1 kg of silicon from about 5.22 kg of ashes [19]. If a hypothetical demonstrator were to use incinerator ashes as a source of silica, the separation process would produce not only silicon but all the other elements in the compounds listed in Tab. 2.4, increasing the value of the operation.

2.2.2.2 Silicon extraction from electronic devices

Old electronic devices are a great and still not unutilized source of already refined silicon. The most common elements used for doping are arsenic, phosphorus, boron and antimony.

2.3 Assumptions and simplifications

2.3.1 The selective-ionization assumption

The methods explained in §1.2.3 have different goals: to separate isotopes of the same element, to recover oxygen from extraterrestrial planetary bodies, to separate the light and heavy components of nuclear waste for subsequent treatment. In focusing on the recovery of pure elements from oxides, especially metals or metalloids, a combination of the working models of these methods can lead to very high yields. The idea behind selective ionization is extremely helpful in removing the most problematic element, oxygen, which has a high first ionization energy and is considered an impurity in the recovered metal (even if by itself can be even considered a product if properly collected).

In a device that uses vaporization and ionization for raw material separation, like the one depicted in Fig. 1.4, the metal-oxygen ionization gap can be used to remove the neutral oxygen from the metal anions. In fact, the substantial gap between the first ionization energy of metals and oxygen allows ionization of metal atoms without ionization of oxygen atoms: the neutral oxygen is insensible to EM fields while the metal anions are manipulated end extracted according to one or a combination of the methods shown in §1.2.3.

The ionization fraction of selected elements as a function of temperature is shown in Fig. 2.3. These curves represent the equilibrium ratio of ionized to neutral atoms vs. temperature, and are obtained using the Saha equation (Eq. 2.2) applied to the single atomic species. Only the first ionization level is assumed to have the same mass-to-charge ratio for each atom of the same element for subsequent separation.

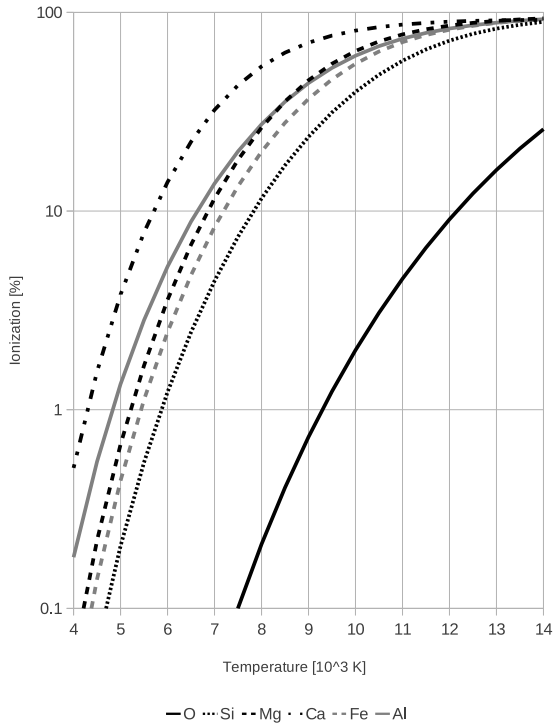

Figure 2.3: *Ionization Vs Temperature of major constituents of the Earth's crust at P=1 atm*

$$\frac{n_i n_e}{n_0} = 2\frac{Z_i}{Z_0}\frac{(2\pi m_e k_b)^{\frac{3}{2}}}{\hat{h}^3}T^{\frac{3}{2}}\exp\left(\frac{-E_{ion}}{k_B T}\right) \tag{2.2}$$

In Eq. 2.2 the partition functions Z_i and Z_0 are taken from Irwin [20]. The curves shown in Fig. 2.3 were calculated to reproduce the same image from Carroll [8], but a 20% difference in the calculated ionization level at the same temperature and pressure is present, mainly due to the partition functions calculation. Unfortunately no reference is made to the partition function used for the calculation of the curves in Carroll [8], so no verification can be made.

Fig. 2.3 is the starting point of the selective ionization application to the silicon production process. At 10000 K the plasma contains a very small percentage of ionized oxygen and an high percentage of ionized metals. The atomic oxygen can be pumped away while the remaining ions can be electromagnetically directed through a separator. If the input material is

only a single oxide, it can be separated from impurities, such as the oxygen atoms. If the input material is a mixture of oxides, the different elements can be separated one by one.

2.4 Impacts on the demonstrator concept

The assumption of the selective ionization implies that in a plasma created by thermal decomposition the difference in first ionization energy allows an almost exclusive ionization of Si respect to O_2. This phenomenon implies that in the specific problem under examination the O_2 will be most likely pumped away by the vacuum system, while the Si ions will continue their trajectory undisturbed. This condition has obviously to be verified in the proposed situation, where a mixture of gases is present and where the decomposition is not only due to thermal phenomena but also to power deposition. With these considerations the separation stage appears therefore almost useless, and also the second stage, originally planned to increase the ionization of the plasma, is reduced in importance if the first stage is able to achieve an adequate ionization efficiency.

Three main design consequences can be derived from the assumption of selective ionization in the first stage:

- Reduced importance of 2^{nd} stage;
- Reduced importance of 3^{rd} stage;
- Focus on 1^{st} stage due to its multiple importance, as a source capable of operating with a high boiling point oxide material in inlet, and as an efficient ionization mechanism.

The effort is therefore concentrated in identifying a 1^{st} stage capable of ionizing and accelerating at the same time. Such a device must be a sort of torch, in which the material is somehow heated to vaporization and decomposition, with subsequent ion formation. An important aspect to keep into consideration is that all the material that is vaporized shall be separated and pumped away: this means that a working gas like argon, as used in common industrial plasma torches, would represent a source of losses because energy has to be spent to heat and ionize it, and later it recombines to be pumped away, providing no benefit.

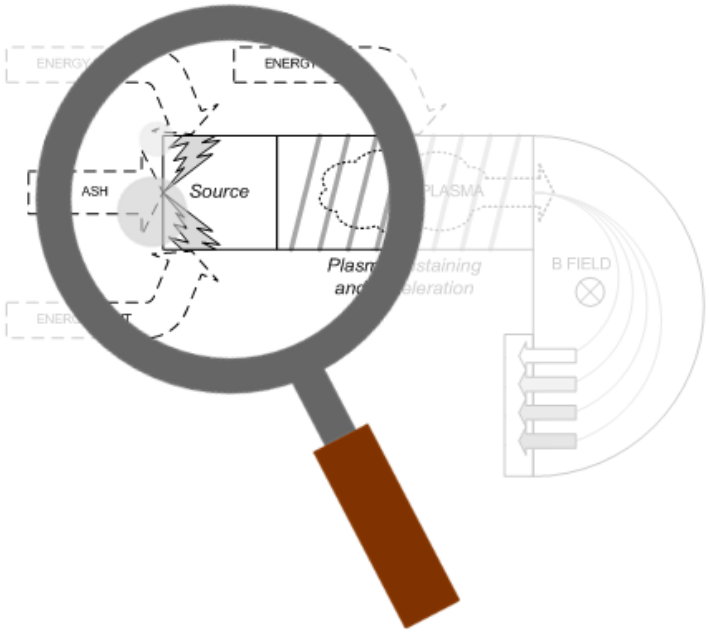

Figure 2.4: *Focusing on the first stage*

Plasma torch concepts capable of functioning without a working gas have been investigated. The most promising ideas between the different concepts conceived and proposed, appeared to be:

- The MPD sublimation torch
- The Self-feeding torch

2.4.1 The MPD sublimation torch concept

The MagnetoPlasmaDynamic Thruster (MPDT) is an in-space propulsion concept [21] under development since the '60s that has flown only once (Japanese Space Flyer Unit 1995). The main advantage of this class of electric propulsion is high thrust at low propellant consumption (high specific impulse) at the expenses of high power requirements on the order of 100kW and 1MW.

A MPDT is characterized by a coaxial geometry consisting of a central cathode, an annular anode, and some form of interelectrode insulator. The propellant, usually a noble gas, is introduced from the rear and is ionized by

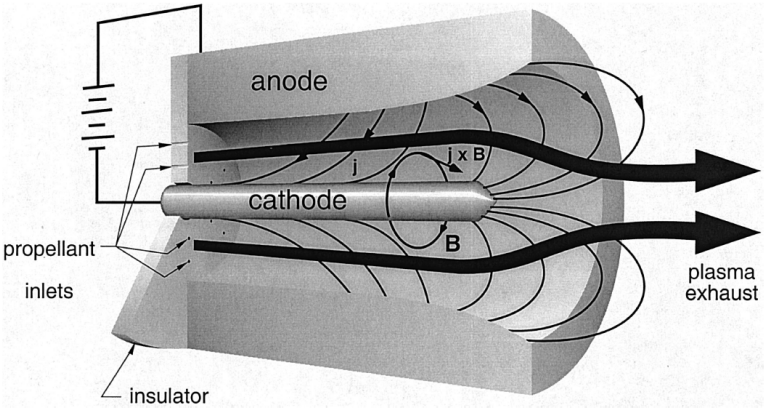

Figure 2.5: *MPDT schematic and working model. Source: [22].*

an azimuthally uniform electric arc bridging the gap between the electrodes. The interaction between the arc current and the moving plasma produces the body forces that accelerate the propellant downstream. A more detailed explanation of the working model can be understood with the help of Fig. 2.6.

The interaction between the plasma flowing axially and the current density **j** flowing radially produces a self-induced magnetic field B_θ described by the Maxwell relation:

$$\nabla \times \mathbf{B} = \mu_0 \mathbf{j} \tag{2.3}$$

B_θ is linear in z. At this point the interaction of this field with the current density produces a Lorentz body force following the relation:

$$\mathbf{f_B} = \mathbf{j} \times \mathbf{B} \tag{2.4}$$

This force has two components, the “blowing” component of force, f_z, that produces an axial acceleration of the propellant, and the “pumping” component of force, f_r, that establishes a radial gradient in the gasdynamic pressure. The blowing force accelerates the propellant downstream and the pumping force compresses the propellant radially toward the centerline, causing a "pinch" effect that forms a hot plasma just beyond the cathode tip. This pinch effect contributes to erosion of the cathode that limits thruster lifetime.

Focusing our attention on f_z we can integrate over the interelectrode volume obtaining the thrust:

$$F = \frac{\mu J^2}{4\pi}\left(ln\frac{r_{an}}{r_{ct}} + A\right) \tag{2.5}$$

where r_{an} is the inner radius of the anode, r_{ct} is the radius of the cathode, and J is the total arc current. A is a constant depending on the geometry of the thruster. As can be seen $F \propto J^2$. Considering the general relation $F = \dot{m}u_e$, the exhaust velocity u_e scales as:

$$u_e \propto \frac{J^2}{\dot{m}} \tag{2.6}$$

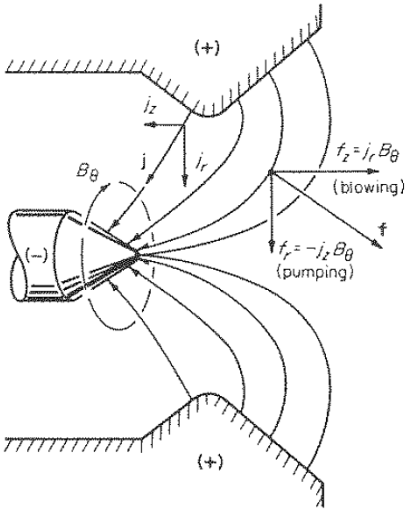

Figure 2.6: *Magnetogasdynamic model of the MPD accelerator. r is the radial coordinate, θ the azimuthal and z the axial coordinate from left to right. Source: [21].*

From the equations it seems that as long as one is able to supply more power to the system, the exhaust velocity will quadratically increase with the current. Unfortunately, experiments have shown that this is not true due to the existence of a critical value $\left(J^2/\dot{m}\right)^*$ above which the thruster begins operating in a different regime called "onset". This regime is characterized by strong instabilities in the plasma and electric arcs associated with explosive spot formation. Thruster operation in the onset regime results in rapid erosion and deterioration of the anode, leading to severe lifetime limitations. It has been found that the cause of this *onset* phenomenon is a lack

of electrons in the interelectrode space (so called *anode starvation*) [23]. Though the onset phenomenon has impeded the development of the MPD thruster for in-space propulsion applications, it can be utilized as a means for vaporizing solid material.

2.4.1.1 MPDT application to solid ablation

A possible application of the MPDT working model, taking advantage of the pinch effect, is silica vapor production. A cylinder of compressed silica can be placed at the center of an annular cathode shaped to encourage arc attachment, as depicted in Fig. 2.7. The advantage of such design is that the pinch effect allows the arc column to adhere to the silica cylinder, concentrating the hottest zone in the region where ablation is needed. This arc *attached* to the silica cylinder ablates the cylinder surface, producing ions and the electric carriers needed for current conduction, avoiding both starvation of the interelectrode medium and spot formation on the anode surface. If used as the first stage of the separator device, the blowing force (see Fig. 2.6) would eject the ions at high speed, avoiding the necessity of an intermediate stage with this purpose. The feasibility of using silica as an electrode should also be taken into consideration, as demonstrated by Addona and Munz [24].

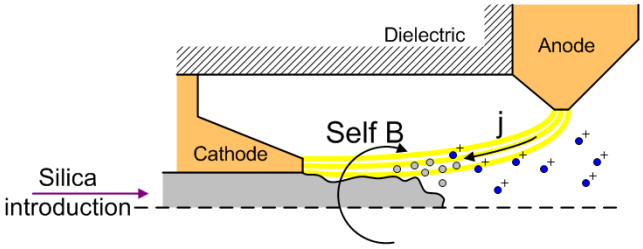

Figure 2.7: *First stage MPDT configuration*

The above approach has three main problems:

- the arc suffer from instabilities, there can be misalignment and impingement only on some areas of the anode producing the damage or destruction of the device;
- the hot plasma shall not come in contact with the dielectric/chamber wall, otherwise the plasma could be cooled to a temperature where recombination reactions occur frequently, or the walls could be heated to the point of damage;

- minor: the self created B field, azimuthal, could interfere with subsequent stages of the demonstrator that utilize and applied magnetic field.

One possible approach to solving these problems is application of an axial B field, which can be achieved by placing a solenoid around the anodes, as shown in Fig. 2.8. This axial field causes an azimuthal component of force on radially-directed current in the arc, producing a swirling current trajectory demonstrated to have a stabilizing effect. In addition, the Lorentz force caused by the axial magnetic field confines the radial motion of ions, reducing collisions with the walls and expelling the ions axially from the device.

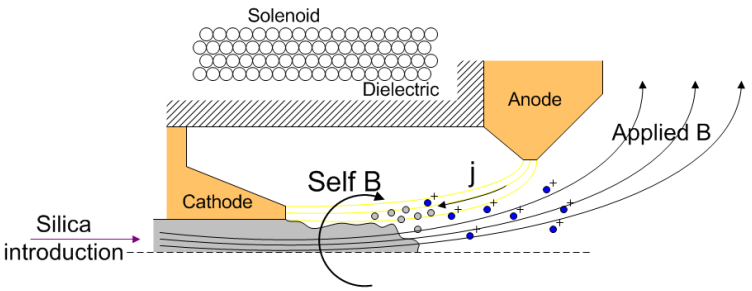

Figure 2.8: *Previous configuration with applied B field*

2.4.2 The self-feeding torch

The self-feeding torch was developed in the frame of the Archimedes program [9, 25] (see §1.2.2). The necessity to avoid insertion of additional external working gas led to the idea of using the volatile part of oxides as the working gas for the RF torch. The sequence of operations of such device is the following:

1. The material to be separated is melted and introduced into the torch;

2. The liquid material, adhering to the chamber walls, drains toward the bottom. The volatile part of the compound that leaves the liquid material (i.e. the component of the mixture that has a lower boiling point or the result of initial decomposition that occurs depending on the vapor pressure) allows the beginning of the RF plasma creation;

3. An equilibrium condition between the RF plasma and the liquid film at the wall occurs with a double effect: on one hand the liquid layer protects the wall from the heat flux generated by the RF torch, while on the other hand part of the fluid evaporates due to the heat flux providing gas to be ionized by the RF antenna.

This concept is quite simple in its operation but at the same times allows many variations, e.g. inserting a cooling fluid between the wall and the antenna.

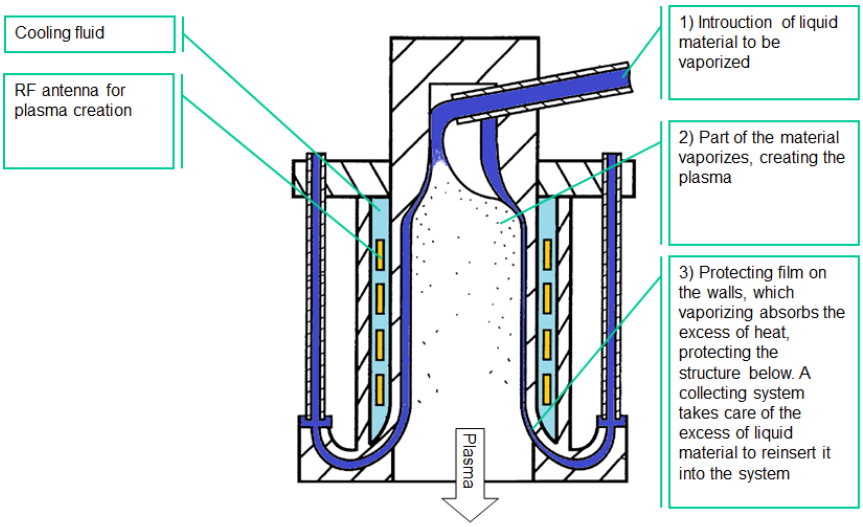

Figure 2.9: *The self-feeding torch concept as proposed in [25]*

.

2.4.3 Trade-off

The choice of selecting the self-fed torch or the MPD sublimation torch derives from a preliminary assessment regarding the power required to perform the operation and the means of performing this operation.

MPD sublimation torch The MPD sublimation torch has been discarded due to the low maturity of the concept, because the idea introduces significant differences with respect to the state-of-the-art of MPD devices. The MPD thruster contains a centerline cathode made of conductive material. During operation, often in pulsed mode, the cathode at low currents is subject to a non negligible voltage drop which increases the ion flux on

the cathode itself and erosion at the cathode tip. Nevertheless at high current and power the voltage drop is shifted towards the anode, while at the cathode it is possible to observe a local low current density and local high plasma number density. In the proposed concept, which has never been tested as far as the author is aware, the cathode is present only in the back of the chamber, while in the middle of it a cylinder made of silica is present. Silica is non-conductive, therefore the same mechanism of pumping toward the center of the thruster shall be verified. In addition cathode erosion, in devices with metallic electrode, is present only at low current (therefore low heat flux) at the tip of the cathode itself. With the silica cylinder centerline this is not possible, virtually lacking the two conditions that allowed erosion and sublimation. This means that in addition to the verification of the assumption of silica dissociation, a completely separate theoretical and numerical model of the torch concept should be developed.

Self-feeding torch The self-feeding concept is a concept which is more reliable. It can be found in literature and investigations have been performed on it. Except for the concept of fluid silica flowing around the walls to protect them from the heat flux and to provide the background gas for the silica estraction, the concept is a normal RF plasma torch. In addition the silica, being already fluid, requires less energy to provide the same amount of processed material

For the above consideration investigation of the self-feeding torch is selected, leaving the MPD sublimation torch for future investigations.

CHAPTER 3

Numerical analysis

As from §2.4.3 the self feeding torch results to be the most viable concept that can be applied in the frame of this research. To quantitatively evaluate the torch performances it is necessary to answer the issues described in Chapter 2, meaning to evaluate the sustainability by comparing the energy cost per unit of product and to verify the assumption that brought to system simplification.
Performance evaluation implies the analysis of the internal processes of the torch, such as the plasma formation and the silica evaporation. These task cannot be performed analytically, therefore numerical models are mandatory. The analysis was initially intended to be progressive, starting from a low fidelity global plasma model, capable of evaluating the domain averaged system evolution in time for a preliminary understanding of the working conditions, and then a multiphysics 2D axisymmetric FEM model, capable of simulating the actual torch geometry and the thermochemical processes in each point of the domain.

The two models shares the list of reactions which describes the plasma behavior. This list includes plasmas reaction and chemical reactions, each

with its own reaction rate or cross section. The work performed to collect this information was not easy: other than the physics of oxygen, which reactions are commonly available, the plasma reactions involving silicon and its oxygen compounds were very difficult to gather. Models of plasma made of SiO_2 appear to be not available in literature, as far as the author is aware. The majority of the papers focus on Plasma Enhanced Chemical Vapor Deposition (PECVD), which involves hydrogen, or on the production on nanometric SiO_2, in plasma torches where silica reaches only fusion temperature. In order to collect the fundamental equations to build the model, reaction has to be found in astrophysics and atmospheric related papers.

3.1 0D model

The 0D model is based on the work of Bosi [26], which led to a collaboration outside the PhD path for the application of this model to N_2O and N_2H_4 [27], being the code initially developed for Ar. The model was applied to the evaluation of the behavior of chemical reactive species with a plasma capable of triggering a self sustained decomposition reaction. It comprises two models which talks together: the plasma model, which is devoted to calculate the electron and ion densities and the electron temperature, and the chemical model which, on the basis of the reactions enthalpy balance, is able to calculate the ions and neutrals temperature, evaluating the self sustaining decomposition conditions.

3.1.1 Model description

The model simulates the 0D evolution in time of a mixture of reacting gases ionized by an inbound power (RF). It basically behaves like a pug flow reactor, with inflow, outflow, bulk reactions and wall reactions (mainly recombinations).
The plasma is considered enclosed in a volume, surrounded by walls. As the plasma is established, electrons and ions diffuse through the volume reaching the walls. Electrons are created in the volume through plasma bulk reactions, and lost at walls through recombination.

3.1.1.1 Processes considered

The model takes into a number of processes which involve charged and neutral particles:

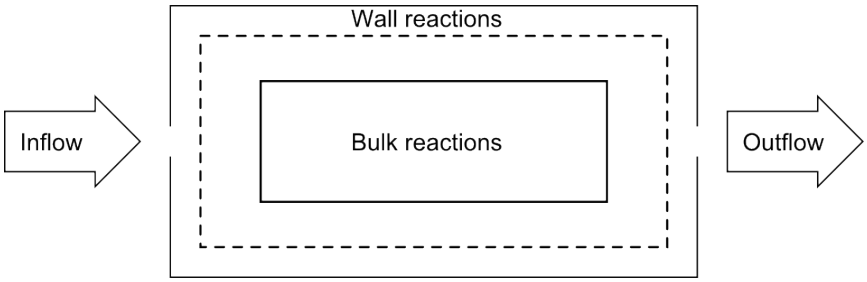

Figure 3.1: *Pug flow reactor*

Wall plasma processes Wall plasma processes are recombinations that lead to disappearance and generation of particles. The surface acts as a third-body-collision partner and usually absorbs the exceeding energy released in these processes. The disappearance of electron is considered lost by the system. The processes involves two main groups of particles;

- **Charged particle processes** When ions and electrons hit the wall, they recombine and are lost. Since electrons have high thermal energy they are lost faster and leave the plasma with a positive net charge, which set-up a negative wall potential respect to the bulk. The potential drop, confined in a region of several Debye lengths (see Eq. 3.6) called sheath, acts as a barrier for the more slow electrons to cross the sheath, while ions accelerate through it leading to the balance of the particle fluxes. The potential drop across the plasma and the sheath and the flux of charged particles across the sheath are evaluated. Diffusivity at the plasma-sheath interface and electron-energy loss terms are calculated.
- **Neutral particle processes** The wall can be considered a third body partner for some reactions in which also some neutral species are involved. The reaction rate depends on the density of the species at the wall and also on a dimensionless recombination factor, which depends on the properties of the surface and the particular species considered. Diffusion of such neutral particles is calculated.

Bulk plasma processes The reactions which happen in the core of the volume, i.e. in a pug reaction not at the wall, are called bulk plasma processes. These involve collisions and radiation. Collisions are responsible for the generation of new species and provide transfer of en-

ergy from the electrons to the other species, and are two types: elastic and inelastic.

- **Elastic collisions** They can be polarization-scattering and coulomb-scattering: the former dominates in weakly ionized plasmas while the latter dominates in fully ionized plasmas or whenever the collision time is less or equal the characteristic time scale.
- **Inelastic collisions** They are ionization, dissociation, attachment, excitation, de-excitation, etc. In both cases the reaction cross section allows to calculate the number of events per volume per second.

In case an electron is involved in the collision, the processes are named electron collision processes. These include elastic scattering, excitation, dissociation, ionization, recombination with ions, attachment and detachment. Neutral gas phase processes involve recombination, de-excitation, detachment. Ion-ion recombination and ion dissociation, being processes between heavy species, are also included in the neutral gas phase framework because are handled at the same way.

The model is based on the following main equations:

- Electrons energy balance equation:

$$\frac{d}{dt}\left(\frac{3}{2}n_e k_B T_e\right) = P_{abs} - P_{loss} \tag{3.1}$$

where P_{abs} is the power deposited to the electrons by the RF antenna, and is a model input, product of the power input and efficiency. P_{loss} is the power lost by electrons in the plasma and is the sum of:

$$P_{loss} = [\text{bulk losses}] + [\text{wall losses}] + [\text{exhaust losses}] \tag{3.2}$$

- Continuity equation for each i-th chemical species:

$$\begin{aligned}\frac{dn_i}{dt} = {} & [\text{Bulk plasma processes}] + [\text{inflow}]+ \\ & - [\text{outflow}] \pm [\text{wall recombination/losses}]\end{aligned} \tag{3.3}$$

$$\frac{dn_i}{dt} = \sum_i K_{i,j} n_i n_j + \frac{inflow}{V_r} + \\ + \frac{outflow}{V_r} \pm \tilde{N}_{events,recombination/losses} \tag{3.4}$$

where $K_{i,j}$ is the rate constant process involving the i-th species with the j-th species.

- Neutrals and ions energy balance equations

$$\frac{d}{dt}\left(\sum \tilde{u}_i\right) = inflow\ h_{in} - outflow\ h_{out} + Q \tag{3.5}$$

where h_{in} and h_{out} are the molar enthalpies entering and exiting the system, $\tilde{u}_i$ is the internal energy of the species, Q is the energy released or absorbed by the system due to reactions occurring inside the chamber.

The model boundary conditions are:

- Mass flow rate
- Power input
- Geometry, from which volume V_r and surface available for wall reactions are derived
- Magnetic field

and the models output is represented by the behavior over time of:

- Species density
- Electron temperature
- Neutral/Ions temperature

The model has been validated in [26] with Argon and N_2O, while due to the lack of available literature experimental data the correctness of the application to N_2H_4 could not be verified [27].

3.1.2 Evaluation of applicability

The model was initially intended to be used as a verification of the selective ionization process described in §2.3.1. During the model development and application to N_2O and N_2H_4 the complexity in switching chemical species was clear. The implementation of the species informations, which already took a lot of time to be gathered, was a time consuming operation, therefore it was clear that the time to specialize the model exceeds model possible benefits.

Decision was made to dismiss the 0D model avoiding the implementation of the SiO_2 kinetics. The decision took place after the understanding that the multiphysics 2D axisymmetric FEM model, planned to be used after the global model, was able to perform the same assessment faster and more accurately.

3.2 Multiphysics model

A multiphysics 2D axisymmetrical FEM model (COMSOL^{TM}) of the first stage of the demonstrator has been set up with the following objectives:

- To verify the silicon ions separation in terms of number density respect to the other species inside the plasma
- To evaluate the output of the torch in terms of species composition and species velocity, in order to understand the necessity and requirements of the second and third stages
- To evaluate the power level required to perform the ionization and extraction of the silicon ions, by evaluating trends in varying the input parameters

3.2.1 Model description

The models simulates the torch behavior, with the molten SiO_2 injection and the power deposition. The geometry resembles those of the torch in §2.4.2, while at its ending a volume is placed, as a section of the vacuum chamber, to allow fluid expansion and neutrals ion pumping out.
The torch have lab size dimensions:

- R_t = 2 cm
- L_t = 7 cm

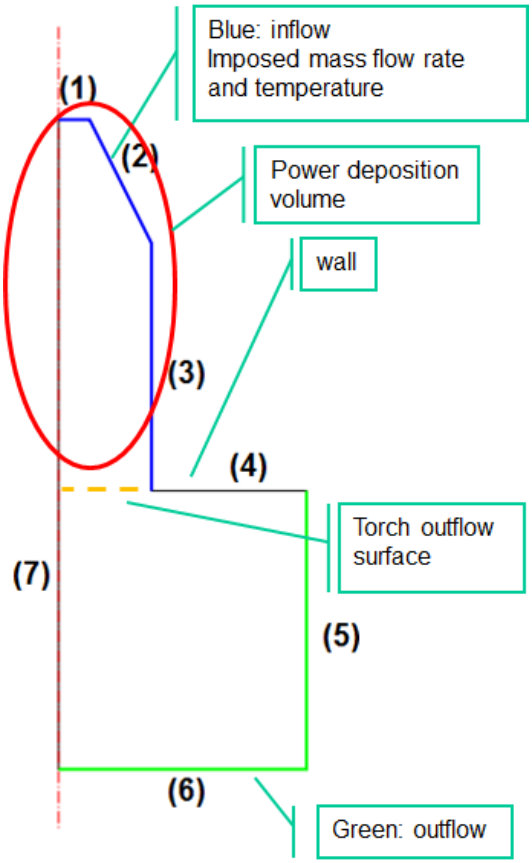

Figure 3.2: *2D axisymmetric FEM model geometry and description. Walls are numbered to allow understanding of the boundary and initial conditions*

The model takes into account the following phenomena:

- Silica evaporation inside the chamber;
- Plasma creation inside the chamber due to power deposition;
- Fluid flow inside the chamber;
- Thermal dynamics due to the enthalpies of reaction.

According to Fig. 3.2 the model has an axisymmetric geometry. From boundaries (1), (2) and (3) the SiO_2 is injected simulating the evaporation from the liquid silica layer which protects the wall from the torch heat flux. This evaporating material establish a laminar flow which is affected by the

power deposition in the volume of the torch (the red circle in Fig. 3.2). In the volume a plasma is therefore created, and the provided energy is spent to ionize the plasma and to increase the electron temperature and the ion/neutral temperature. From the torch ouflow surface the plasma and the neutrals flows into a bigger volume which purpose is to simulate a part of the volume of the separation chamber, in which the neutrals (mainly molecular oxygen) are pumped away and the ions are not affected due to the high output speed and, in case, by the applied uniform magnetic field of the separator stage. The power is deposited into the plasma (e.g. inductively by an antenna), increasing the electron temperature. The energy increment triggers the decomposition and ionization reactions, which in turns increase the electron density and the electrons impacts, till the reaching of dynamic equilibrium with the inbound mass flow.

The model comprises a *fluid-dynamical* model (§3.2.1.1), a *thermal* model (§3.2.1.2) and a *plasma* model (§3.2.1.3) coupled one to each other. As introduced above, ions and neutrals are supposed to have a single temperature, different from the electrons one. This implies that a single fluid model is used, where the plasma is seen as a unique conducting fluid and globally neutral, that reacts to external inputs. This approach is possible because the plasma is *collisional*, due to the relatively high pressure level in the torch, and two conditions applies:

- the time scales of interest are much higher than the characteristics frequency of the system. In particular characteristic electron-neutral collision frequency of this kind of system is much higher ($\nu_{e-n} \sim O(1E9\ s^{-1}$ [28]) that the exciting frequencies, which are on the order of MHz ($O(1E6\ s^{-1})$.

- the characteristic length of the system must be much higher than the Debye length. As we will see in the worst case an electron temperature of 5 eV and an electron density of 1E16 m^{-3} (§3.2.3.1) and §3.2.3.2) lead to a maximum Debye length of

$$\lambda_D = \sqrt{\frac{\epsilon_0 k_B T_e[K]}{n_e q^2}} \sim 1.7E-4\ m \tag{3.6}$$

  which is orders of magnitude smaller than the chamber diameter or length.

Related to the above bullets, the collisionality of the plasma is verified, meaning that the mean free path before an electron-neutral collision $\lambda_{e-n} = v_{e,th}/\nu_{e-n}$ is much lower than the characteristics dimensions of the system. Considering above values of electron temperature, from which $v_{e,th}$ is calculated through Eq. 3.37, and of electron-neutral collision frequency, a value of $\lambda_{e-n} \sim O(1E-3\ m) \ll R_t, L_t$ is found.

The logic of the model is represented in Fig. 3.3 below:

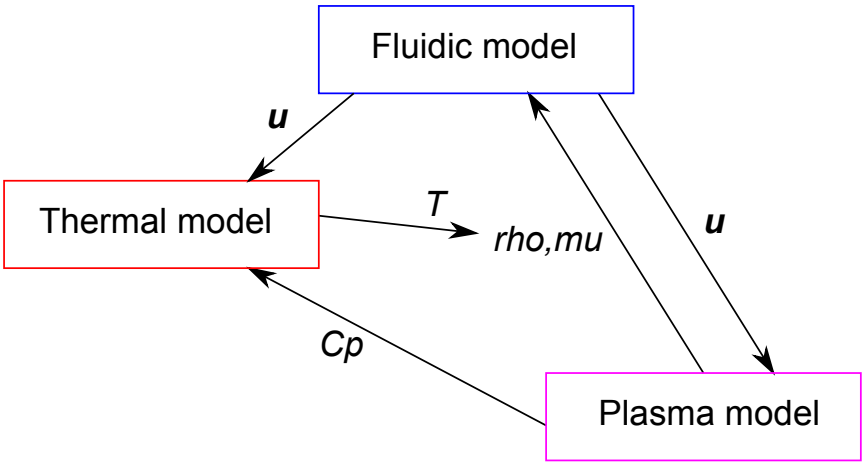

Figure 3.3: *Multiphysics model logic*

The model input is a general power deposition per unit volume P_{in}, which is used inside the electron energy balance equation (Eq. 3.7 [29]) that rules the deposition of energy inside the plasma. The choice to not specialize the model toward a particular energy deposition technology was preferred to focus the attention on what happens inside the plasma, and what are the outcome of the device starting from actual deposited power levels, in agreement with the goals of the work identified in Chapter 2. From the practical point of view such power deposition can be performed using ICP or helicon plasma sources, but the effect of this technologies on the overall behavior is taken into account using in §4.3 a typical source efficiency value. The electron energy balance equation is:

$$\frac{\partial n_e}{\partial t} + \nabla \cdot \mathbf{\Gamma}_e + \mathbf{E} \cdot \mathbf{\Gamma}_e = R_e - (\mathbf{u} \cdot \nabla) n_e + \frac{P_{in}}{q} \tag{3.7}$$

$$\mathbf{\Gamma}_e = -(\mu_e \cdot \mathbf{E}) n_e - \mathbf{D}_e \cdot \nabla n_e \tag{3.8}$$

$$\mathbf{E} = -\nabla V \tag{3.9}$$

Where n_e is the electron energy density, R_e is the energy loss/gain due to inelastic collisions, μ_e is the electron energy mobility (see Eq. 3.52), $\mathbf{D}_e$ is the electron energy diffusivity, P_{in} is the power deposited into the plasma and is modeled as a power deposition for unit of volume (W/m^3), $\mathbf{E}$ is the electric field and V is the potential. Assuming a Maxwellian Electron Energy Distribution Function (EEDF) the following relations hold [30]:

$$\mathbf{D}_e = \mu_e T_e \tag{3.10}$$

$$\mu_e = \frac{5}{3}\mu_e \tag{3.11}$$

$$\mathbf{D}_e = \mu_e T_e \tag{3.12}$$

Eq. 3.7 is coupled to the momentum balance equation (Eq. 3.13) of the fluid model, as the neutral fluid velocity field $\mathbf{u}$ is the output of this equation. $\mathbf{u}$ also enters in the continuity equations for electrons, in the continuity equation for ion/neutrals and the ion/neutral energy balance.

$$\rho\frac{\partial \mathbf{u}}{\partial t} + \rho\left(\mathbf{u}\cdot\nabla\right)\mathbf{u} = \nabla\cdot\left[-\rho\mathbf{I} + \mu\left(\nabla\mathbf{u} + (\nabla\mathbf{u})^T\right) - \frac{2}{3}\mu\left(\nabla\cdot\mathbf{u}\right)\mathbf{I}\right] \tag{3.13}$$

The momentum balance equation usually contains a term of external force. Nevertheless in the proposed model the boundary conditions foresee no external electric field $\mathbf{E}$ or magnetic field $\mathbf{B}$ applied to the torch volume, therefore no Lorentz force is applied to the quasi neutral conductive fluid, and the momentum balance equation results a standard Navier-Stokes equation.

As said, the coupling with the plasma part is provided by the neutral fluid velocity field $\mathbf{u}$, but also through the density ρ and the dynamic viscosity μ terms, which are calculated averaging on the mixture. Starting from the mean molar mass M_n:

$$\frac{1}{M_n} = \sum_{k=1}^{N}\frac{w_k}{M_k} \tag{3.14}$$

where w_k is the mass fraction of the species k, and M_k its molar mass.

Therefore ρ and μ are:

$$\rho = \frac{pM_n}{RT} \tag{3.15}$$

$$\mu = \mu(T, M_k, \mu_k) \qquad \text{(see Brokaw [31] for details)} \tag{3.16}$$

$$\tilde{C}_p = \frac{\sum_k x_k \tilde{C}_{p,k}}{\sum_k x_k M_k} \tag{3.17}$$

Eq. 3.13 is coupled to the thermal model, and in particular to the heat equation Eq. 3.18, through ρ and μ, which depend on T, and again through the fluid velocity field $\mathbf{u}$. The heat equation is also coupled to the plasma model through the specific heat C_p from Eq. 3.17, conveniently converted from molar basis to mass basis units.

$$\rho C_p \frac{\partial T}{\partial t} + \rho C_p \mathbf{u} \cdot \nabla T = \nabla \cdot (k \nabla T) + Q \tag{3.18}$$

where Q is the heat provided to the gas due to system reactions:

$$Q = -\sum_j \Delta H_j r r_j \tag{3.19}$$

ΔH_j and rr_j are the enthalpy and the reaction rate of the j-th reaction, where:

$$\Delta H_j = \sum_i \tilde{\nu}_{kj} h_k \tag{3.20}$$

$$rr_j = k_j^f \prod_{k=1}^{N} c_k^{\tilde{\nu}_{kj}} - k_j^b \prod_{k=1}^{N} c_k^{\tilde{\nu}_{kj}} \tag{3.21}$$

where $c_k = w_k \rho / M_k$ is the molar concentration of the k-th species, $\tilde{\nu}_{kj}$ is the stoichiometric matrix with the stoichiometric coefficients and k_j^f and k_j^b are the rate coefficients calculated through the Arrhenius law or the integration of the cross section depending on the input data.

The objectives of the model described in the previous paragraph are to be verified in the torch volume and at the torch outflow surface, and in particular the ions velocities which impact the device design in case a further

ionization or accelerating stage is needed.

The model takes into consideration 18 chemical species, listed in Tab. 3.1 , and for each of them the termochemical properties are specified (see §3.2.2.2).

O	O2+	Si
O+	O2a1d	Si+
O1d	O2b1s	SiO
O1s	O2(45)	SiO+
O-	O2-	SiO2
O2	O3	SiO2+

Table 3.1: *Species taken into consideration by the 2D axisymmetric FEM model*

3.2.1.1 Fluid-dynamical modelling

The possibility of using the Navier-Stokes equation is based on the continuum assumption. This can be easily verified by calculating the Knudsen number:

$$Kn = \frac{\lambda_{mfp}}{L_t} \tag{3.22}$$

The λ_{mfp} is given by the ratio of the average velocity of the colliding particle and the neutral collision frequency. Under the approximation of the hard-sphere gas in the kinetic theory the mean free path can be approximated as:

$$\lambda_{mfp} = \frac{\mu}{\rho}\sqrt{\frac{\pi m}{2k_B T}} \tag{3.23}$$

where m is the molecular mass. By using the molecular mass of SiO, the most abundant species in the volume, it is possible to obtain $\lambda_{mfp} \sim 4E{-}3\ m$ in the worst case of 25 Pa background pressure, which gives $Kn \sim O(10)$, which is the same order of magnitude of the ratio λ_{e-n}/L_t.

A laminar flow is modeled for the fluid-dynamics of the system. As the Knudsen number, the Reynolds number is calculated *a posteriori* to be $Re \sim O(1-10) \ll 2000$, verifying this assumption .

The boundary conditions and the equations governing the dynamics are the following:

Boundary	**Condition**
(1) (2) (3)	Imposed mass flow rate
	$$-\int_S \rho\,(\mathbf{u}\cdot\mathbf{n})\,dS = \dot{m} \quad (3.24)$$
(4)	No slip condition
	$$\mathbf{u} = 0 \quad (3.25)$$
(5) (6)	Output pressure imposed
	$$p = p_0 \quad (3.26)$$
(7)	Axis of symmetry
	$$-\int_S \rho\,(\mathbf{u}\cdot\mathbf{n})\,dS = 0 \quad (3.27)$$
Volume	Continuity equation
	$$\frac{\partial\rho}{\partial t} + \nabla\cdot(\rho\mathbf{u}) = 0 \quad (3.28)$$
Volume	Momentum balance
	$$\rho\frac{\partial\mathbf{u}}{\partial t} + \rho\,(\mathbf{u}\cdot\nabla)\,\mathbf{u} = \nabla\cdot\left[-\rho\mathbf{I} + \mu\left(\nabla\mathbf{u} + (\nabla\mathbf{u})^T\right) - \frac{2}{3}\mu\,(\nabla\cdot\mathbf{u})\,\mathbf{I}\right] \quad (3.13 \text{ revisited})$$
	$$\frac{1}{M_n} = \sum_{k=1}^{N}\frac{w_k}{M_k} \quad (3.14 \text{ revisited})$$
	$$\rho = \frac{pM_n}{RT} \quad (3.15 \text{ revisited})$$
	$$\mu = \mu\,(T, M_k, \mu_k) \quad (3.16 \text{ revisited})$$

Table 3.2: *Fluid-dynamical boundary conditions and equation governing the model*

The physics of the SiO_2 evaporation is taken into account in Eq. 3.24 with the definition of the input mass flow rate $\dot{m}$. According to Schick [32], the most important reaction in the vaporization of silica is:

$$SiO_{2(l)} \rightarrow SiO_{(g)} + 0.5O_{2(g)} \quad (3.29)$$

while $SiO_{2(g)}$ results to be produced in at least one order of magnitude less quantity. The model has been therefore set to have, as a boundary condition, the injection from the walls of a mixture of SiO and O_2 in stoichiometric

condition, plus minor quantities of other molecules for numerical purposes. The mixture is reported in Tab. 3.3, which is derived from Schick [32] from SiO_2 decomposition in neutral conditions (i.e. without air or other gas in the environment).

Species	Mass fraction
O2	0.332
O	0.01
SiO	0.657
SiO2	0.001

Table 3.3: *Inlet mass flow rate mixture*

The range of mass flow rates used in the model is 1E-7 - 1E-5 kg/s.

3.2.1.2 Thermal modelling

The thermal modeling of the system comprises the heat equation with heat generation from the system chemical reactions. Due to the evaporation of silica on the walls the temperature of the vapor that leaves the surface is assumed constant and equal to the boiling temperature of the fluid T_b. This temperature strongly depends on the pressure inside the chamber, and therefore T_b is calculated from the vapor pressure of silica, assuming that the Eq. 3.30 valid for neutral conditions as from [32] is valid throughout the whole simulation.

$$p_{SiO}[atm] = 2p_{O_2} = \exp\left(18.41\left(1 - \frac{3160}{T_b[K]}\right)\right) \tag{3.30}$$

therefore

$$p_{vap}[atm] = 1.5\exp\left(18.41\left(1 - \frac{3160}{T_b[K]}\right)\right) \tag{3.31}$$

Starting from the imposed pressure, and expressing the pressure in Pascal, the equation can be inverted to obtain the boiling point.

$$T_b[K] = \frac{3160}{1 - \ln\left(\frac{p_{vap}[Pa]}{1.5 \cdot 101325}\right)/18.41} \tag{3.32}$$

Null heat flux is imposed at the other surfaces, therefore the only energy flux is due to the inflow and outflow of enthalpy.

Boundary	Condition
(1) (2) (3)	Imposed wall temperature and inlet flow temperature
$$T = T_0 \quad (3.33)$$	
(4)	No conductive flux
$$-\mathbf{n} \cdot (-k\nabla T) = 0 \quad (3.34)$$	
(5) (6)	No conductive flux, only convective outflow
$$-\mathbf{n} \cdot (-k\nabla T) = 0 \quad (3.35)$$	
(7)	Axis of symmetry
$$-\mathbf{n} \cdot (-k\nabla T) = 0 \quad (3.36)$$	
Volume	Heat equation
$$\rho C_p \frac{\partial T}{\partial t} + \rho C_p \mathbf{u} \cdot \nabla T = \nabla \cdot (k\nabla T) + Q \quad (3.18 \text{ revisited})$$	
$$\tilde{C}_p = \frac{\sum_k x_k \tilde{C}_{p,k}}{\sum_k x_k M_k} \quad (3.17 \text{ revisited})$$	
$$Q = -\sum_j \Delta H_j r_j \quad (3.19 \text{ revisited})$$	
$$\Delta H_j = \sum_i \tilde{\nu}_{kj} h_k \quad (3.20 \text{ revisited})$$	

Table 3.4: *Thermal boundary conditions and equation governing the model*

3.2.1.3 Plasma modeling

The modeling of the plasma decomposition of the inbound gas mixture is the most complex physics taken into consideration in the FEM model. It comprises both plasma reactions, which involve electrons impact, and chemical reactions, which are responsible of the heating of the neutral mixture.

As introduced the equation that rules the deposition of energy inside the plasma is the electron energy balance in Eq. 3.7. The power is injected into the plasma, increasing the electron temperature. The energy increment triggers the decomposition and ionization reactions, which in turns increases the electron density and the electrons impacts, till the reaching of dynamic equilibrium with the inbound mass flow.

An important aspect is represented by the wall recombination, which represents a sink of electrons and ions because charged particles hits the wall and recombine with the opposite charge, disappearing in case of electrons (but providing an energy flux toward the wall) or mutating into the neutral atoms or molecules in case of ions. The fluxes of electrons $\mathbf{\Gamma_e}$ and electron energy $\mathbf{\Gamma_e}$ to the wall are calculated in Eqs. 3.39 and 3.40, and are proportional to the the thermal velocity $v_{e,th}$ defined as

$$v_{e,th} = \sqrt{\frac{8k_B T_e[K]}{\pi m_e}} \tag{3.37}$$

For sake of clarity in the following equations the quantities that refers to electron have $[.]_e$ as subscript, while those referring to the electron energy have $[.]_\mathrm{e}$ as subscript.

Boundary	**Condition**
(1) (2) (3) (4)	Ground
$V = 0$ (3.38)	
(1) (2) (3) (4)	Normal flux of electrons and electron energy
$\mathbf{n} \cdot \mathbf{\Gamma_e} = \left(\frac{1}{2} v_{e,th} n_e\right)$ (3.39) $\mathbf{n} \cdot \mathbf{\Gamma_e} = \left(\frac{5}{6} v_{e,th} n_\mathrm{e}\right)$ (3.40)	
(5) (6)	Zero charge building on the boundary
$-\mathbf{n} \cdot \mathbf{D} = 0$ (3.41)	
(5) (6)	No flux of electron density and electron energy density
$-\mathbf{n} \cdot \mathbf{\Gamma_e} = 0$ (3.42) $-\mathbf{n} \cdot \mathbf{\Gamma_e} = 0$ (3.43)	
(7)	Axis of symmetry
$-\mathbf{n} \cdot \mathbf{\Gamma_e} = 0$ (3.44) $-\mathbf{n} \cdot \mathbf{\Gamma_e} = 0$ (3.45)	

Continued on next page

Table 3.5 – continued from previous page

Boundary	Condition
Volume	Electron density and electron energy balance
	$\frac{\partial n_e}{\partial t} + \nabla \cdot \mathbf{\Gamma_e} = R_e - (\mathbf{u} \cdot \nabla) n_e$ (3.46)
	$\mathbf{\Gamma_e} = -(\mu_e \cdot \mathbf{E}) n_e - \mathbf{D}_e \cdot \nabla n_e$ (3.47)
	$\frac{\partial n_\mathrm{e}}{\partial t} + \nabla \cdot \mathbf{\Gamma_e} + \mathbf{E} \cdot \mathbf{\Gamma}_e = R_\mathrm{e} - (\mathbf{u} \cdot \nabla) n_\mathrm{e} + \frac{P_{in}}{q}$ (3.7 revisited)
	$\mathbf{\Gamma_e} = -(\mu_\mathrm{e} \cdot \mathbf{E}) n_\mathrm{e} - \mathbf{D_e} \cdot \nabla n_\mathrm{e}$ (3.8 revisited)
	$\mathbf{E} = -\nabla V$ (3.9 revisited)
	$\mathbf{D}_e = \mu_e T_e$ (3.10 revisited)
	$\mu_\mathrm{e} = \frac{5}{3}\mu_e$ (3.11 revisited)
	$\mathbf{D_e} = \mu_\mathrm{e} T_e$ (3.12 revisited)
	$R_e = \sum_{j=1}^{M} x_j k_j N_n n_e$ (3.48)
	$R_\mathrm{e} = \sum_{j=1}^{P} x_j k_j N_n n_e \Delta e_j$ (3.49)
Volume	Continuity equation for each species
	$\rho \frac{\partial w_k}{\partial t} + \rho (\mathbf{u} \cdot \nabla) w_k = R_k$ (3.50)
	$R_k = M_k \sum_{J=1}^{N} \tilde{\nu}_{kj} r r_j$ (3.51)
Volume	Reaction rate calculation
	$r r_j = k_j^f \prod_{k=1}^{N} c_k^{\tilde{\nu}_{kj}} - k_j^b \prod_{k=1}^{N} c_k^{\tilde{\nu}_{kj}}$ (3.21 revisited)

Table 3.5: *Plasma boundary conditions and equation governing the model*

where R_e is the electron source term, Δe_j is the energy loss for reaction j-th, N_n is the total neutral density, M_k is the atomic weight of the species k-th.

In the torch volume the values of power injected P_{in} are $12.5W - 125W - 1250W$.

3.2.1.4 FEM discretization

Linear FEM elements are used for the discretization. Quadratical discretization for electric potential, electron density and electron energy density greatly

increased Degrees of Freedom (DoF) number without introducing improvements in the solution.

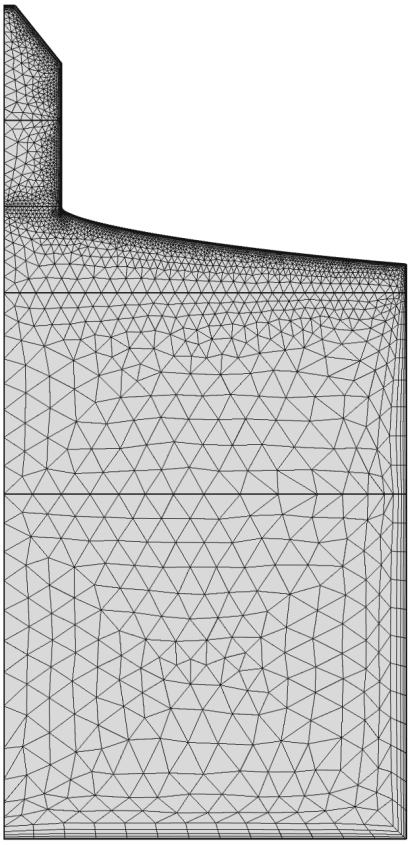

Figure 3.4: *2D axisymmetrical model mesh*

The geometry is 2D axisymmetrical, and the domain is discretized with triangular elements and quadrilateral boundary layer elements. The torch domain in which the power deposition occurs is meshed with finer elements respect to those of the "chamber" region. Fig. 3.4 shows the mesh.

A sensitivity analysis was performed on the mesh. Results are provided in Fig. 3.5 where the maximum electron density is plotted versus subsequent mesh refinement. As can be seen above 6000 elements the solutions reaches a trend where further refinements provide only minimal improvements in the solution, which do not justify the increased computational load.

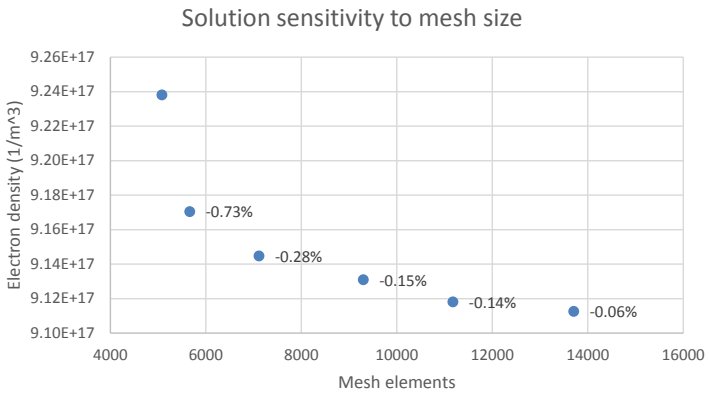

Figure 3.5: *2D axisymmetrical model mesh sensitivity analysis*

3.2.2 Input experimental data

The model needs as input several information about the reactions occurring inside the chamber and physical properties of the substances involved. These data comes from experimental investigation, therefore extensive research on literature and databases was necessary. The information needed by the model are basically of two kinds:

Set of involved reactions listing the reactions which occur inside the volume and on the surface of the chamber.

Thermochemical properties for each of the involved species: specific heat, enthalpy of formation and entropy are necessary to calculate the heat of reaction and therefore to calculate the temperature of the neutrals as specified in Eq. 3.18.

3.2.2.1 Reaction set

A big effort was put in identifying an exhaustive set of equations capable of simulating silica decomposition and thermal behavior. Unfortunately silica plasma processing is generally investigated for the production of nanometric silica particle (fumed silica) for industrial uses. In such references the phenomenon is mainly described and modeled in its global behavior, with the purpose of comparing results to macroscopic experimental values [33–35]. Even if in case of numerical simulation of the plasma flame [36] the model is mainly focused in reproducing its fluidic behavior rather than simulating the behavior of any single specie inside the chamber,

and the material usually reaches the melting point at maximum. A field in which there is an extensive literature of processes and kinetic plasma models is Plasma Enhanced Chemical Vapour Deposition (PECVD) where unfortunately the most used class of silicon compound is those of silanes, due to their gaseous form and their capability to be easily decomposed in a plasma environment. The area of research which provides the most useful information is instead the modeling of atmospheric processes. Surprisingly it appears that silicon ions are generated in the Earth's upper atmosphere by collisions of material ablated from incoming meteoroids with atmospheric molecules [37,38], and from charge transfer of silicon-based neutral species with major atmospheric ions [39]. Being atmosphere composed mainly by nitrogen and oxygen it is clear that the interaction of silicon with those elements is of great interest to understand aspects of atmospheric dynamics. The reactions kinetics can be expressed in two main forms, by using the reaction cross section or by providing the forward rate constant, from both of which the reaction rate can be obtained [40]. In Tab. 3.6 the bulk reactions, which happens inside the plasma volume, are listed along with the source where they were retrieved. In Tab. 3.7, for the reaction whose kinetic can be expressed by using a reaction rate, the expression of the latter is provided. It has to be underlined that apparently no complete kinetic models of silica plasma decomposition are available in literature, therefore this set of reactions can be a useful source of rate constants and references for those involved in building similar models.

#	Reaction	Type	eV	Source
1	e + O2 => e + O2	Elastic		[41]
2	e + O2 => O + O-	Attachment	-	[42]
3	e + O2 => e + O2	Excitation	0.02	[42]
4	e + O2 => e + O2	Excitation	0.19	[42]
5	e + O2 => e + O2	Excitation	0.19	[42]
6	e + O2 => e + O2	Excitation	0.38	[42,43]
7	e + O2 => e + O2	Excitation	0.38	[42–44]
8	e + O2 => e + O2	Excitation	0.57	[42–44]
9	e + O2 => e + O2	Excitation	0.75	[42–44]
10	e + O2 => e + O2a1d	Excitation	0.977	[42–44]
11	e + O2a1d => e + O2	Excitation	-0.977	COMSOL
12	e + O2 => e + O2b1s	Excitation	1.627	[42–44]
13	e + O2b1s => e + O2	Excitation	-1.627	COMSOL
14	e + O2 => e + O2(45)	Excitation	4.5	[42,44]
15	e + O2(45) => e + O2	Excitation	-4.5	COMSOL
16	e + O2 => e + O + O	Excitation	6	[42,44]
17	e + O2 => e + O + O1d	Excitation	8.4	[41,44]
18	e + O2 => e + O + O1s	Excitation	9.97	[44]

Continued on next page

Table 3.6 – continued from previous page

#	Reaction	Type	eV	Source
19	e + O2 => 2e + O2+	Ionization	12.06	[42]
20	e + O2a1d => e +O2a1d	Elastic		[41]
21	e + O2a1d => e + O + O	Excitation	4.6	[41]
22	e + O2a1d => 2e + O2+	Ionization	11.1	[41]
23	e + O2b1s => e + O2b1s	Elastic		[41]
24	e + O2b1s => e + O + O	Excitation	6	[41]
25	e + O2b1s => 2e + O2+	Ionization	10.39	[44]
26	e + O2(45)=> e + O + O	Excitation	1.5	COMSOL
27	e + O2(45)=>2e + O2+	Ionization	7.58	COMSOL
28	e + O => e + O	Elastic		COMSOL
29	e + O => e + O1d	Excitation	1.968	[44]
30	e + O1d => e + O	Excitation	-1.968	COMSOL
31	e + O => e + O1s	Excitation	4.192	[44]
32	e + O1s => e + O	Excitation	-4.192	COMSOL
33	e + O => 2e + O+	Ionization	13.192	[44]
34	e + O1d => e + O1s	Excitation	2.224	COMSOL
35	e + O1d => 2e + O+	Ionization	11.224	COMSOL
36	e + O1s => 2e + O+	Ionization	9	COMSOL
37	e + O2 + O2 => O2 + O2-	Attachment		COMSOL
38	e + O2+ => O + O	Recombination		COMSOL
39	e + O2+ => O + O1d	Recombination		COMSOL
40	O2a1d + O2 => O2 + O2	Metastable quenching		COMSOL
41	O2a1d + O => O2 + O	Metastable quenching		COMSOL
42	O2b1s + O2 => O2 + O2	Metastable quenching		COMSOL
43	O2b1s + O => O2 + O	Metastable quenching		COMSOL
44	O2(45) + O2 => O2 + O2	Metastable quenching		COMSOL
45	O1d + O2 => O + O2	Metastable quenching		COMSOL
46	O1d + O => O + O	Metastable quenching		COMSOL
47	O1s + O2 => O + O2	Metastable quenching		COMSOL
48	O1s + O => O + O	Metastable quenching		COMSOL
49	O + O + O2 => O2 + O2	Recombination		COMSOL
50	O + O + O => O + O2	Recombination		COMSOL
51	O+ + O2 => O + O2+	Charge exchange		COMSOL
52	O- + O => O2 + e	Detachment		COMSOL
53	O- + O2 => O2- + O	Charge exchange		COMSOL
54	O- + O+ => 2O	Recombination		COMSOL
55	O- + O2+ => 3O	Recombination		COMSOL
56	O2- + O2+ => 2O2	Recombination		COMSOL
57	O2- + O+ => O2+O	Recombination		COMSOL
58	e + Si => 2e + Si+	Ionization	8.15	[45]
59	e + SiO => 2e + SiO+	Ionization	11.49	[45]
60	e + SiO2 => 2e + SiO2+	Ionization	12.13	[45]
61	2O + O2 => O3 + O			[46]
62	2O2 + O => O3 + O2			[46]
63	2O3 => O + O2 + O3			[47]
64	O + O2 => O3			[48]
65	O2+ + Si => Si+ + O2	Charge exchange		[49]
66	O2a1d + O3 => 2O2 + O	Metastable quenching		[46, 47]

Continued on next page

Table 3.6 – continued from previous page

#	Reaction	Type	eV	Source
67	Si + O2 => SiO + O(3P)			[39]
68	Si + O3 => SiO + O2			[39]
69	Si+ + O2 => SiO+ + O	Charge exchange		[50]
70	Si+ + O2 => SiO2+	Charge exchange		[51]
71	Si+ + O2(a1Dg) => SiO+ + O	Charge exchange		[52]
72	Si+ + O3 => (SiO+ + O2)*0.52 + (SiO + O2+)*0.48	Charge exchange		[52]
73	SiO + O3 =>SiO2 + O2			[52]
74	SiO+ + e => Si + O	Attachment		[49, 53]
75	SiO+ + O => Si+ + O2	Charge exchange		[54]
76	SiO+ + O3 => SiO2 + O2+	Charge exchange		[55]
77	SiO2 + O => SiO + O2			[52]
78	SiO2+ + e => Si + O2	Attachment		[56]
79	SiO2+ + O2 => SiO2 + O2+	Charge exchange		[50, 55]
80	e + O+ + e => O + e	Recombination		[57]
81	e + O+ + Si => O + Si	Recombination		[57]
82	e + O+ + SiO => O + SiO	Recombination		[57]
83	e + O+ + O2 => O + O2	Recombination		[57]
84	e + O+ + O => O + O	Recombination		[57]
85	O+ + O3 => O2+ + O2	Charge exchange		[57]
86	O+ + O + Si => O2+ + Si	Recombination		[57]
87	O+ + O + SiO => O2+ + SiO	Recombination		[57]
88	O+ + O + O2 => O2+ + O2	Recombination		[57]
89	O+ + O + O => O2+ + O	Recombination		[57]

Table 3.6: *List of bulk reactions implemented in the 2D axisymmetric FEM model*

#	Reaction	Unit
37	$Na^2 * 3.6E-40 * (T_e^{-0.5})$	$m^6/s/mol^2$
38	$Na * 1.95E-13 * (300[K]/T)^{0.7}$	$m^3/s/mol$
39	$Na * 1.95E-13 * (300[K]/T)^{0.7}$	$m^3/s/mol$
40	$Na * 3E-24 * \exp(-200[K]/T)$	$m^3/s/mol$
41	$Na * 2E-22$	$m^3/s/mol$
42	$Na * 2.317E-28 * T^{0.5}$	$m^3/s/mol$
43	$Na * 4.634E-22 * T^{0.5}$	$m^3/s/mol$
44	$Na * 2E-19$	$m^3/s/mol$
45	$Na * 3.2E-17 * \exp(67[K]/T)$	$m^3/s/mol$
46	$Na * 8.0E-18$	$m^3/s/mol$
47	$Na * 4.8E-18 * \exp(67[K]/T)$	$m^3/s/mol$
48	$Na * 3.33E-17 * \exp(-300[K]/T)$	$m^3/s/mol$
49	$Na^2 * 9.268E-42 * (T^{-0.63})$	$m^6/s/mol^2$
50	$Na^2 * 3.334E-41 * (T^{-0.63})$	$m^6/s/mol^2$
51	$Na * 1.9E-18 * T^{-0.4}$	$m^3/s/mol$
52	$Na * 5.0E-16$	$m^3/s/mol$
53	$Na * 1.0E-20$	$m^3/s/mol$
54	$Na * 2.3E-13 * (T/300[K])^{-0.5}$	$m^3/s/mol$

Continued on next page

Table 3.7 – continued from previous page

#	Reaction	Unit
55	$Na * 2.3E-13 * (T/300[K])^{-0.5}$	$m^3/s/mol$
56	$Na * 2.3E-13 * (T/300[K])^{-0.5}$	$m^3/s/mol$
57	$Na * 2.3E-13 * (T/300[K])^{-0.5}$	$m^3/s/mol$
61	$Na^2 * 2E-46 * \exp(345[K]/T)$	$m^6/s/mol^2$
62	$Na^2 * 6.4E-47 * \exp(663[K]/T)$	$m^6/s/mol^2$
63	$Na * 1.648E-15 * \exp(-11400[K]/T)$	$m^3/s/mol$
64	$Na * 1.4E-20$	$m^3/s/mol$
65	$Na * 1E-15$	$m^3/s/mol$
66	$Na * 7.26E-16 * \exp(-11400[K]/T)$	$m^3/s/mol$
67	$Na * 9.49E-117 + Na * 1.8E-16 * \exp(-T/115[K])$	$m^3/s/mol$
68	$Na * 4E-16$	$m^3/s/mol$
69	$Na * 1E-19$	$m^3/s/mol$
70	$Na * 1E-19$	$m^3/s/mol$
71	$Na * 3.6E-17$	$m^3/s/mol$
72	$Na * 6.5E-16$	$m^3/s/mol$
73	$Na * 4.4E-19$	$m^3/s/mol$
74	$Na * 2.00E-13 * (T/300[K])^{-0.5}$	$m^3/s/mol$
75	$Na * 2E-16$	$m^3/s/mol$
76	$Na * 6E-16$	$m^3/s/mol$
77	$Na * 5E-19$	$m^3/s/mol$
78	$Na * 3E-13$	$m^3/s/mol$
79	$Na * 1.5E-19$	$m^3/s/mol$
80	$Na^2 * 7.0E-32 * (300[K]/(T_e * 11604[K/V]))^{4.5}$	$m^6/s/mol^2$
81	$Na^2 * 6.0E-39 * (300[K]/(T_e * 11604[K/V]))^{1.5}$	$m^6/s/mol^2$
82	$Na^2 * 6.0E-39 * (300[K]/(T_e * 11604[K/V]))^{1.6}$	$m^6/s/mol^2$
83	$Na^2 * 6.0E-39 * (300[K]/(T_e * 11604[K/V]))^{1.7}$	$m^6/s/mol^2$
84	$Na^2 * 6.0E-39 * (300[K]/(T_e * 11604[K/V]))^{1.8}$	$m^6/s/mol^2$
85	$Na * 1E-16$	$m^3/s/mol$
86	$Na^2 * 1E-41$	$m^6/s/mol^2$
87	$Na^2 * 1E-42$	$m^6/s/mol^2$
88	$Na^2 * 1E-43$	$m^6/s/mol^2$
89	$Na^2 * 1E-44$	$m^6/s/mol^2$

Table 3.7: *Rate constant of bulk reactions implemented in the 2D axisymmetric FEM model*

It has to be underlined that despite many of the previous cross sections and rate constant were already available in the commercial FEM software, they have been reviewed to verify their consistency with trusted sources. Many incorrectness have indeed been identified, and some of them were also able to provide a non negligible shift in the solution. Fig. 3.6 provides a plot of the cross section of the reaction #33 `e + O => 2e + O+`, showing the strong difference in slope between the two curves.

In addition to plasma bulk reactions, surface reactions which happens

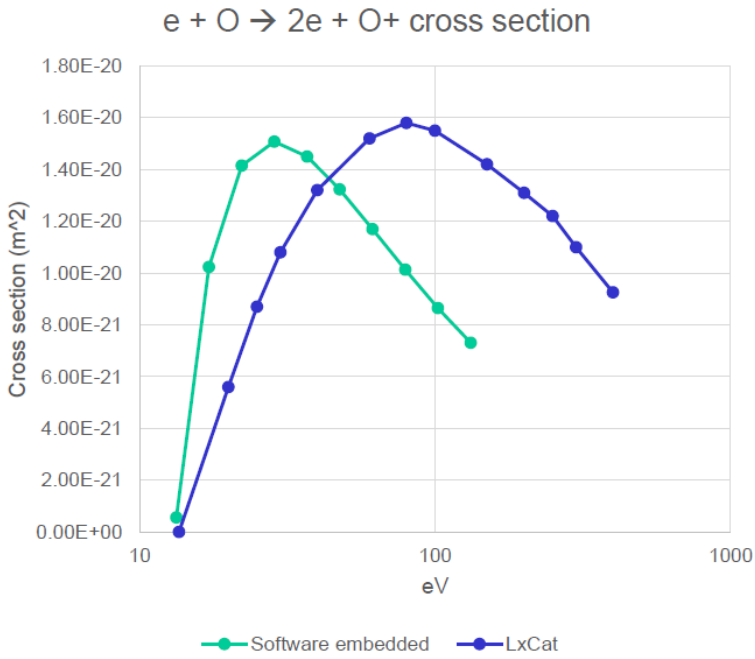

Figure 3.6: *Comparison of cross sections from different sources for the reaction #33* `e + O => 2e + O+`

on the walls of the geometry (boundaries 1-2-3-4 of Fig. 3.2) are modeled. Wall plasma processes are mainly recombination reactions which lead to disappearance and generation of species.
Wall recombination process can can be mainly of two kinds:

- charged particles processes
- neutral particles processes

Charged particle processes results in a ion-electron recombination at wall, with the electron provided by the wall itself, which results in the generation of one or more neutral species. Neutral particles interaction with walls results in the generation of different neutral species. A third phenomenon happening at wall is the electron disappearance, which is a dissipative energy process that draws away the power deposited in the plasma, and which is ruled by Eqs. 3.39 and 3.40. Each wall reaction is identified by a sticking coefficient, which describes the probability for the reaction to happen when a particle comes in contact to the wall. In Tab. 3.8 the

wall plasma processes implemented in the 2D axisymmetric FEM model are listed along with the related sticking coefficients.

#	Reaction	Sticking coefficient
1	O2a1d => O2	1
2	O2b1s => O2	1
3	O2(45) => O2	1
4	O2+ => O2	1
5	O1d => O	1
6	O1s => O	1
7	O+ => O	1
8	O + O => 0.5 O2	0.001
9	Si+ => Si	1
10	SiO+ => SiO	1
11	SiO2+ => SiO2	1

Table 3.8: *Sticking coefficients of wall plasma processes implemented in the 2D axisymmetric FEM model*

The reduced electron mobility is used and imposed to be $4E24\ sA/(m^3kg)$, which has been used in simulation involving Ar [58] and O2 gases [59]. This value may be a little bit too high considering values on the order of $1E23\ sA/(m^3kg)$ obtained from characteristic electron-neutral collision frequency for CO2 ($7.5E8\ s^{-1}$), CO ($2.25E9\ s^{-1}$) and Ar ($1.9E9\ s^{-1}$) [28] for the range of pressure of interest of this simulation (25-75 Pa) through Eq. 3.52

$$\mu_e = \frac{q_e}{m_e \nu_{e-n}} \tag{3.52}$$

nevertheless it has be maintained for sake of comparison with previous models. A future open point may be to implement a more detailed relation for electron mobility calculation.

3.2.2.2 Thermochemical data

The second set of input data to be retrieved is those of the species thermodynamic properties. These are expressed in the form of the NASA polynomials, where 14 coefficients define the following relations for the thermodynamic properties [60].

$$\frac{Cp_0}{R} = a_1 + a_2T + a_3T^2 + a_4T^3 + a_5T^4 \tag{3.53}$$

$$\frac{H_0}{RT} = a_1 + \frac{a_2}{2}T + \frac{a_3}{3}T^2 + \frac{a_4}{4}T^3 + \frac{a_5}{5}T^4 + \frac{a_6}{T} \tag{3.54}$$

$$\frac{S_0}{R} = a_1 ln(T) + a_2T + \frac{a_3}{2}T^2 + \frac{a_4}{3}T^3 + \frac{a_5}{4}T^4 + a_7 \tag{3.55}$$

where H_0 is defined as

$$H_0(T) = \Delta H_{0f}(298) + [H_0(T) - H_0(298)] \tag{3.56}$$

the value for the chemical species involved are obtained from NASA Thermodynamic database [61] based on JANAF Tables [62]. Enthalpy values for ions and excited state molecules are those for the neutral state with in addition the energy variation due to excitation/ionization.

```
O                 L 1/90O  1.   0.   0.   0.G   200.000  6000.000     15.99940 1
 2.54363697E+00-2.73162486E-05-4.19029520E-09 4.95481845E-12-4.79553694E-16    2
 2.92260120E+04 4.92229457E+00 3.16826710E+00-3.27931884E-03 6.64306396E-06    3
-6.12806624E-09 2.11265971E-12 2.91222592E+04 2.05193346E+00 2.99687009E+04    4

O2                TPIS89O  2.   0.   0.   0.G   200.000  6000.000     31.99880 1
 3.66096083E+00 6.56365523E-04-1.41149485E-07 2.05797658E-11-1.29913248E-15    2
-1.21597725E+03 3.41536184E+00 3.78245636E+00-2.99673415E-03 9.84730200E-06    3
-9.68129508E-09 3.24372836E-12-1.06394356E+03 3.65767573E+00 0.00000000E+00    4

O3                L 5/90O  3.   0.   0.   0.G   200.000  6000.000     47.99820 1
 1.23302914E+01-1.19324783E-02 7.98741278E-06-1.77194552E-09 1.26075824E-13    2
 1.26755831E+04-4.08823374E+01 3.40738221E+00 2.05379063E-03 1.38486052E-05    3
-2.23311542E-08 9.76073226E-12 1.58644979E+04 8.28247580E+00 1.70545228E+04    4

Si                J 3/83SI 1.   0.   0.   0.G   200.000  6000.000     28.08550 1
 2.58061157E+00-2.06044654E-04 1.93051677E-07-4.56485107E-11 3.36411716E-15    2
 5.33829933E+04 5.60657423E+00 3.76476150E+00-7.12070985E-03 1.57318301E-05    3
-1.53824969E-08 5.53194933E-12 5.32050782E+04 3.02168772E-01 5.41222513E+04    4

Si+               J 3/83SI 1.E -1.   0.   0.G   298.150  6000.000     28.08495 1
 2.64794579E+00-1.60109008E-04 6.54024155E-08-1.16224655E-11 7.55961272E-16    2
 1.48703413E+05 4.73171848E+00 4.24419073E+00-7.51160863E-03 1.33368333E-05    3
-1.09406149E-08 3.41357223E-12 1.48408792E+05-2.78917334E+00 1.49438151E+05    4

SiO               J 9/67SI 1.O  1.   0.   0.G   300.000  5000.000     44.08490 1
 3.74788350E+00 8.19919430E-04-3.25253960E-07 5.73249620E-11-3.51089440E-15    2
-1.33174300E+04 3.66100339E+00 3.25282760E+00 4.18231260E-04 3.78062020E-06    3
-5.10244830E-09 1.94713170E-12-1.30903400E+04 6.66174329E+00-1.20776829E+04    4
```

```
SiO2              J 9/67SI 1.O  2.   0.   0.G   300.000  5000.000     60.08430 1
 5.86203950E+00 1.77197840E-03-7.51941940E-07 1.41805840E-10-9.88564170E-15    2
-3.87678160E+04-6.84718711E+00 3.26280580E+00 8.50165840E-03-5.73881440E-06    3
 1.28965730E-11 9.75449760E-13-3.80359710E+04 6.66807529E+00-3.67355093E+04    4
```

3.2.3 Results

The simulation have been performed simulating all the possible combination between the parameters in Tab. 3.9, for a total of 27 simulations.

Parameter	Values	Unit
Power input	12.5 - 125 - 1250	W
Mass flow rate	1E-7 - 1E-6 - 1E-5	kg/s
Pressure	25 - 50 - 75	Pa

Table 3.9: *Simulations parameters and values*

Simulations results are summarized in the following paragraphs. Graphs report the points corresponding to the simulation results. The lines which connect these points are the results of power law fittings.

3.2.3.1 Electron temperature

As from Fig. 3.7 the maximum electron temperature never exceeds 5 eV. This result confirmed the validity of the choice of maintaining reaction involving negative ions, i.e. modeling an electronegative plasma, as the cross section of the involved electronegative reactions shows higher values in the low electron temperature region [40, 63].

3.2.3.2 Electron density

Figs. 3.8 and 3.9 provides the results for the average electron density in the torch volume (i.e. non including the vacuum chamber of the separation stage volume) with respect to the input power and the background pressure. The main observation is the strong dependence of the electron density on the input power, rather than on the background pressure. This is pretty straightforward considering that the variation of the electron energy depends linearly from the input power P_{in} in Eq. 3.7 which in turns increases the electron density due to increased collision number. In Fig. 3.8 it may appear that, while at low pressures the mass flow rate increment results in an increasing of the electron density, at high background pressure the electron density is basically independent on the input mass flow rate. This is actually only due to the logarithmic scale chosen for the representation, in

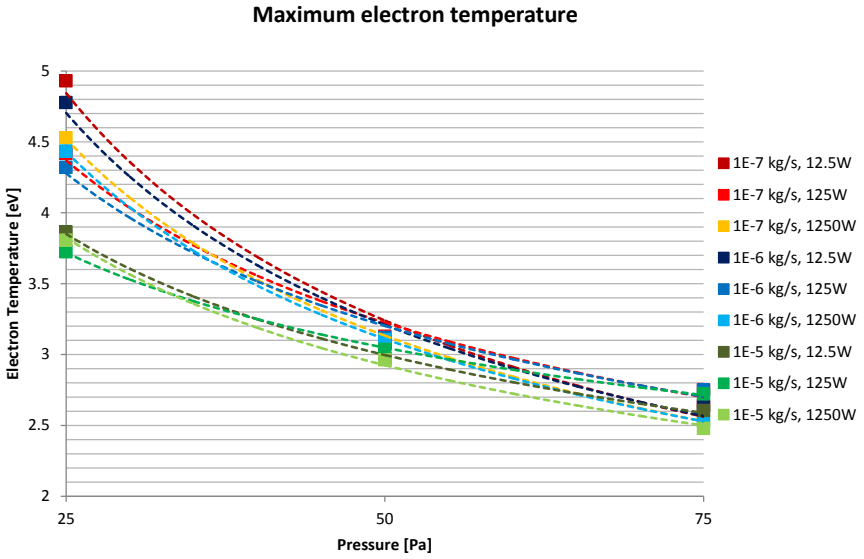

Figure 3.7: *Electron temperature Vs Background pressure*

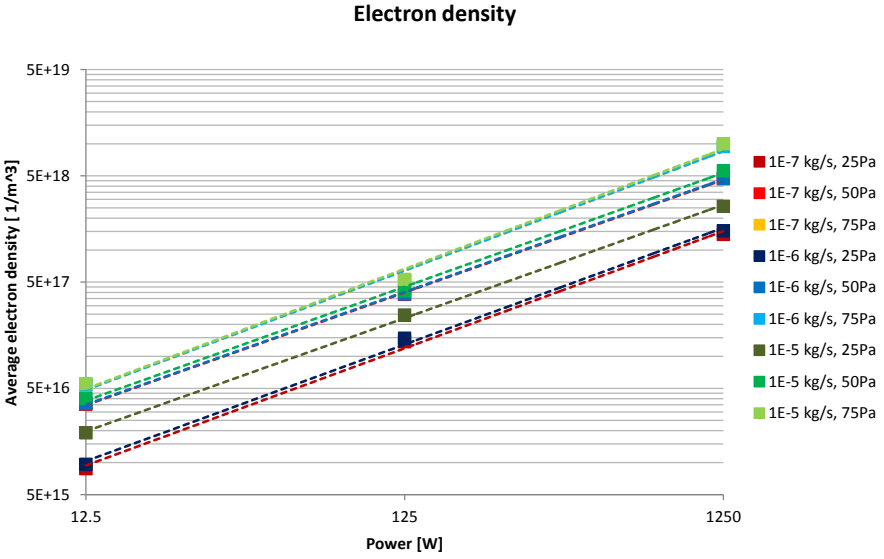

Figure 3.8: *Electron density Vs Input power*

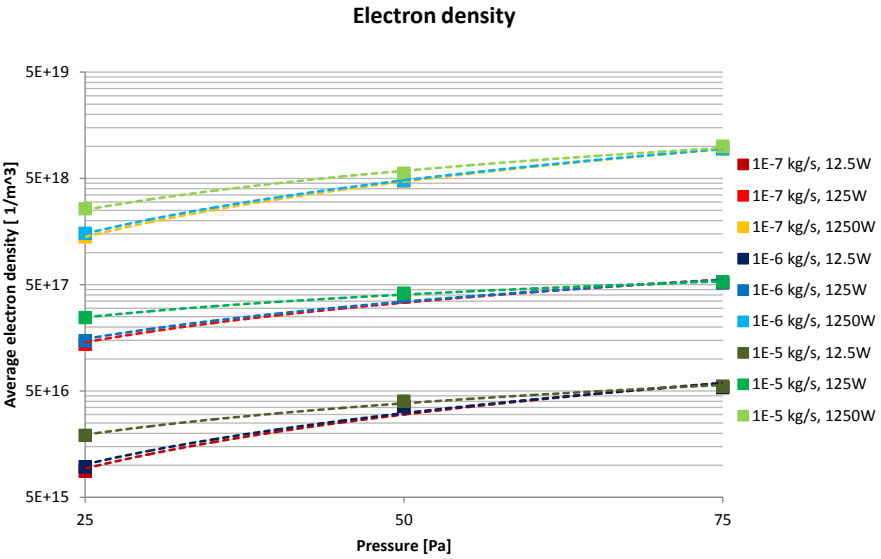

Figure 3.9: *Electron density Vs Background pressure*

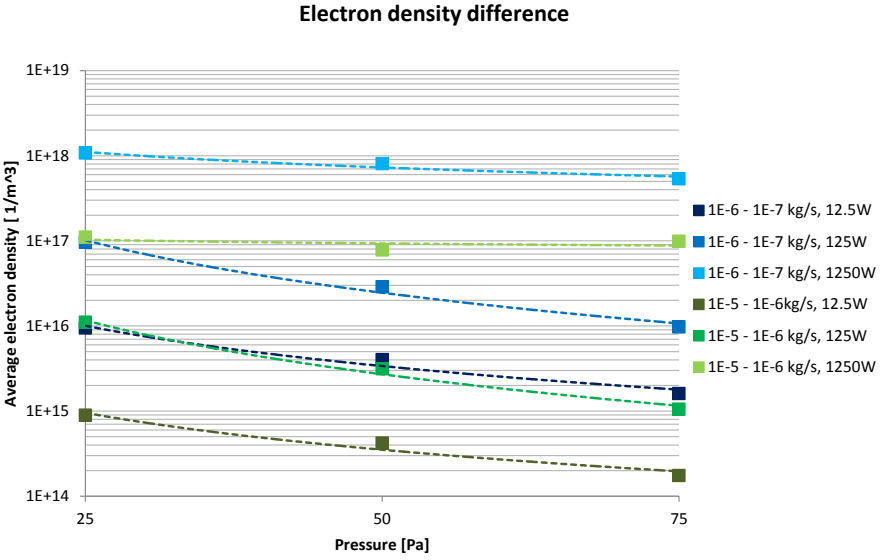

Figure 3.10: *Difference of Electron density between simulation at different input mass flow rate plotted vs Background pressure*

fact in Fig. 3.10 the difference between the electron density obtained at 1E-5 kg/s of input mass flow rate and those obtained at 1E-6 kg/s of input mass flow rate are plotted. Analogously a second set of curves plot the difference between the electron density obtained at 1E-6 kg/s of input mass flow rate and those obtained at 1E-7 kg/s of input mass flow rate. As can be seen there actually is a dependency on mass flow rate at high pressures, while the greatest absolute increments happen at low pressure due to the stronger relative increase in neutral densities and therefore collisions number.

3.2.3.3 Neutrals and ions number densities

By analyzing the plot of the number density of the different species plotted with respect to the background pressure or the power input, the main observation is that it is indeed possible to achieve an interesting production of silicon ions. By observing Figs. 3.11, 3.12 and 3.13 one can infer that the production is shifted toward $Si+$ at higher background pressure, due to increased number of collisions which occur.

In addition, in a view of extracting only silicon ions and avoiding ions of other species, from the same plot it is possible to observe that only for high powers the number density of silicon ions is higher of those of SiO and of SiO_2. The last observation is that, as one can better see from the related

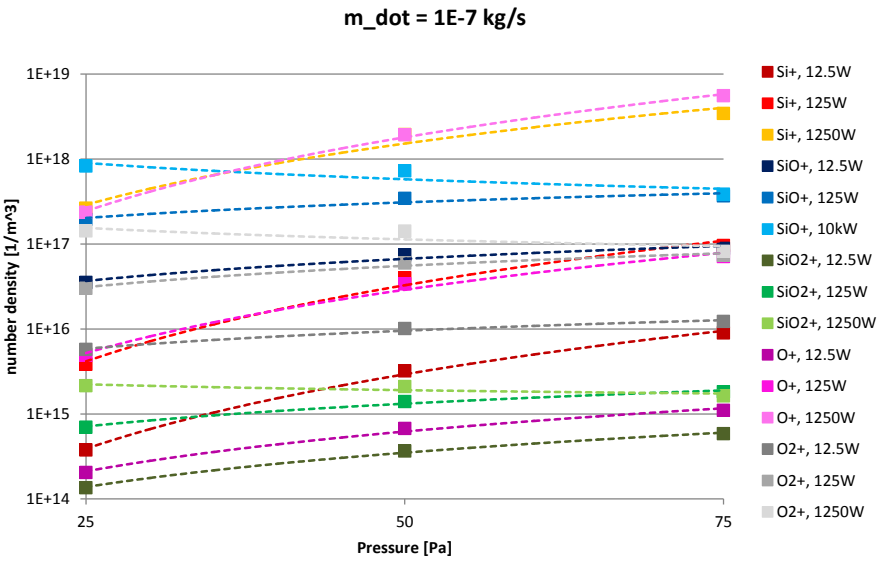

Figure 3.11: *Species number density Vs Background pressure @ 1E-7 kg/s input mass flow rate*

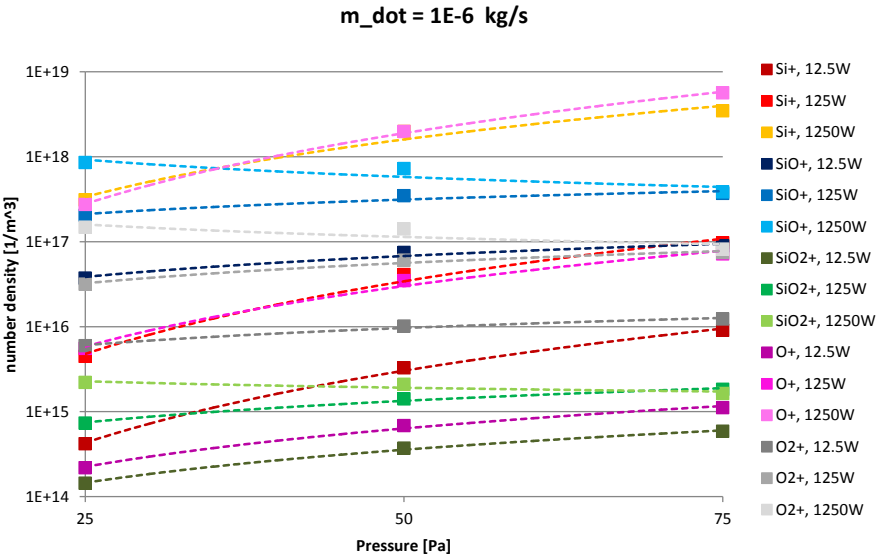

Figure 3.12: *Species number density Vs Background pressure @ 1E-6 kg/s input mass flow rate*

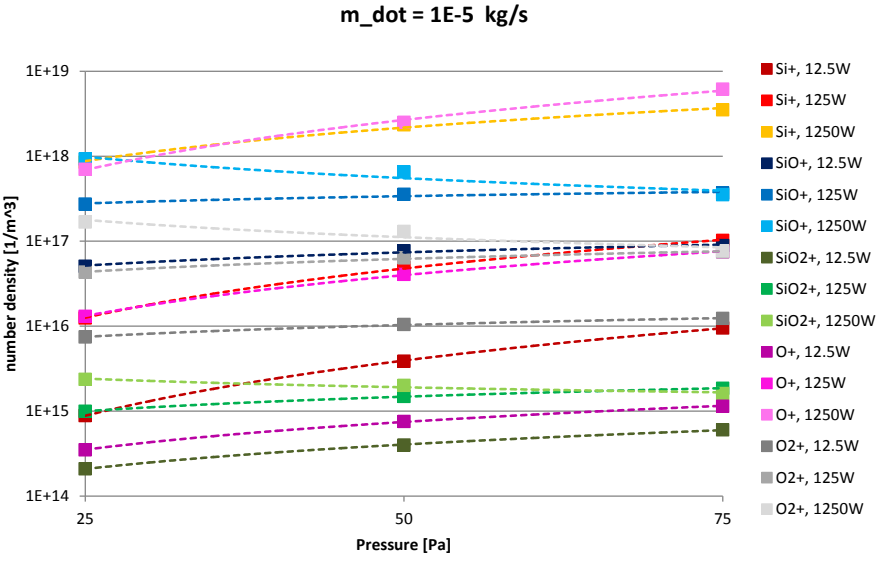

Figure 3.13: *Species number density Vs Background pressure @ 1E-5 kg/s input mass flow rate*

tables in Appendix A, final number densities are similar independently from the input mass flow rate. This is primarily due to fact that, at a certain background pressure, which is set at the output of the domain, mixture properties such as density are fixed, and therefore collision number. What changes by maintaining almost fixed density and geometry is the velocity field, whose magnitude increases at the increasing of the mass flow rate.

In Figs. 3.14, 3.15 and 3.16 the same number density is plotted versus input power, confirming the above considerations. In both series of graphs it is clear that, even at the most favorable condition for silicon production, the ion with the highest number density is $O+$. This is due mainly to the combination of the input conditions and reactions chain. The input mass flow includes about one third of O_2 and two thirds of SiO: generally speaking the number of O atoms is double than those of Si. In addition the chain of reactions that brings to $O+$ is more favorable in terms of requested total energy. According to Tab. 3.6, despite the threshold energy for monoatomic oxygen ionization of reaction #33 is pretty high, 13.2 eV, the threshold energy for the reaction #16 $e + O_2 => e + O + O$ is only 6 eV, for a total of 19.3 eV. If one considers the threshold energy for SiO ionization in reaction #60, 12.1 eV, and the ionization of Si in reaction #58, 8.2 eV, the required energy is 20.2 eV. This, in addition, does not even consider reaction #74 $SiO + +e => Si + O$, which introduces a further energy expenditure, and

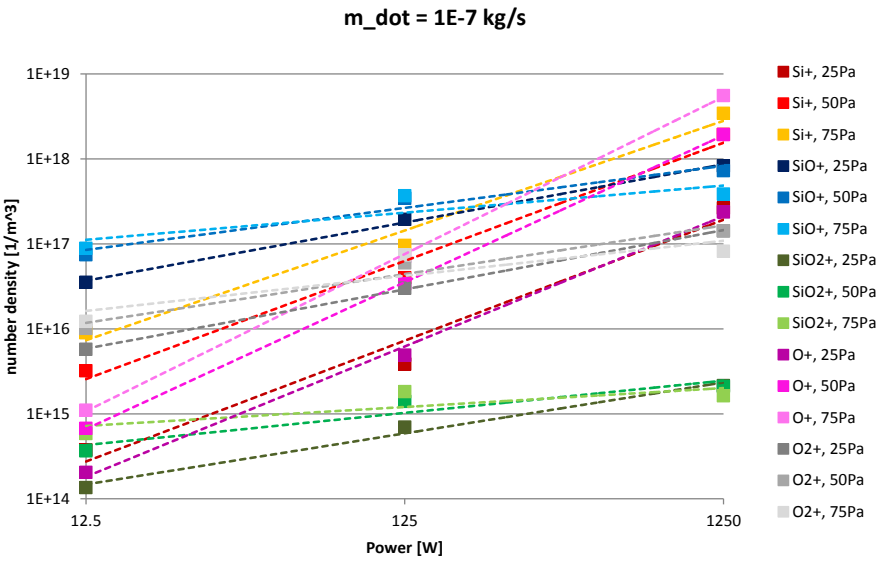

Figure 3.14: *Species number density Vs Input power @ 1E-7 kg/s input mass flow rate*

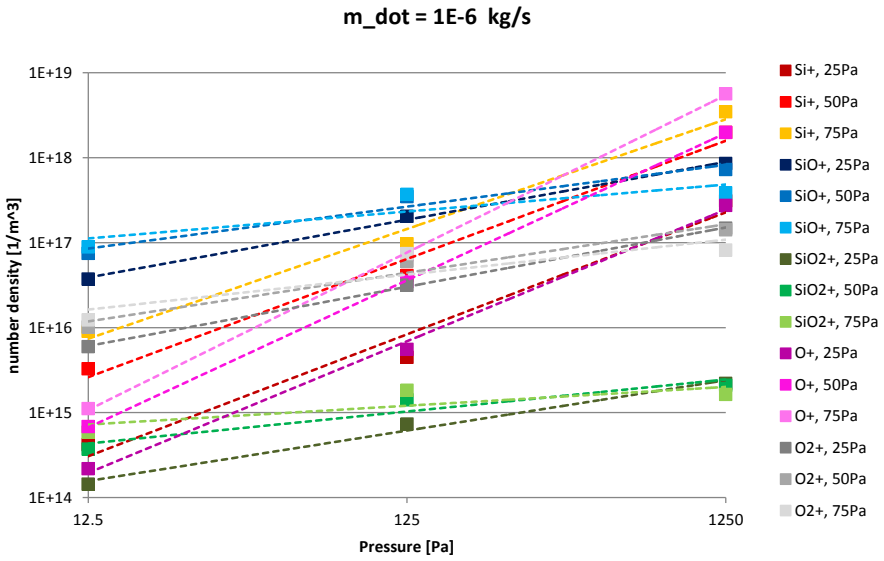

Figure 3.15: *Species number density Vs Input power @ 1E-6 kg/s input mass flow rate*

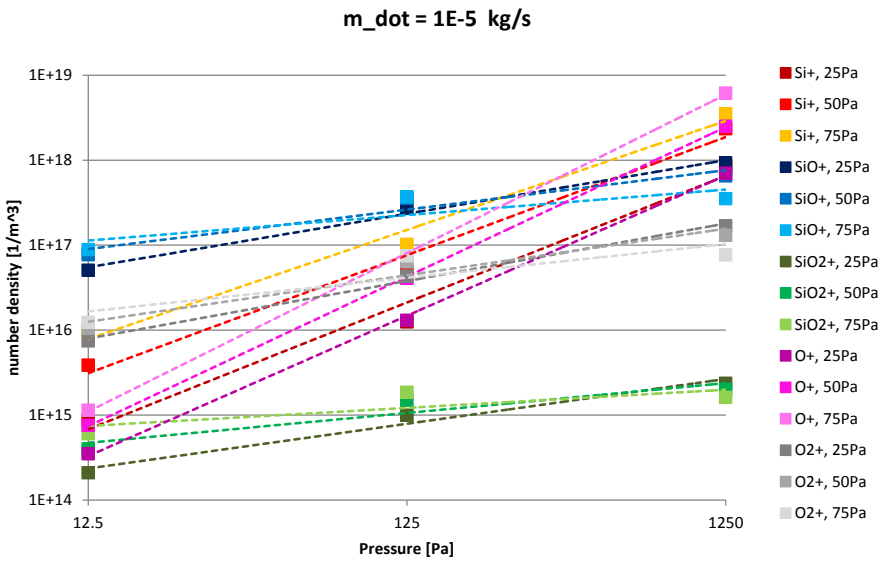

Figure 3.16: *Species number density Vs Input power @ 1E-5 kg/s input mass flow rate*

the fact that the amount of monoatomic oxygen is, as said, potentially the double of those of silicon. Obviously there are other chain reactions paths that brings to silicon and monoatomic oxygen ions, but the two mentioned above already provide and explanation of the simulation results.

The practical output of this explanation is that in the outflow of the torch a non negligible quantity of $O+$ ions shall be taken into consideration, especially at low power and low pressure regimes where $SiO+$ is also present in large quantities.

3.2.3.4 Neutrals and ions temperature

The heat equation 3.18 allows the heat of reactions to influence the temperature of ions and neutrals, as part of the energy P_{in} provided does not go into ionization or ion acceleration but goes into plasma heating. This heating results into a thermal flux of ions and electrons to the walls, which at the end evaporates the molten silica providing additional material for the plasma creation. Fig. 3.17 provides the temperatures reached by the plasma at the different input conditions.

The main comment is that the reached temperatures are highly above those related to vapor pressure of silica vaporization at the imposed background pressure, as calculated with Eq. 3.32, therefore the process is verified to be sustainable in the long term.

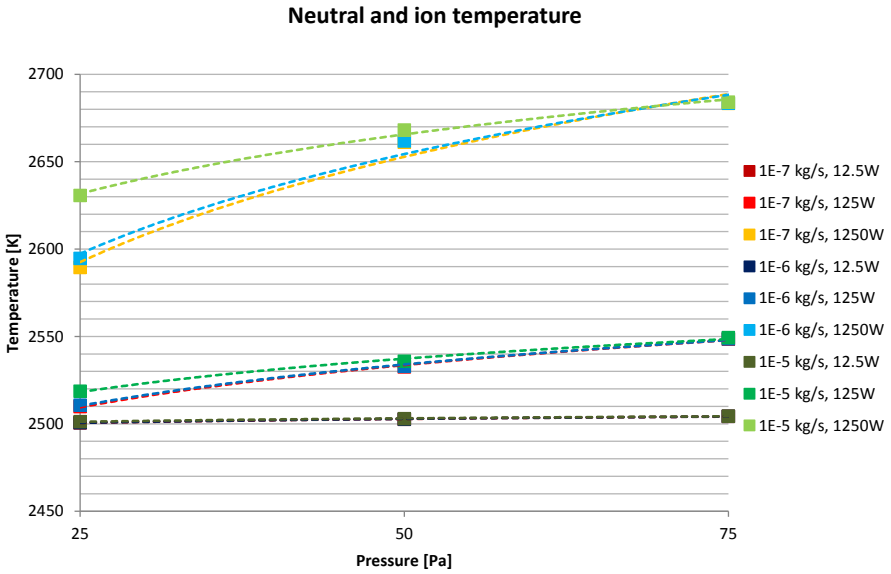

Figure 3.17: *Neutral and ion temperature Vs Background pressure*

3.2.3.5 Ionization ratios

Figs. 3.18, 3.19 and 3.20 show the species ionization ratio, which is the ratio between an ion number density and the number density of the related neutral species.

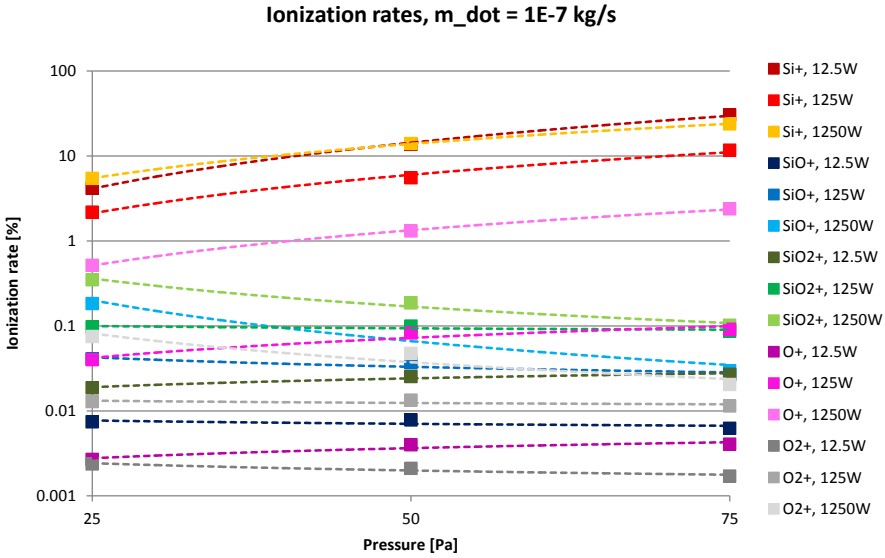

Figure 3.18: *Ionization ratios @ 1E-7 kg/s input mass flow rate*

The main outcome of the plots is that at any combination of pressure and temperature the ionization ratio of silica is higher that the ionization ratio of any other species, including oxygen. The important conclusion of this analysis is that the concept of selective ionization is verified: silicon is the most ionized species and therefore it makes sense to try to enhance this ionization with an optimized combination of mass flow rate, background pressure and input power.

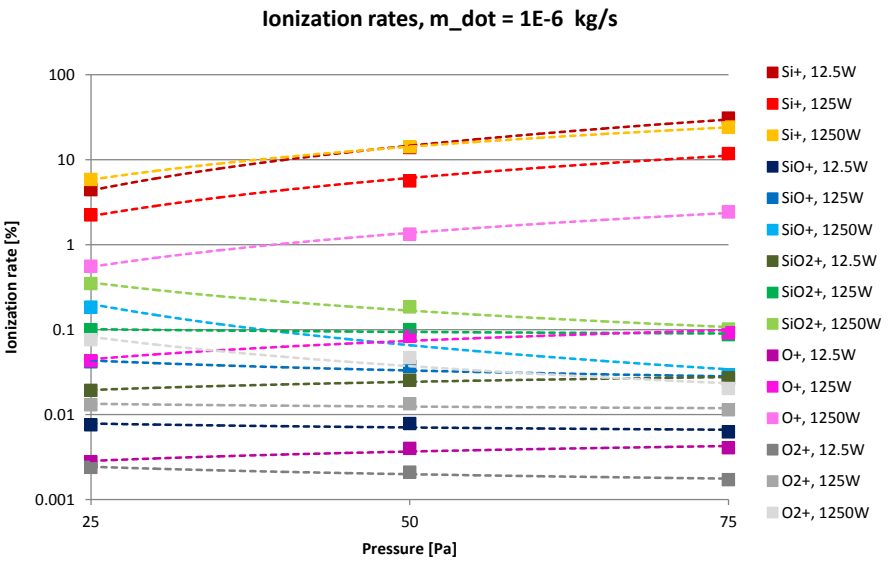

Figure 3.19: *Ionization ratios @ 1E-6 kg/s input mass flow rate*

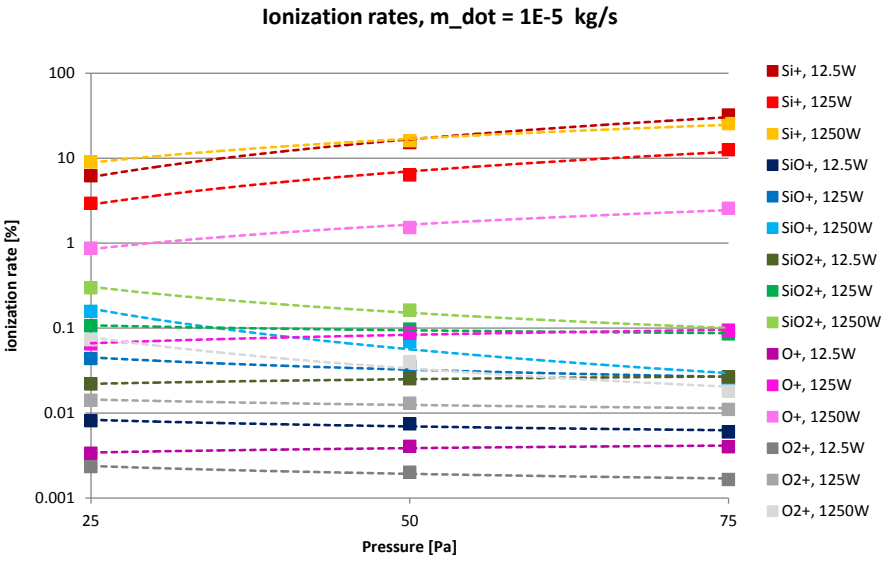

Figure 3.20: *Ionization ratios @ 1E-5 kg/s input mass flow rate*

3.2.3.6 Output fluxes

The main goal of the simulation is to verify if the output of the plasma torch can be considered adequate to avoid the implementation of a further ionization/acceleration stage and of a separation stage. Figs. 3.21, 3.22 and 3.23 represent the mass flow rate of each ion species coming out from the torch volume.

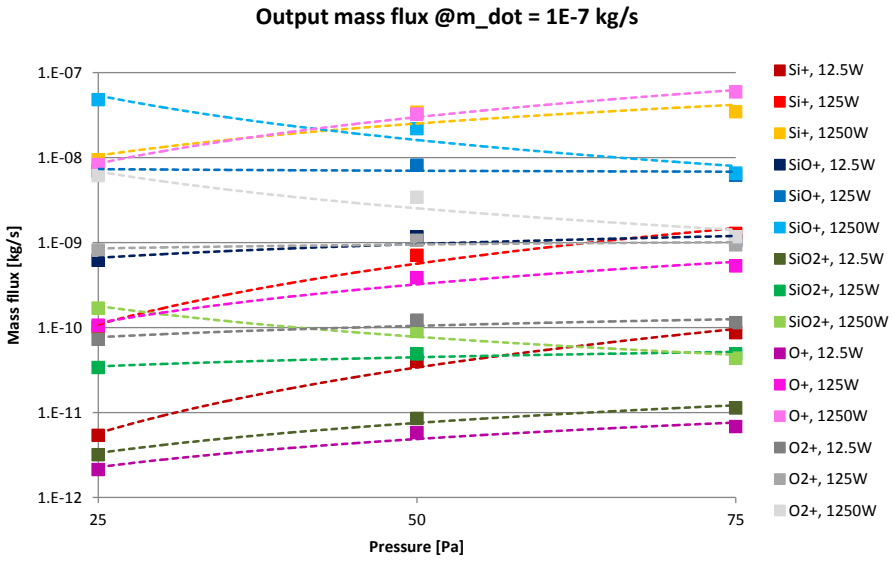

Figure 3.21: *Output ions mass flow rate Vs Background pressure @ 1E-7 kg/s input mass flow rate*

According to the previous observation, results does not depend on input mass flow rate. Not surprisingly the outcome is very similar to the number density plot depicted in Figs. 3.11, 3.12 and 3.13, with a predominance of the $Si+$ and $O+$ flux. At high pressure and high power ranges it appears that the demonstrator concept is actually working: of the silicon compounds only $Si+$ is considerably ejected from the torch. Unfortunately two additional consideration shall be done:

- the $O+$ flux is higher than the $Si+$ flux, even if with the same order of magnitude. This flux will not be affected by the pumping extracting neutral species, therefore in a straight path it will collide in the same spot where the silicon ions are collected. This will likely nullify any effort devoted to preserve the purity of the output silicon, because

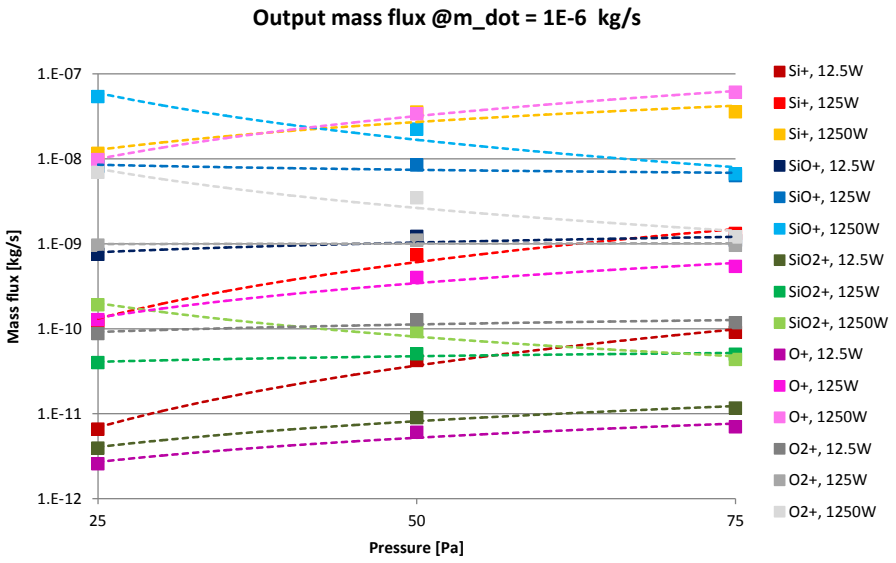

Figure 3.22: *Output ions mass flow rate Vs Background pressure @ 1E-6 kg/s input mass flow rate*

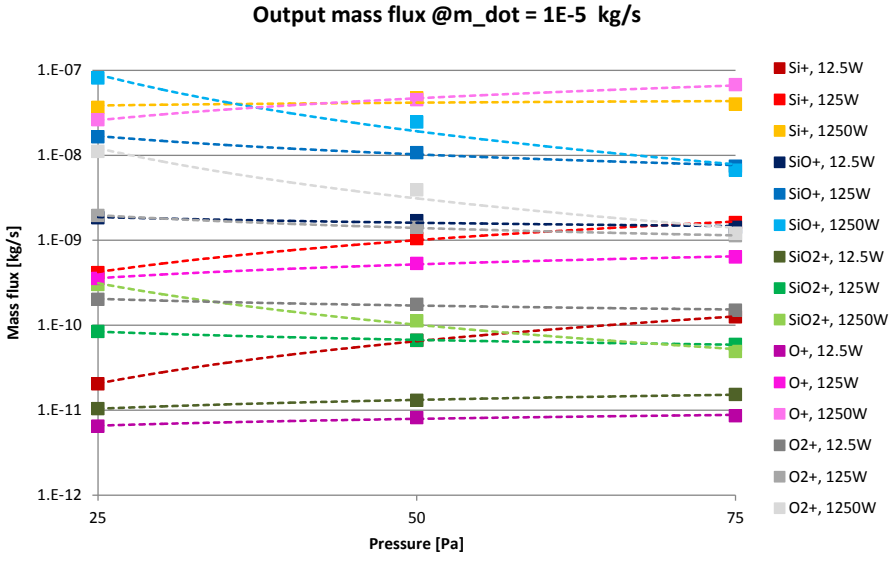

Figure 3.23: *Output ions mass flow rate Vs Background pressure @ 1E-5 kg/s input mass flow rate*

during the path to the collector and during the impact the chances of recombination will be very high, resulting in a mixture of silicon compounds. For this reason a **separator stage appear to be necessary**, and therefore an accelerator stage capable of providing to the ions the required velocity, considering that at 75 Pa and 1250 W the output ion velocity is on the order of few hundreds meters per second (see Appendix A, Figs. A.4, A.5 and A.6 and related tables). This solution, at the expenses of a higher required power, will likely increase the purity of the final product, because also the limited amount of $SiO+$ will be eliminated.

- the presence of the neutral species shall not be forgotten. Fig. 3.24 and Tab. 3.10 shows the ratios of the silicon ion flux out of the torch with respect to the input mass flow rate. As one can see, with a mass flow rate of 1E-7 kg/s the yield of the silicon ions is above 30%, which is somewhat obvious considering that irrespectively from the input mass flow rate, the number density results basically the same. The outcome of this consideration is that it is not needed a very high mass flow rate that cannot be treated, and this will result also in a lower energy expenditure for the melting of the silica. As a sake of completeness the output flux of the other neutral species is reported in Appendix A, Figs. A.1, A.2 and A.3.

		$\dot{m}$ (kg/s)	$\dot{m}$ (kg/s)	$\dot{m}$ (kg/s)
		1.00E-07	1.00E-06	1.00E-05
Pressure (Pa)	**Power (W)**	**Si+/$\dot{m}$**	**Si+/$\dot{m}$**	**Si+/$\dot{m}$**
25	12.5	0.0054%	0.0007%	0.0002%
50	12.5	0.0398%	0.0042%	0.0007%
75	12.5	0.0871%	0.0090%	0.0013%
25	125	0.1001%	0.0122%	0.0042%
50	125	0.7098%	0.0740%	0.0105%
75	125	1.2848%	0.1317%	0.0162%
25	1250	9.4483%	1.1560%	0.3673%
50	1250	34.1773%	3.5475%	0.4764%
75	1250	34.5755%	3.5584%	0.4002%

Table 3.10: *Ratio between $Si+$ flux and input mass flow rate Vs Background pressure*

3.2.4 Impact on demonstrator design

Summarizing the outcomes of the this chapter, the main considerations are:

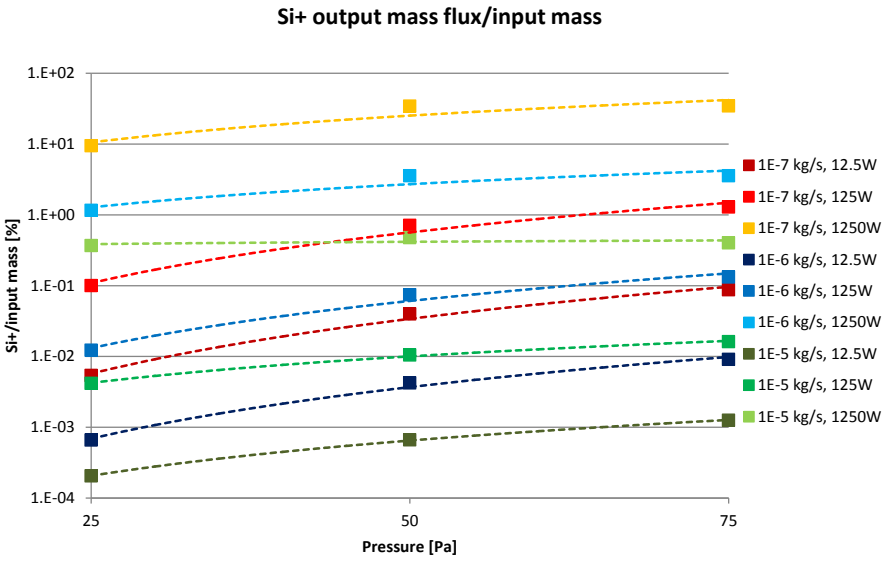

Figure 3.24: *Ratio between $Si+$ flux and input mass flow rate Vs Background pressure*

- plasma characteristics vary strongly with background pressure and power input, but less with input mass flow rate, and in particular ion densities and output ion fluxes remain almost constant. It is therefore desirable to inject a low mass flow rate in order to have a high silicon yield, which can reach values above 30% with 1E-7 kg/s input mass flow rate
- silicon ionization ratio is the highest of all the other species, at any considered pressure and power level. This confirms the assumption of the selective ionization concept depicted in §2.3.1.
- $Si+$ outflow at high pressures and power levels greatly exceeds $SiO+$ ions, but it is slightly lower than $O+$ ions. This does not allow to avoid the presence of a separator stage, preceded by an accelerator stage to uniform ion velocities.

Therefore it appears that:

- an accelerator stage is necessary
- a separation stage is necessary

- if operating at low pressure a further ionization stage is recommended to improve $Si+$ yield

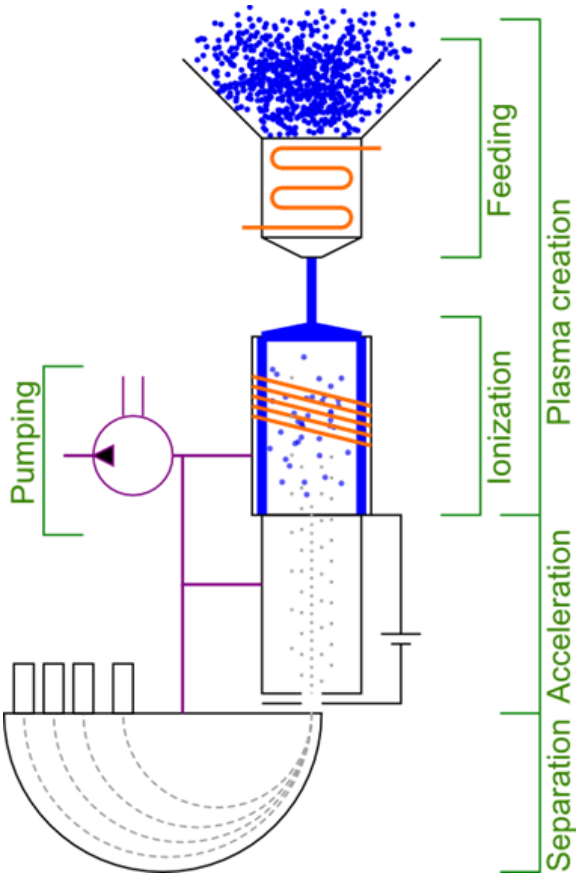

Figure 3.25: *Demonstrator concept simplified schematic*

Fig. 3.25 shows the concept of the demonstrator with in addition the two stages previously identified. The demonstrator is therefore divided into the following stages:

Feeding stage Energy required to melt and heat the silica till boiling (which depends on the pressure inside the chamber)

Ionization stage The plasma source to ionize the SiO_2 and obtain $Si+$

Acceleration stage To accelerate the ions till the required speed, in order to have for all the ions of the same species approximately the same radius in the separator stage

Separation stage Thanks to the cyclotron radius divides and collects the different ion species

Pumping stage Service stage for the whole system, creating the vacuum condition necessary for the plasma source operation

CHAPTER 4

Demonstrator design

In this chapter the outputs form the 2D multiphysical FEM model, and especially form §3.2.3.6, are used to size the lab demonstrator of the device capable of extracting pure silicon starting from raw silica.

4.1 Experimental data for demonstrator design

In additional to experimental data retrieved and listed in §3.2.2 additional thermophysical proprieties of compounds had to be gathered in order to perform the calculations for the demonstrator design. As with other experimental data involving SiO_2, discrepancies were found between different sources, demonstrating the complexity of the involved physics. Below a discussion of the fundamental properties collected. For sake of completeness also some properties not used in the following chapters are reported.

4.1.1 Melting point (glass transition temperature)

Being SiO_2 a silicate, it shows the tetrahedral coordination typical of silicon compounds, with four oxygen atoms surrounding a central Si atom. The

relative position between those tetrahedra leads to the formation a number of distinct crystalline forms (polymorphs) in addition to amorphous forms. Another consequence is that there is not a specific melting point, but rather a glass transition temperature which varies between the different silica forms. Perry [64] reports value of 1743 K for quartz and 1973 K for cristobalite. A reliable source of data is the work from Richet at al. [65], which resulted in the findings reported in Tab. 4.1. Results from Richet are taken as reference.

SiO_2 form	Glass transition temperature (K)	Source
Amorphous	1490	[65]
Quartz	1700	[65]
Cristobalite	1999	[65]
Quartz	1743	[64]
Cristobalite	1973	[64]

Table 4.1: *Glass transition temperatures for different SiO_2 forms and sources*

4.1.2 Boiling point

The boiling point at ambient pressure varies strongly between the different sources. Perry [64] reports a very low value of 2503 K. Schick [32] performed an extensive review and discussion of available experimental data. The most reliable value is 3085 K, which is also somewhat closer to 3160 K reported by Fegley [66] and to 3070 ± 75 reported by Grayson [67]. The value by Schick are taken as baseline due to its correspondence with the most reliable vapor pressure relation explained in §4.1.4.

Boiling point (K)	Source
2503	[64]
3070 ± 75	[67]
3085	[32]
3160	[66]

Table 4.2: *Boiling point for SiO_2 and sources*

4.1.3 Enthalpy of fusion

Also in this case data from Richet et al. [65] are of valuable interest, providing a value of 8.9 ± 1.0 kJ/mole for cristobalite and 9.4 ± 1.0 kJ/mole for quartz. Schick [32] reports a value of 2500 ± 500 cal/mol equal to 10.46 ± 2.1 kJ/mol, in line with the abovementioned more precise results. Perry reports a value of 8.8 kJ/mole for cristobalite and a very high 14.2 kJ/mole

for quartz. In this perspective the quartz value from Richet are chosen as baseline. Alternative values from non peer reviewed sources or without clear source indication were discarded.

SiO_2 form	Enthalpy of fusion (kJ/mole)	Source
-	10.46 ± 2.1	[32]
Quartz	9.4 ± 1.0	[65]
Cristobalite	8.9 ± 1.0	[65]
Quartz	14.2	[64]
Cristobalite	8.8	[64]

Table 4.3: *Enthalpy of fusion for different SiO_2 forms and sources*

4.1.4 Enthalpy of vaporization

Few values are available for the enthalpy of vaporization. One is 341 ± 31 kJ/mol taken at 3130 K from Fegley [66]. He calculates this value using the *Trouton's rule*, which correlates enthalpy of vaporization, boiling point and entropy of vaporization according to the relation:

$$\Delta S_{vap} = \frac{\Delta H_{vap}}{T_b} \tag{4.1}$$

Schick [32], instead, calculated a value by taking into considerations all the contribution to the heat of reaction of the most occurring reaction in silica vaporization, meaning Eq. 3.29:

$$SiO_{2(l)} \rightarrow SiO_{(g)} + 0.5O_{2(g)} \qquad \text{(3.29 revisited)}$$

Schick work resulted in a value of 721.8 ± 14.3 kJ/mol, which appear not to change strongly from 2000 K to 3000 K. For the same reaction Elhadj et al. [68] provide an experimental value of 260.7 kJ/mol which is indeed closer to Fegley than to Schick. The main difference that can be observed is the environmental condition of the reaction. Elhadj et al. performed a laser

Enthalpy of vaporization (kJ/mol)	Source
260.7	[68]
341 ± 31	[66]
721.8 ± 14.3	[32]

Table 4.4: *Enthalpy of vaporization for SiO_2 and sources*

vaporization experiment in different atmospheres, like air, nitrogen and hydrogen, while Schick calculations were referred to neutral conditions. The latter are the condition which are mostly similar to this work conditions, because the ”atmosphere" present in the simulation is derived only by silica decomposition. In a view of worst case scenario, and compatibility with previously selected data, Schick value is again selected.

4.1.5 Vapor pressure

The vapor pressure relations identified are quite in disagreement. Pitkanen et al. [69] develop Eq. 4.2 to fit Samsonov's experimental data [70, 71].

$$p_{vap}[Pa] = 10^{(-24.7924\ \log(T[^\circ C])^2+189.2613\ \log(T[^\circ C])-353.6596)} \tag{4.2}$$

Inexplicably, they choose a series of experimental data to fit which does not agree to the other parameter they choose for the simulation, in particular with Grayson [67] boiling point at ambient pressure. Schick relation [32], Eq. 3.32 already anticipated in §3.2.1.2, is able instead to correctly catch the boiling point.

$$p_{vap}[atm] = 1.5 \exp\left(18.41\left(1 - \frac{3160}{T[K]}\right)\right) \qquad \text{(3.32 revisited)}$$

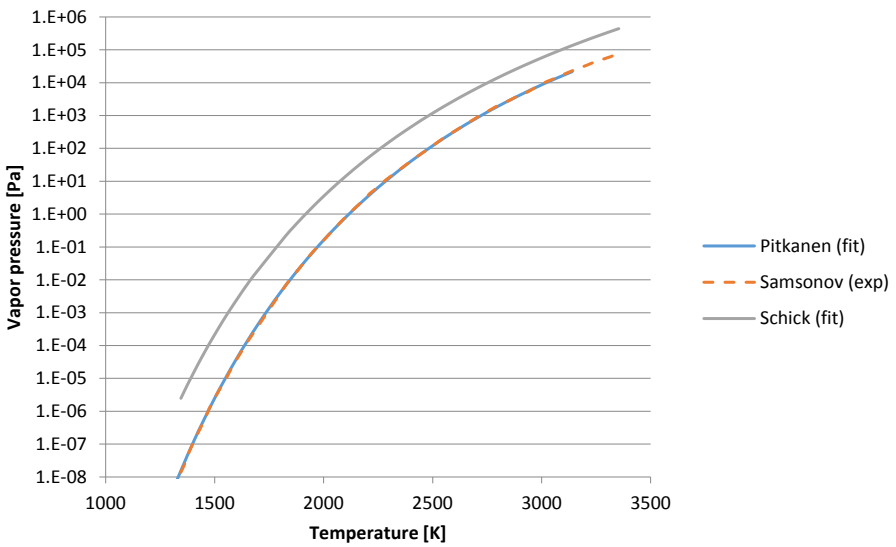

Figure 4.1: *Vapor pressure data and relations from different sources*

In order to be also consistent with previous choices, Schick expression is selected. Fig. 4.1 shows the different fits and experimental data.

4.1.6 SiO_2 condensed phase thermochemical data

In order to calculate some important energy contribution, such as the energy required to melt and bring silica to vaporization, equations for solid and liquid silica have to be identified. In §3.2.2.2 analogous data were provided in terms of NASA polynomials for gaseous SiO_2. From JANAF tables [62] it is possible to retrieve data for quartz, here assumed to be the solid phase of silica, and molten silica. Tables 4.5 and 4.6 provides the values of specific heat, enthalpy and entropy in the form of coefficients of the Shomate equations:

$$Cp_0 = A + B\,\hat{t} + C\,\hat{t}^2 + D\,\hat{t}^3 + \frac{E}{\hat{t}^2} \tag{4.3}$$

$$H_0 - H_{0\ 298.15} = A\,\hat{t} + B\,\frac{\hat{t}^2}{2} + C\,\frac{\hat{t}^3}{3} + D\,\frac{\hat{t}^4}{4} - \frac{E}{\hat{t}} + F - H \tag{4.4}$$

$$S_0 = A\,ln(\hat{t}) + B\,\hat{t} + C\,\frac{\hat{t}^2}{2} + D\,\frac{\hat{t}^3}{3} - \frac{E}{2\,\hat{t}^2} + G \tag{4.5}$$

where

$$\begin{aligned} Cp_0 &= \text{specific heat } (J\ mol^{-1}\ K^{-1}) \\ H_0 &= \text{standard enthalpy } (kJ\ mol^{-1}) \\ S_0 &= \text{standard entropy } (J\ mol^{-1} K^{-1}) \\ \hat{t} &= \text{temperature } (K) \,/\, 1000 \end{aligned}$$

SiO_2 solid (Quartz)		
Temperature (K)	**298. - 847.**	**847. - 1996.**
A	-6.076591	58.7534
B	251.6755	10.27925
C	-324.7964	-0.131384
D	168.5604	0.02521
E	0.002548	0.025601
F	-917.6893	-929.3292
G	-27.96962	105.8092
H	-910.8568	-910.8568

Table 4.5: *Coefficients for Shomate equations for SiO_2 solid (Quartz) phase*

SiO_2 liquid	
Temperature (K)	**1996. - 4500.**
A	85.772
B	-0.000016
C	0.000004
D	-3.81E-07
E	-0.000017
F	-952.87
G	113.344
H	-902.661

Table 4.6: *Coefficients for Shomate equations for SiO_2 liquid phase*

4.2 Demonstrator stages design

4.2.1 Feeding stage

The feeding stage task is to heat the input raw silica till melting and boiling. Actually in the energy cost also the enthalpy of vaporization is considered, as a worst case. We will see that this will impact the final results only slightly, as the other stages require much more power.

The initial input condition is represented by the imposed pressure in the chamber. By using Eq. 3.30, as explained in §4.1.5, it is possible to calculate the boiling point. After this step it is possible to calculate the enthalpy to boil silica and the power related to the processed mass flow rate.

$$P_{boil} = \left[(H_{0\ T_{boil}} - H_{0\ T_{298.15}}) + \Delta H_{vap} \right] \frac{\dot{m}}{M} \tag{4.6}$$

where M is silica molar mass. It is obvious that, if instead of $\dot{m}$, a mass of silica is used, the result of Eq. 4.6 will be the energy used to vaporize that mass.

4.2.2 Ionization stage: torch

This contribution to the overall budget is the output calculated in Chapter 3. This stage is represented by the torch depicted in Fig. 2.9 with the geometry described in §3.2.1. It is fed with the molten silica coming from the feeding stage, and the outputs are the ion fluxes shown in §3.2.3.6. Considering the model results, the sizing will be based on the combination of the following input conditions:

Power 1250 W

Pressure 75 Pa

Mass flow rate 1E-7 kg/s SiO_2

The above conditions result in an output flux of $Si+$ of 3.46E-8 kg/s, equal to a yield of 34.5%.

4.2.3 Acceleration stage stage

The acceleration stage is necessary to provide at the entrance of the separator know values of the ion speed: this is possible only if the ions are accelerated with a final velocity v_{out} much higher than the one they have at the torch exit, as per Eq. 4.7.

$$\frac{v_{in}}{v_{out}} = \frac{v_{in}}{v_{in} + \Delta v} << 1 \tag{4.7}$$

with Δv calculated by a simple energy balance between the potential energy provided by an accelerating electric field and the kinetic energy owned by the ions after the acceleration:

$$\frac{1}{2} m_{ion} \Delta v^2 = q \Delta V \Rightarrow \Delta v = \sqrt{\frac{2q\Delta V}{m_{ion}}} \tag{4.8}$$

By imposing an electric field of $\Delta V = 1000$ V it is possible to obtain the output velocities listed in Tab. 4.7.

Ion	Atomic mass [uma]	ΔV [V]	v_{out} [m/s]	Fluxes [kg/s]	Power [W]
O+	16	1000	109821	5.93E-08	357.7
O2+	32	1000	77655	1.17E-09	3.5
Si+	28	1000	83017	3.46E-08	119.1
SiO+	44	1000	66225	6.56E-09	14.4
SiO2+	60	1000	56711	4.36E-11	0.1

Table 4.7: *Acceleration stage output velocities and power required*

Comparing these output velocities with the input velocities (output of the torch stage) it is possible to verify that the ratio is always much smaller than one. Tab. 4.8 provides this data for the three major ion species in the torch output flow. v_{in} values are taken from tables listed in §A.3.

Ion	Atomic mass [uma]	ΔV [V]	v_{in} [m/s]	v_{out} [m/s]	Ratio
O+	16	1000	405	109821	0.004
Si+	28	1000	283	83017	0.003
SiO+	44	1000	253	66225	0.004

Table 4.8: *Ratio of acceleration stage input and output velocities*

In Tab. 4.7 the power required to accelerate those fluxes of ions is also provided. These values are calculated considering the kinetic energy gain at the expenses of the electric field. For the i-th ion species the associated power is:

$$P_{acc_i} = \frac{\dot{m}_i v_{out}}{2} = \frac{\dot{m}_i \left(v_{in} + \Delta v\right)}{2} \tag{4.9}$$

by summing all the contributions the total power is 495 W. It has to be cosidered that the power spent for the acceleration results in a double problem for the overall design, meaning that the energy that has to be provided for the acceleration is later recovered in form of heat, at the moment of the impact of the ions on the collector surface. This energy has to be dissipated, and a suitable heat exchange device shall be put in place, with additional energy costs, to remove an amount of power $P_{diss} = P_{acc} = 495$ W.

4.2.4 Separation stage

As ions exit the acceleration stage, they are subjected in the separator stage to a constant and uniform B field, perpendicular to the inlet velocity. In

this condition they will experience a particular composition of the Lorentz force, which in its general form is described by the equation:

$$\mathbf{F} = q\,(\mathbf{E} + \mathbf{v} \times \mathbf{B}) \qquad \text{(1.1 revisited)}$$

Being generated by a cross product, the Lorentz force always acts perpendicular to the direction of motion, thus causing the particle to rotate. In absence of electric fields the rotation result to be circular, and the radius of this circle can be determined equating the magnitude of the Lorentz force and the centripetal force as

$$\frac{m v_{out}^2}{r_c} = q v_{out} B \tag{4.10}$$

Therefore the cyclotron radius is expressed as

$$r_c = \frac{m v_{out}}{qB} \tag{4.11}$$

Starting from the v_{out}, from the acceleration stage calculated above, it is possible to apply a suitable magnetic field which imposes a cyclotron radius r_c adequate to be generated in the frame of a laboratory demonstration plant. Tab. 4.9 provide such calculations

Ion	**Atomic mass [uma]**	ΔV **[V]**	v_{out} **[m/s]**	**B field [T]**	r_c **[m]**
O+	16	1000	109821	0.12	0.15
O2+	32	1000	77655	0.12	0.21
Si+	28	1000	83017	0.12	0.20
SiO+	44	1000	66225	0.12	0.25
SiO2+	60	1000	56711	0.12	0.29

Table 4.9: *Cyclotron radius for the involved species and input conditions*

With an applied B field of 0.12 T it is possible to obtain a maximum radius of about 0.3 m, for an overall dimension of 0.6 m, equal to the diameter. The motivation is that the ions must be allowed to perform a 180° turn. In this way the ions with the same inlet speed and same mass/charge ratio, but slightly different inlet angle, at 180° from the starting point collide in the same position, even if they describes slightly different trajectories [2, 72].

The magnetic field is created by two solenoids made of copper wires, which are separated by a gap as wide as the torch diameter (4 cm). These

solenoids can be thought as discs which are wrapped by thousands of turns of a copper wire. A first attempt tried to calculate the power required to generate the required B field by using the well known Biot Savart law

$$|B| = \mu \frac{N_c}{h} I \text{ hence } I = \frac{Bh}{\mu N_c} \tag{4.12}$$

where h is the solenoid length, I the current, N_c the number of turns. This formula allows the calculation of the magnetic field at the center of the coil, but unfortunately it is too simple for this particular case, and also provides an underestimation of the power required. A more consistent approach makes use of the analytical expression for the magnetic induction of a simple planar circular current loop in spherical coordinates [73]. In order to fall into this case the solenoid shall be seen as a single turn coil having an equivalent current equal to

$$I_{eq} = \frac{N_c}{N_{c,eq}} I \tag{4.13}$$

where $N_{c,eq}$ is the number of equivalent coil turns, 1 in this case.

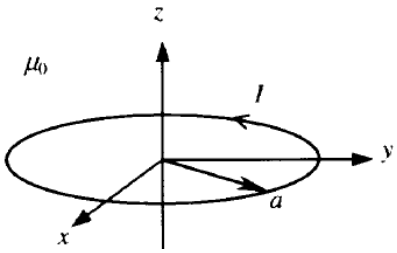

Figure 4.2: *Spherical coordinates on a single turn coil*

The current loop has radius r_a, is located in the $x - y$ plane, centered at the origin, and carries a current I_{eq} coherent to the right hand rule, as shown in Fig. 4.2. It is assumed that the cross section of the conductor is negligible. The vector potential $\mathbf{A}$ of the loop is given by [74]:

$$\begin{aligned} A_\phi(r,\theta) &= \frac{\mu_0 I r_a}{4\pi} \int_0^{2\pi} \frac{\cos\phi' d\phi'}{\sqrt{a^2 + r^2 - 2r_a r \sin\theta \cos\phi'}} = \\ &= \frac{\mu_0}{4\pi} \frac{4 I r_a}{\sqrt{r_a^2 + r^2 + 2sr\sin\theta}} \left[\frac{(2-k^2)K(k^2) - 2E(k^2)}{k^2} \right] \end{aligned} \tag{4.14}$$

where r, θ and ϕ are the spherical coordinates, K and E are the elliptic integrals [75]

$$K(k^2) = \int_0^{\pi/2} \frac{d\theta}{\sqrt{1 - k^2 \sin^2 \theta}} \tag{4.15}$$

$$E(k^2) = \int_0^{\pi/2} \sqrt{1 - k^2 \sin^2 \theta}\, d\theta \tag{4.16}$$

and k^2 is the argument of the elliptic integrals

$$k^2 = \frac{4 r_a r \sin\theta}{r_a^2 + r^2 + 2 r_a r \sin\theta} \tag{4.17}$$

By projecting $\mathbf{B} = \nabla \times \mathbf{A}$ on r and z it is possible to calculate the components of the magnetic field at specified distance from the center of the single turn coil, meaning at 2 cm above/below one coil, or the center of the volume of the separator, as shown in Fig. 4.3. By summing the contribution from the two coils it is possible to calculate the total B_r and B_z and the core of the separating chamber, meaning the field perceived by the particles.

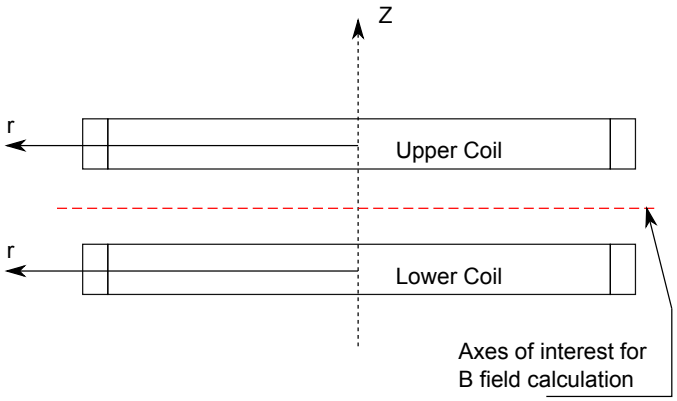

Figure 4.3: *Configuration of the upper and lower coils*

This approach results in a required power of 2.75 kW for each coil. This result is calculated considering the number of turns to be distributed on multiple rows, to reduce the solenoid overall height. This operation shall be performed carefully, because the radial dimension of this stack of turns shall not be comparable with the diameter of the device, otherwise the simplification of equivalent single turn coil cannot be applied. The stack

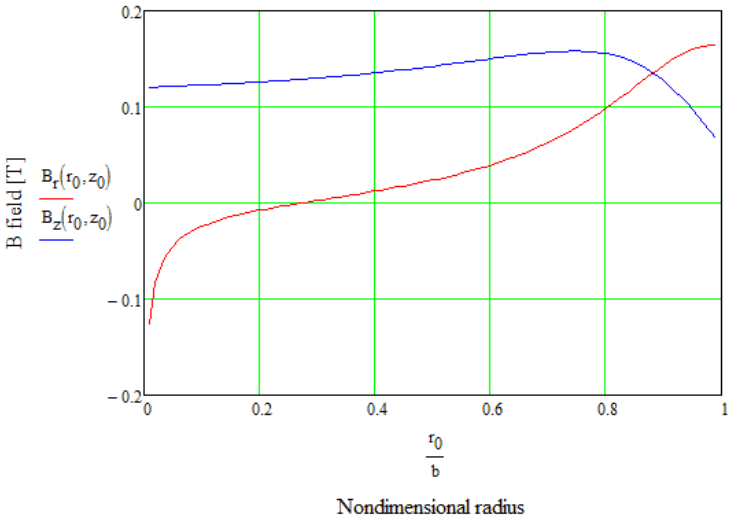

Figure 4.4: *Radial and axial magnetic flux density in the separator center*

dimension (which can be seen as the thickness of the circular annulus containing the solenoid) defines the wire diameter. This value, along with the total length of the wire, provides the resistance of the wire itself according to the relation

$$R_w = \frac{\rho_c l_w}{A_w} \tag{4.18}$$

The resistance is used to calculate voltage and required power as per the Joule's law

$$P_{coil} = I^2 R_w \tag{4.19}$$

This power ultimately goes to heat the wire. The heatings provide an increase of the wire temperature, which changes its resistivity. To calculate ρ_c an equilibrium temperature of 100°C is assumed (a 80°C increment from the 20°C ambient temperature), therefore the modified copper resistivity is calculated with the following equation:

$$\rho_c = \rho_{c,20}\left(1 + \alpha_{\rho_c}\Delta T\right) \tag{4.20}$$

where α_{ρ_c}=0.004 K^{-1}.

The resulting solenoid (one of the two) is depicted in Fig. 4.5. Tab. 4.10 provides an insight about the final solenoid configuration.

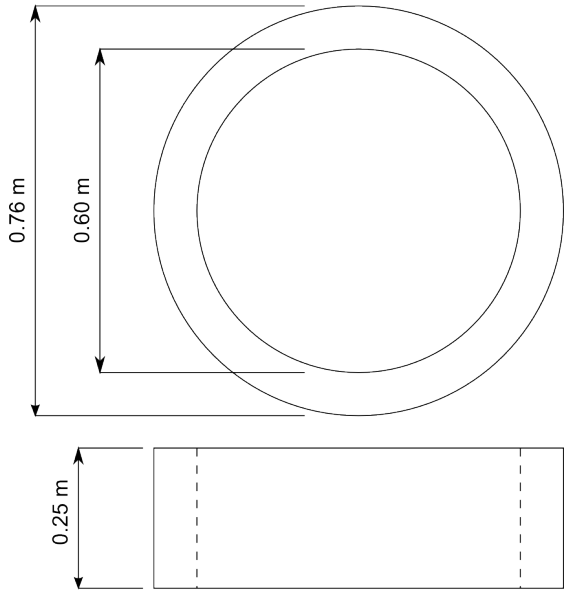

Figure 4.5: *Schematic of one solenoid with overall dimensions*

Description	Value	Units
Height of the solenoid	0.25	m
Resistivity of copper @ 20°C	1.72E-08	V*m/A
Resistivity of copper	2.27E-08	V*m/A
Radius of the devices	0.3	m
Magnetic field applied	0.12	T
Number of turn	2000	#
Number of layer of turns	25	#
Wire radius	0.0015	m
Lenght of the cable	3770	m
Thickness of the solenoid pack of layers	0.08	m
Resistance of the cable	11.4	ohm
Current to create the B field	15.5	A
Required and dissipated power (single solenoid)	2748.5	W
Voltage	177.3	V

Table 4.10: *Solenoid configuration*

4.2.5 Pumping stage

The chosen operative pressure, capable of guaranteeing an adequate $Si+$ outflow, is 75 Pa. This pressure level, equal to 0.75 mbar, is easily achievable with a rotary pump, which are generally capable of achieving 1E-2 mbar. A diffusion pump is therefore not necessary. The vacuum volume is represented by the chamber volume, which is a cylinder having a radius of 0.3m and a height equal to the torch diameter, 0.04m. Actually only half of this volume is necessary, because ions need only a 180° turn. A final volume of less than 6 liter has to be considered.

To evaluate pump power requirement the best approach is to identify a suitable commercial product able to guarantee such conditions. As a reference dual stage rotary vane pump Varian DS 302 is chosen, which is capable of a free air displacement of 237 dm^3/min and a pumping speed of 11.6m^3/h with a power consumption of 0.45 kW.

4.3 Energy consumption

Following all the considerations exposed above, where the calculation methodologies are described, all the contributions from all the stages need to be aggregated to obtain an overall value of power consumption. As introduced in Chapter 1 this value is essential to compare the outcome of this work with present silicon production processes, and evaluate the overall economical sustainability of the idea.

With all the contributions explained in §4.2 it is possible to fill a breakdown in Table 4.11 summarizing all the energy costs. Results shows the amount of energy to recover 1 kg of pure silicon. In particular the $Si+$ throughput of 3.46E-8 kg/s reported in §3.2.3.6 is used to calculate the time required to extract such amount of silicon, assuming no losses at the collectors, and such amount of time is used with the power of each stage to calculate the amount of energy required.

The total requested energy results to be about 220 GJ/kg of silicon. The total power required is actually not impressive, 7.2 kW, but the total time of collection of about 8000h lead to the results shown.

Feeding stage				
Heating and melting	30.83	MJ		
Atomization stage				
Power injected into the plasma	1.25	kW		
Efficiency	0.92	-		
Power required	1.36	kW		
Energy required	36153	MJ	10042	kWh
Time required	8034	h	28922211	s
Accelerator stage				
Power required	0.49	kW		
Energy required	14312	MJ	3975	kWh
Separation stage				
Power separation	5.50	kW		
Energy required	158986	MJ	44163	kWh
Pumping stage				
Power required	0.45	kW		
Energy required	13015	MJ	3615	kWh
Total				
Total required energy	222496	MJ	57820	kWh
Power required	7.20	kW		

Table 4.11: *Device required energy estimation*

4.3.1 Power dissipation

As already anticipated in §4.2.3 and §4.2.4 in some stages the energy used to perform the required task is later dissipated in terms of heat. In the accelerator stage the energy used to accelerate the ion flux is retrieved at the collectors, due to the impact of the high velocity ions. In the separator stage the energy used to create the magnetic field increases, due to Joule heating, the solenoid temperature, therefore, has to be properly dissipated in order to maintain the wire at the design temperature.

Considering only the abovementioned contributions a total of about 6 kW power need to be dissipated. This can be pursued with a suitable heat exchanger which, in the end, may require additional power, increasing the energy bill. Exchanger design is not part of this work.

4.4 Comparison with present production processes

One of the goal of this work is **to verify if the overall energy cost per unit mass of silicon can be competitive with present production processes**. As already introduced in §2.2.1, and in particular referring to calculations in Tab. 2.3, the overall energy cost to produce 1 kg of monocristalline ingot is 1057 kWh or 3805 MJ.

The above value has to be compared with the **220 GJ requested by the demonstrator**, which in turn leads to the conclusion that **58 times energy** is required to obtain the same outcome. This surely demonstrate that from the energy point of view the proposed process is **not sustainable**.

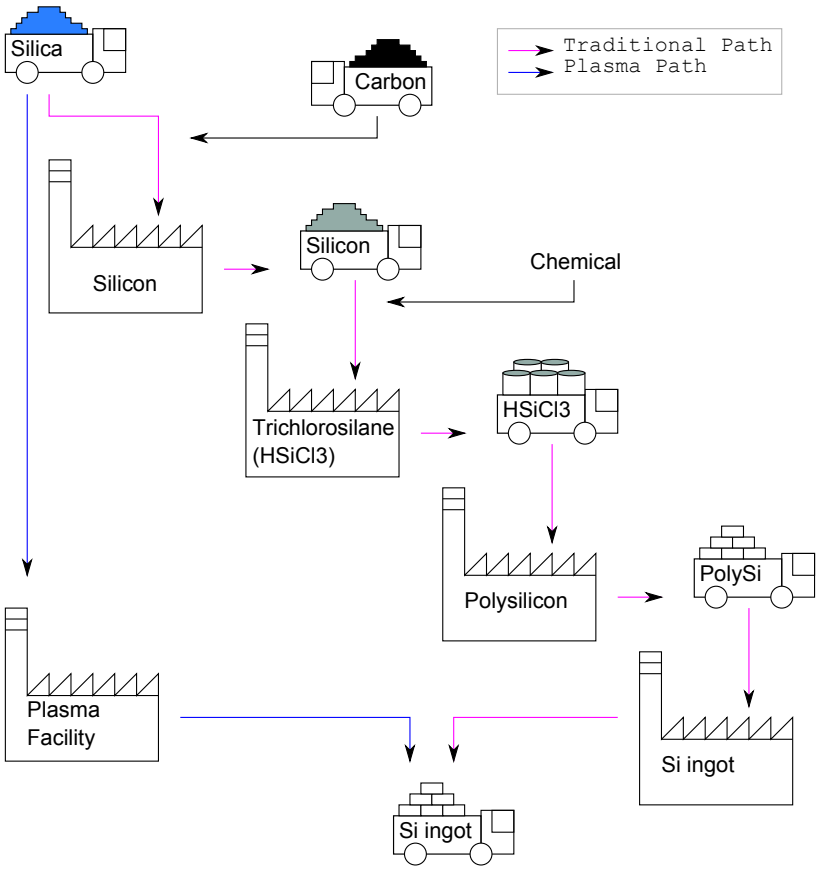

Figure 4.6: *Comparison of present production process chain with this work*

4.4.1 Considerations on the overall present production process

It is necessary to underline that the energy cost is only a part of the inputs required by the present industrial silicon ingots production process.

If, from an energetic/cost point of view, the concept proposed in this research appears not sustainable, in term of overall sustainability some considerations can be made. In Fig. 4.6 a representation of the traditional production chain is compared with the concept proposed in this work. Other than the external contributions depicted, many kilograms of other chemicals, water and fossil fuels are used other than electric energy in the process, and all these items requires energy to be produced. To provide some numbers 32 kg water, 0.7 kg N_2, 1.6 kg fossil fuels, 72 g chemicals are needed for the production of a 2 g chip, which contain 0.26 g of silicon based semiconductor [17].

Apart from energy costs, these substances are an important source of pollution from the semiconductor industry, and because in this field the technology changes very fast and secrecy prevails, environmental protection rules tend to be not attended or bypassed [76].

In contrast with the above requirements, in the presented process only electrical energy is required for the production. This energy greatly exceeds traditional values, but the overall environmental impact is greatly reduced, especially if the electric energy is taken from renewable energy sources.

CHAPTER 5

Conclusions

In Chapter 1 and especially in Chapter 2, three main goals were defined and specialized to the particular case of the silicon production. The purpose of these goals were to drive the research, in order to provide an evaluation of the proposed idea based on the fundamental principles of:

Feasibility meaning the evaluation of the actual technological realization of the proposed general idea.

Validity meaning that the feasibility study has to be performed in a correct way, with *a priori* or *a posteriori* verifications.

Sustainability meaning that the process, other than being feasible, is also sustainable from an energetic/economical point of view.

By analyzing the results and data provided in the previous chapters the final outcomes are the following:

Technological feasibility Simulation results shows that the yield of silicon ions is much greater of those of other species or molecules, therefore the feasibility of the concept has been demonstrated. See §3.2.3.6.

Verification of assumptions during demonstrator preliminary design The **selective ionization**, according to which some preliminary choices were performed, **appears verified** in terms of ionization ratio, leading to a very high ionization rate of silicon compared with those of monoatomic or biatomic oxygen. Nevertheless the input conditions, and therefore the high neutral density of oxygen respect to to silicon, lead to comparable numbers densities which results in the need of an acceleration and a separator stage. See §3.2.3.5.

Economical sustainability, comparison with present production methods The yield of the process is low, therefore the total energy consumption per kg of final product is much greater than the traditional present production process. See §4.3.

5.1 Open points

- A strong impact on the overall energy cost is represented by the separator stage. Alternative methods may be identified to generate the same magnetic field. As an example, if only permanent magnet could be used, zeroing the required energy from this stage, the overall cost would be reduced to 16 times the traditional production process cost. In general optimization procedures on each single stage may further significantly reduce the overall cost, making the technology more appealing.
  For the magnetic field generation, an intermediate approach would be to use a ferromagnetic material inside the solenoids, having a shape going from one solenoid to another, closing the force field lines between the two, except from the space of the vacuum chamber, as per Fig. 5.1. This solution has already taken into consideration because capable of providing substantial power savings, and can be easily calculated using the magnetic net approach.

  Unfortunately the $\mathbf{B}_{\mathbf{vac}}$ field required in vacuum result in a $\mathbf{B}_{\mathbf{fm}}$ field in the ferromagnetic material that brings the metal to saturation. This ultimately would flat $\mathbf{B}_{\mathbf{vac}}$ making the solution useless. Investigations need to be further carried out in order to find a ferromagnetic material with a high saturation level, and at the same time a relatively high relative permeability μ_r in order to reduce power consumption in generating the same magnetic fields.

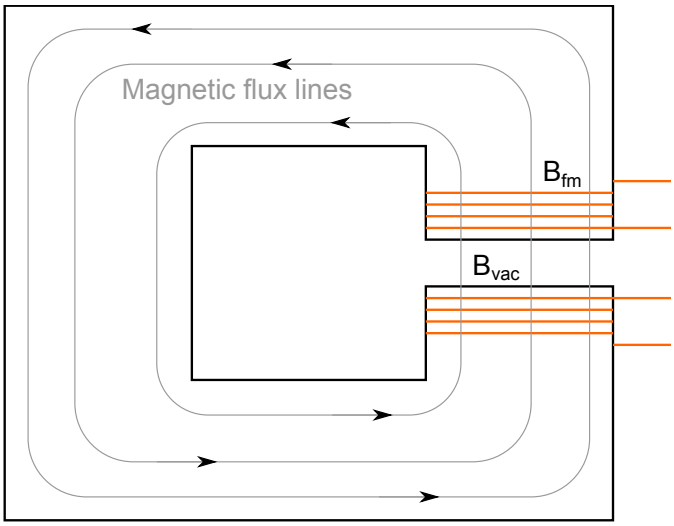

Figure 5.1: *Options of solenoids with ferromagnetic material core*

- at the moment the power is provided to the FEM model as general volume power deposition. An interesting open point would be to actually simulate the coupling with an ICP or another RF source. This will provide a higher insight about the efficiency of the torch. In addition this modification opens the possibility to insert additional elements, such as a containing magnetic field, which could act as a magnetic nozzle driving the ions which escape from the torch. This would likely increase the ions output velocity.
- In the present configuration, depending on the input material, the device can recover a big quantity of O_2, but also heavy metals or rare Earth materials can be recovered, increasing the overall economical sustainability of the concept. In particular rare Earth element recovery from semiconductor waste are acquiring a great importance due to political events and developing countries requirements.
- The SiO_2 kinetic model developed, and related reaction rate database is not present in literature. It can be used in a variety of applications, e.g. CVD simulation. An exploitation is therefore advisable.

Nomenclature

Roman Symbols

$\mathbf{A}$	Magnetic vector potential ($V\ s\ m^{-1}$)
$\mathbf{a}$	Acceleration ($m\ s^{-2}$)
A_w	Wire section (m^2)
$\mathbf{B}$	Magnetic flux density (T)
$\mathbf{B_{fm}}$	Magnetic flux density in ferromagnetic material (T)
$\mathbf{B_{vac}}$	Magnetic flux density in vacuum (T)
c	Molar concentration ($mol\ m^{-3}$)
$\tilde{C}_p$	Specific heat (molar basis) ($J\ mol^{-1}\ K^{-1}$)
C_p	Specific heat ($J\ kg^{-1}\ K^{-1}$)
$\mathbf{D}$	Displacement field ($C\ m^{-2}$)
$\mathbf{D_e}$	Electron energy diffusivity ($m^2\ s^{-1}$)
$\mathbf{D}_e$	Electron diffusivity ($m^2\ s^{-1}$)
$\mathbf{E}$	Electric field ($V\ m^{-1}$)
E_{ion}	Ionization energy (J)
$\mathbf{F}$	Force applied to the ion (N)

f_B Lorentz body force (N)

$\hat{h}$ Plank constant ($J\ s^{-1}$)

h Molar enthalpy ($J\ mol^{-1}$)

$H_{0\ T_{298.15}}$ Standard enthalpy at 298.15K ($J\ mol^{-1}$)

$H_{0\ T_{boil}}$ Standard enthalpy at boiling point ($J\ mol^{-1}$)

ΔH_{vap} Enthalpy of vaporization ($J\ mol^{-1}$)

I Solenoid current (A)

I_{eq} Equivalent solenoid current (A)

J Arc current (A)

j Current density ($A\ m^{-2}$)

K Rate constant ($m^3\ s^{-1}$ for order 2 reaction)

k Thermal conductivity ($W\ m^{-1}\ K^{-1}$)

k^b Backward rate coefficient (s^{-1} or $mol\ m^{-3}\ s^{-1}$ or $mol^2\ m^{-6}\ s^{-1}$)

k_B Boltzmann constant ($J\ K^{-1}$)

k^f Forward rate coefficient (s^{-1} or $mol\ m^{-3}\ s^{-1}$ or $mol^2\ m^{-6}\ s^{-1}$)

Kn Knudsen number ($-$)

L_t Torch length (m)

l_w Wire length (m)

$\dot{m}$ Mass flow rate ($kg\ s^{-1}$)

M Molar mass ($kg\ mol^{-1}$)

m Molecular weight (kg)

m_e Electron mass (kg)

m_{ion} Ion mass (kg)

M_n Mean molar mass of the mixture ($kg\ mol^{-1}$)

$\tilde{N}$ Particle number ($-$)

n Neutral or ion density (m^{-3})

n_0	Neutral density (m^{-3})
N_c	Number of coil turns ($-$)
$N_{c,eq}$	Number of equivalent coil turns ($-$)
n_e	Electron density (m^{-3})
$n\mathrm{e}$	Electron energy density ($V\ m^{-3}$)
n_i	Ion density (m^{-3})
N_n	Total neutral density (m^{-3})
p	Pressure (Pa)
P_{abs}	Absorbed power (W)
P_{acc}	Power to accelerate ions (W)
P_{boil}	Power to vaporize input raw silica (W)
P_{coil}	Power requested by a single solenoid (W)
P_{in}	Power deposited into the plasma ($W\ m^{-3}$)
P_{loss}	Power losses (W)
p_{SiO}	SiO vapor pressure (Pa)
p_{vap}	Vapor pressure (Pa)
Q	Total heat source due to chemical reactions ($W\ m^{-3}$)
q	Electron or ion charge (single ionization assumed) (C)
R	Universal gas constant ($J\ mol^{-1}\ K^{-1}$)
r_a	Radius of the current loop (m)
r_{an}	Anode inner radius (m)
r_c	Cyclotron radius (m)
r_{ct}	Cathode radius (m)
$R\mathrm{e}$	Energy loss/gain due to inelastic collisions ($V\ m^{-3}\ s^{-1}$)
rr	Reaction rate ($mol\ m^{-3}\ s^{-1}$)
R_t	Torch radius (m)

R_w Wire resistance (Ω)

ΔS_{vap} Entropy of vaporization ($J\ mol^{-1}\ K^{-1}$)

T Temperature (K)

t Time (s)

T_b Boiling temperature (K)

T_e Electron temperature (eV)

$\mathbf{u}$ Mass averaged fluid velocity vector ($m\ s^{-1}$)

$\tilde{u}$ Internal energy (J)

u_e Exhaust velocity (ms^{-1})

ΔV Accelerating potential (V)

Δv Ion velocity increment ($m\ s^{-1}$)

$\tilde{\mathbf{v}}$ Stoichiometric coefficients matrix ($-$)

$\mathbf{v}$ on velocity ($m\ s^{-1}$)

V Potential (V)

$v_{e,th}$ Electron thermal velocity ($m\ s^{-1}$)

v_{in} Input ion velocity in acceleration stage (output of torch) ($m\ s^{-1}$)

v_{out} Output ion velocity from acceleration stage ($m\ s^{-1}$)

V_r Pug flow reactor volume (m^3)

w Mass fraction ($-$)

x Molar fraction ($-$)

Z_0 Neutral partition function ($-$)

Z_i Ion partition function ($-$)

Greek Symbols

α_{ρ_c} Temperature coefficient of resistivity (K^{-1})

ϵ_0 Vacuum permittivity ($F\ m^{-1}$)

λ_D Debye length (m)

λ_{e-n}	Mean free path before electron-neutral collision (m)
λ_{mfp}	Gas mean free path (m)
μ	Dynamic viscosity ($N\ s\ m^{-2}$)
μ_0	Magnetic permeability of vacuum ($N\ A^{-2}$ or $H\ m^{-1}$)
μ_e	Electron energy mobility ($m^2\ V\ s^{-1}$)
μ_e	Electron mobility ($m^2\ V\ s^{-1}$)
μ_r	Relative magnetic permeability ($-$)
ν_{e-n}	Electron-neutral collision frequency (s^{-1})
ρ	Mixture density ($kg\ m^{-3}$)
ρ_c	Copper resistivity ($\Omega\ m$)

Bibliography

[1] Global Footprint Network. *Earth Overshoot Day 2014*. 2014.

[2] E. O. Lawrence. Methods of and apparatus for separating materials. *US Patent 2709222*, May 24, 1955.

[3] M.W. Grossman and T.A. Shepp. Plasma isotope separation methods. *Plasma Science, IEEE Transactions on*, 19(6):1114 –1122, dec 1991.

[4] V. Bardakov, G. Kichigin, N. Strokin, and E. Tsaregorodtsev. Plasma-optical mass separation of isotopes in the magnetic field of linear current. *Technical Physics*, 55:1504–1508, 2010. 10.1134/S1063784210100178.

[5] A. Morozov and V. Savelev. Axisymmetric plasma-optic mass separators. *Plasma Physics Reports*, 31:417–424, 2005. 10.1134/1.1925791.

[6] A. Morozov and N. Semashko. On the mass separation of quasineutral beams. *Technical Physics Letters*, 28:1052–1053, 2002. 10.1134/1.1535500.

[7] W. H. Steurer. Extraterrestrial material processing. *Jet Propulsion Laboratory*, Doc. JPL-82-41, 1982.

[8] W. F. Carroll. Research on the use of space resources. *Jet Propulsion Laboratory*, Doc. JPL-83-36, 1983.

[9] J. Gilleland, S. Agnew, B. Cluggish, R. Freeman, R. Miller, S. Putvinski, L. Sevier, and K. Umstadter. Application of archimedes filter for reduction of hanford hlw. *WM02 Conference*, Tucson, AZ, February 24-28, 2002.

[10] C. E. Ahlfeld, J. G. Gilleland, and J. D. Wagoner. Commercial application of plasma mass separation in the archimedes filter plant. *WM03 Conference*, Tucson, AZ, February 23-27, 2003.

[11] A.M. Yegorov, E.I. Skibenko, Yu.V. Kovtun, and V.B. Yuferov. Magneto-plasma separation as a method for reprocessing of spent fuel and radioactive waste. *Problems of Atomic Science and Technology*, 6(Series: Plasma Physics (14)):147–149, 2008.

[12] D. A. Dmitrii A Dolgolenko and Y. A. Muromkin. Plasma isotope separation based on ion cyclotron resonance. *Phys.-Usp.*, 52(4):345, 2009.

[13] T.S. Bigelow, F.J. Tarallo, and N.R. Stevenson. Production of stable isotopes utilizing the plasma separation process. *Nuclear Instruments and Methods in Physics Research Section B: Beam Interactions with Materials and Atoms*, 241(1-4):652 – 654, 2005. The Application of Accelerators in Research and Industry - Proceedings of the Eighteenth International Conference on the Application of Accelerators in Research and Industry (CAARI 2004).

[14] P. Meubus and a. Huczko. A study of chromic oxide decomposition in an RF argon plasma. *Plasma Chemistry and Plasma Processing*, 6(2):159–177, June 1986.

[15] P Meubus and A. Huczko. A study of CrO vapor decomposition in approximated isothermal RF plasma reactors. *The Canadian Journal of Chemical Engineering*, 67(1):127–136, February 1989.

[16] A Huczko and P Meubus. Vapor phase reduction of chromic oxide in an Ar-H2 Rf Plasma. *Metallurgical Transactions B*, 19(December):927–933, 1988.

[17] E. D. Williams, R. U. Ayres, and M. Heller. The 1.7 kilogram microchip: Energy and material use in the production of semiconductor devices. *Environ. Sci. Technol.*, 36:5504–5510, 2002.

[18] C. C. Chan. Behavior of metals in msw incinerator fly ash during roasting with chlorinating agents. *PhD Thesis, University of Toronto*, 1997.

[19] G. Parissenti and A. Niro. Power dissipation in heavy metals recovery from incinerator ashes. *XXVIII Congresso UIT sulla Trasmissione del Calore*, Brescia, 21-23 Giugno 2010.

[20] A. W. Irwin. Polynomial partition function approximations of 344 atomic and molecular species. *The Astrophysical Journal Supplement Series*, 45:621–633, April 1981.

[21] R.G. Jahn. *Physics of Electric Propulsion*. Dover books on physics. Dover Publications, Incorporated, 2006.

[22] R. G. Jahn and E. Y. Choueiri. *Electric Propulsion, in Encyclopedia of Physical Science and Technology*, volume 5. Academic Press, 3rd edition, 2002.

[23] G. Parissenti. Modeling Explosive Mass Ejection From High-Current Anode Spots. M.sc. thesis, Politecnico di Milano, 2008.

[24] Tony Addona and Richard J. Munz. Silica Decomposition Using a Transferred Arc Process. *Industrial & Engineering Chemistry Research*, 38(6):2299–2309, June 1999.

[25] A. Putvinsky, S. F. Agnew, T. Ohkawa, and L. Sevier. Induction plasma torch liquid waste injector. *US Patent 6410880B1*, Jun 25, 2002.

[26] F. Bosi. F. Bosi M.Sc. thesis, 2012.

[27] F. Bosi, G. Parissenti, M. Pessana, and D. Pavarin. Modelling of plasma-chemical propellant interaction in electrodeless helicon plasma thruster. *5th European Conference for Aeronautics and Space Sciences (EUCASS)*, Munich, Germany, 1-5 July 2013.

[28] Alexander Fridman. *Plasma Chemistry*. Cambridge University Press, Cambridge, 2008.

[29] Evangelos Gogolides and Herbert H. Sawin. Continuum modeling of radio-frequency glow discharges. I. Theory and results for electropositive and electronegative gases. *Journal of Applied Physics*, 72(9):3971, 1992.

[30] G J M Hagelaar and L C Pitchford. Solving the Boltzmann equation to obtain electron transport coefficients and rate coefficients for fluid models. *Plasma Sources Science and Technology*, 14(4):722–733, November 2005.

[31] R. S. Brokaw. Predicting Transport Properties of Dilute Gases. *Industrial & Engineering Chemistry Process Design and Development*, 8(2):240–253, April 1969.

[32] HL Schick. A Thermodynamic Analysis of the High-temperature Vaporization Properties of Silica. *Chemical Reviews*, 60(4):331–362, August 1960.

[33] T. Addona. *The study of a novel thermal plasma process for the production of fumed silica*. PhD thesis, McGill University (Canada), 1998.

[34] D. Harbec, F. Gitzhofer, and a. Tagnit-Hamou. Induction plasma synthesis of nanometric spheroidized glass powder for use in cementitious materials. *Powder Technology*, 214(3):356–364, December 2011.

[35] E Balabanova. Silica nanoparticles produced by thermal arc plasma. modelling. *Journal of Optoelectronics and Advanced Materials*, 5(3):679–686, 2003.

[36] Norma Yadira Mendoza Gonzalez, Mbark El Morsli, and Pierre Proulx. Production of Nanoparticles in Thermal Plasmas: A Model Including Evaporation, Nucleation, Condensation, and Fractal Aggregation. *Journal of Thermal Spray Technology*, 17(4):533–550, October 2008.

[37] EE Ferguson. Ionospheric Si+ and SiO+. *Journal of Geophysical . . .* , pages 10–12, 1970.

[38] TL Brown. The chemistry of metallic elements in the ionosphere and mesosphere. *Chemical Reviews*, 3(3), 1973.

[39] Juan C Gómez Martín, Mark a. Blitz, and John M. C. Plane. Kinetic studies of atmospherically relevant silicon chemistry : Part I: Silicon atom reactions. *Physical Chemistry Chemical Physics*, 11(4):671, 2009.

[40] MA Lieberman and AJ Lichtenberg. *Principles of plasma discharges and materials processing*. Second edition, 2005.

[41] TRINITI database. *LxCat*, page www.lxcat.net, 2014.

[42] PHELPS database. *LxCat*, page www.lxcat.net, 2014.

[43] BIAGI database. *LxCat*, page www.lxcat.net, 2014.

[44] MORGAN database. *LxCat*, page www.lxcat.net, 2014.

[45] K.N. Joshipura, B.G. Vaishnav, and Sumona Gangopadhyay. Electron impact ionization cross-sections of plasma relevant and astrophysical silicon compounds: SiH4, Si2H6, Si(CH3)4, SiO, SiO2, SiN and SiS. *International Journal of Mass Spectrometry*, 261(2-3):146–151, March 2007.

[46] a Yanguas-Gil, J Cotrino, and a R González-Elipe. Global model of a low pressure ECR microwave plasma applied to the PECVD of SiO 2 thin films. *Journal of Physics D: Applied Physics*, 40(11):3411–3422, June 2007.

[47] Jaime H. Lozano-Parada and William B. Zimmerman. The role of kinetics in the design of plasma microreactors. *Chemical Engineering Science*, 65(17):4925–4930, September 2010.

[48] H. Y. Kim, H. W. Lee, S. K. Kang, H. Wk. Lee, G. C. Kim, and J. K. Lee. Modeling the chemical kinetics of atmospheric plasma for cell treatment in a liquid solution. *Physics of Plasmas*, 19(7):073518, 2012.

[49] SS Prasad and WT Huntress Jr. A model for gas phase chemistry in interstellar clouds. I-The basic model, library of chemical reactions, and chemistry among C, N, and O compounds. *The Astrophysical Journal . . .* , 1980.

[50] D. W. Fahey. Reactions of Si+ with H2O and O2 and SiO+ with H2 and D2. *The Journal of Chemical Physics*, 75(2):669, 1981.

[51] Diethard K. Bohme. Chemistry initiated by atomic silicon ions in the gas phase: formation of silicon-bearing ions and molecules. *International Journal of Mass Spectrometry and Ion Processes*, 100:719–736, October 1990.

[52] Juan C Gómez Martín, Mark a Blitz, and John M C Plane. Kinetic studies of atmospherically relevant silicon chemistry. Part II: silicon monoxide reactions. *Physical chemistry chemical physics : PCCP*, 11(46):10945–54, December 2009.

[53] UMIST RATE2012 / astrochemistry.net database. *astrochemistry.net*, page http://udfa.ajmarkwick.net/, 2014.

[54] FC Fehsenfeld. Si+ and SiO+ reactions of atmospheric importance. *Canadian Journal of Chemistry*, 47:1–2, 1969.

[55] Juan C Gómez Martín and John M C Plane. Kinetic studies of atmospherically relevant silicon chemistry. Part III: Reactions of Si+ and SiO+ with O3, and Si+ with O2. *Physical chemistry chemical physics : PCCP*, 13(9):3764–74, March 2011.

[56] RA Goldberg. Silicon ions below 100 km: A case for SiO2+. *Radio Science*, 1975.

[57] B.F. Gordiets A.I. Osipov M. Capitelli, C.M. Ferreira. *Plasma kinetics in atmospheric gases*. Springer Series on Atomic, Optical, and Plasma Physics. Springer, 2000.

[58] COMSOL Thermal plasma model. *COMSOL Multiphysics*, http://www.comsol.com/model/thermal-plasma-8658, 2014.

[59] COMSOL Electronegative inductively coupled plasma model. *COMSOL Multiphysics*, http://www.comsol.com/model/electronegative-inductively-coupled-plasma-12601, 2014.

[60] BJ McBride, S Gordon, and MA Reno. Coefficients for calculating thermodynamic and transport properties of individual species. *Nasa Technical Memorandum NASA TM-4513*, 1993.

[61] BJ McBride. NASA Thermodynamic database. *NASA Glenn Research Center*, http://shepherd.caltech.edu/EDL/public/thermo/nasadat, 2014.

[62] M.W. Chase Jr. Nist-janaf themochemical tables, fourth edition. *Journal of Physical and Chemical Reference Data, Monograph 9*, pages 1–1951, 1998.

[63] P. Cicman, J.D. Skalny, J. Fedor, N.J. Mason, P. Scheier, E. Illenberger, and T.D. Märk. Dissociative electron attachment to ozone at very low energies revisited. *International Journal of Mass Spectrometry*, 260(1):85–87, January 2007.

[64] D. Green and R. Perry. *Perry's Chemical Engineers' Handbook, Eighth Edition*. McGraw Hill professional. McGraw-Hill Education, 2007.

[65] P. Richet, Y. Bottinga, L. Denielou, J.P. Petitet, and C. Tequi. Thermodynamic properties of quartz, cristobalite and amorphous SiO2: drop calorimetry measurements between 1000 and 1800 K and a review from 0 to 2000 K. *Geochimica et Cosmochimica Acta*, 46(12):2639–2658, December 1982.

[66] Bruce Fegley, editor. *Practical Chemical Thermodynamics for Geoscientists*. Academic Press, Boston, 2013.

[67] M. Grayson. *Encyclopedia of glass, ceramics and cement*. Encyclopaedia reprint series. Wiley, New York, NY, 1985.

[68] S. Elhadj, M. J. Matthews, S. T. Yang, and D. J. Cooke. Evaporation kinetics of laser heated silica in reactive and inert gases based on near-equilibrium dynamics. *Optics express*, 20(2):1575–87, January 2012.

[69] A Pitkänen, JM Mäkelä, M Nurminen, A Oksanen, K Janka, J Keskinen, H Keskinen, JK Liimatainen, S Hellstén, and T Määttä. Numerical study of silica particle formation in turbulent h2/o2 flame. *IFRF Combustion journal*, 200509:1–29, 2005.

[70] G.V. Samsonov. *The Oxide handbook*. IFI/Plenum, 1973.

[71] G.V. Samsonov. *The Oxide Handbook*. IFI Data Base Library. IFI/Plenum, 1982.

[72] L. J. Cook, A. T. Forrester, Mahoney J. F., J. Peref, and K. E. Vickers. Apparatus and process for separating materials. *US Patent 4124801*, Nov 7, 1970.

[73] J. C. Simpson, J. E. Lane, C. D. Immer, and R. C Youngquist. Simple analytic expressions for the magnetic field of a circular current loop. *NASA Technical Document 20010038494*, Jan 01, 2001.

[74] J.D. Jackson. *Classical Electrodynamics*. Wiley, 1998.

[75] M. Abramowitz and I.A. Stegun. *Handbook of Mathematical Functions: with Formulas, Graphs, and Mathematical Tables*. Dover Books on Mathematics. Dover Publications, 2012.

[76] F. Yoshida. High-tech pollution. *Economic Journal of Hokkaido University*, 23:73–138, 1994.

Appendices

APPENDIX $\mathcal{A}$

2D axisymmetric multiphysics FEM model results

A.1 Number densities

Pressure (Pa)	Power (W)	e ($1/m^3$)	O ($1/m^3$)	O2 ($1/m^3$)	Si ($1/m^3$)	SiO ($1/m^3$)	SiO2 ($1/m^3$)	O+ ($1/m^3$)	O2+ ($1/m^3$)	Si+ ($1/m^3$)	SiO+ ($1/m^3$)	SiO2+ ($1/m^3$)
25	100	8.8E+15	7.6E+18	2.4E+20	9E+15	4.8E+20	7.3E+17	2E+14	5.7E+15	3.8E+14	3.5E+16	1.4E+14
50	100	3.6E+16	1.7E+19	4.8E+20	2.3E+16	9.5E+20	1.4E+18	6.8E+14	1E+16	3.2E+15	7.4E+16	3.7E+14
75	100	5.4E+16	2.7E+19	7.2E+20	2.9E+16	1.4E+21	2.2E+18	1.1E+15	1.2E+16	9E+15	8.9E+16	5.9E+14
25	1000	1.4E+17	1.2E+19	2.4E+20	1.8E+17	4.7E+20	7.1E+17	4.9E+15	3E+16	3.9E+15	1.9E+17	7.0E+14
50	1000	3.8E+17	4.1E+19	4.5E+20	7.2E+17	9.4E+20	1.4E+18	3.4E+16	6E+16	4E+16	3.5E+17	1.4E+15
75	1000	5.2E+17	7.8E+19	6.5E+20	8.2E+17	1.4E+21	2.1E+18	7.1E+16	7.4E+16	9.6E+16	3.7E+17	1.8E+15
25	10000	1.4E+18	4.6E+19	1.9E+20	4.8E+18	4.5E+20	6.2E+17	2.4E+17	1.4E+17	2.6E+17	8.3E+17	2.2E+15
50	10000	4.7E+18	1.5E+20	3E+20	1.4E+19	8.6E+20	1.1E+18	1.9E+18	1.4E+17	1.9E+18	7.3E+17	2.1E+15
75	10000	9.4E+18	2.3E+20	4E+20	1.4E+19	1.3E+21	1.6E+18	5.6E+18	8.2E+16	3.4E+18	3.9E+17	1.6E+15

Table A.1: *Species number density Vs Background pressure @ 1E-7 kg/s input mass flow rate*

Pressure (Pa)	Power (W)	e ($1/m^3$)	O ($1/m^3$)	O2 ($1/m^3$)	Si ($1/m^3$)	SiO ($1/m^3$)	SiO2 ($1/m^3$)	O+ ($1/m^3$)	O2+ ($1/m^3$)	Si+ ($1/m^3$)	SiO+ ($1/m^3$)	SiO2+ ($1/m^3$)
25	100	9.7E+15	7.9E+18	2.5E+20	9.4E+15	4.9E+20	7.5E+17	2.2E+14	6E+15	4.2E+14	3.7E+16	1.4E+14
50	100	3.6E+16	1.7E+19	4.8E+20	2.4E+16	9.6E+20	1.5E+18	6.8E+14	1E+16	3.3E+15	7.5E+16	3.7E+14
75	100	5.4E+16	2.7E+19	7.2E+20	2.9E+16	1.4E+21	2.2E+18	1.1E+15	1.2E+16	9E+15	8.9E+16	5.9E+14
25	1000	1.5E+17	1.3E+19	2.4E+20	2E+17	4.9E+20	7.4E+17	5.5E+15	3.2E+16	4.5E+15	2E+17	7.3E+14
50	1000	3.9E+17	4.2E+19	4.5E+20	7.3E+17	9.4E+20	1.4E+18	3.5E+16	6E+16	4.1E+16	3.5E+17	1.4E+15
75	1000	5.2E+17	7.8E+19	6.5E+20	8.2E+17	1.4E+21	2.1E+18	7.2E+16	7.4E+16	9.7E+16	3.7E+17	1.8E+15
25	10000	1.5E+18	4.9E+19	1.9E+20	5.3E+18	4.6E+20	6.3E+17	2.7E+17	1.5E+17	3.1E+17	8.5E+17	2.2E+15
50	10000	4.8E+18	1.5E+20	3E+20	1.4E+19	8.7E+20	1.1E+18	2E+18	1.4E+17	2E+18	7.2E+17	2.1E+15
75	10000	9.5E+18	2.3E+20	4E+20	1.4E+19	1.3E+21	1.6E+18	5.6E+18	8.2E+16	3.5E+18	3.8E+17	1.6E+15

Table A.2: *Species number density Vs Background pressure @ 1E-6 kg/s input mass flow rate*

Pressure (Pa)	Power (W)	e ($1/m^3$)	O ($1/m^3$)	O2 ($1/m^3$)	Si ($1/m^3$)	SiO ($1/m^3$)	SiO2 ($1/m^3$)	O+ ($1/m^3$)	O2+ ($1/m^3$)	Si+ ($1/m^3$)	SiO+ ($1/m^3$)	SiO2+ ($1/m^3$)
25	100	1.9E+16	1E+19	3.2E+20	1.4E+16	6.3E+20	9.5E+17	3.5E+14	7.4E+15	8.9E+14	5.1E+16	2.1E+14
50	100	4E+16	1.9E+19	5.2E+20	2.5E+16	1E+21	1.6E+18	7.6E+14	1E+16	3.9E+15	7.7E+16	4.0E+14
75	100	5.5E+16	2.8E+19	7.4E+20	3E+16	1.5E+21	2.3E+18	1.1E+15	1.2E+16	9.5E+15	8.9E+16	6.0E+14
25	1000	2.4E+17	2E+19	3E+20	4.2E+17	6.2E+20	9.4E+17	1.3E+16	4.3E+16	1.2E+16	2.7E+17	1.0E+15
50	1000	4.1E+17	4.7E+19	4.8E+20	7.7E+17	1E+21	1.5E+18	4.1E+16	6.4E+16	4.9E+16	3.6E+17	1.5E+15
75	1000	5.3E+17	8.1E+19	6.8E+20	8.1E+17	1.5E+21	2.2E+18	7.5E+16	7.5E+16	1E+17	3.7E+17	1.9E+15
25	10000	2.6E+18	8.1E+19	2.3E+20	9.5E+18	5.9E+20	7.9E+17	7.1E+17	1.7E+17	8.5E+17	9.3E+17	2.4E+15
50	10000	5.6E+18	1.6E+20	3.2E+20	1.5E+19	9.4E+20	1.2E+18	2.5E+18	1.3E+17	2.3E+18	6.5E+17	2.0E+15
75	10000	1E+19	2.4E+20	4.2E+20	1.4E+19	1.4E+21	1.7E+18	6.1E+18	7.7E+16	3.5E+18	3.5E+17	1.6E+15

Table A.3: *Species number density Vs Background pressure @ 1E-5 kg/s input mass flow rate*

Power (W)	Pressure (Pa)	e ($1/m^3$)	O ($1/m^3$)	O2 ($1/m^3$)	Si ($1/m^3$)	SiO ($1/m^3$)	SiO2 ($1/m^3$)	O+ ($1/m^3$)	O2+ ($1/m^3$)	Si+ ($1/m^3$)	SiO+ ($1/m^3$)	SiO2+ ($1/m^3$)
100	25	8.8E+15	7.6E+18	2.4E+20	9E+15	4.8E+20	7.3E+17	2E+14	5.7E+15	3.8E+14	3.5E+16	1.4E+14
1000	25	1.4E+17	1.2E+19	2.4E+20	1.8E+17	4.7E+20	7.1E+17	4.9E+15	3E+16	3.9E+15	1.9E+17	7E+14
10000	25	1.4E+18	4.6E+19	1.9E+20	4.8E+18	4.5E+20	6.2E+17	2.4E+17	1.4E+17	2.6E+17	8.3E+17	2.2E+15
100	50	3.6E+16	1.7E+19	4.8E+20	2.3E+16	9.5E+20	1.4E+18	6.8E+14	1E+16	3.2E+15	7.4E+16	3.7E+14
1000	50	3.8E+17	4.1E+19	4.5E+20	7.2E+17	9.4E+20	1.4E+18	3.4E+16	6E+16	4E+16	3.5E+17	1.4E+15
10000	50	4.7E+18	1.5E+20	3E+20	1.4E+19	8.6E+20	1.1E+18	1.9E+18	1.4E+17	1.9E+18	7.3E+17	2.1E+15
100	75	5.4E+16	2.7E+19	7.2E+20	2.9E+16	1.4E+21	2.2E+18	1.1E+15	1.2E+16	9E+15	8.9E+16	5.9E+14
1000	75	5.2E+17	7.8E+19	6.5E+20	8.2E+17	1.4E+21	2.1E+18	7.1E+16	7.4E+16	9.6E+16	3.7E+17	1.8E+15
10000	75	9.4E+18	2.3E+20	4E+20	1.4E+19	1.3E+21	1.6E+18	5.6E+18	8.2E+16	3.4E+18	3.9E+17	1.6E+15

Table A.4: *Species number density Vs Input power @ 1E-7 kg/s input mass flow rate*

Power (W)	Pressure (Pa)	e ($1/m^3$)	O ($1/m^3$)	O2 ($1/m^3$)	Si ($1/m^3$)	SiO ($1/m^3$)	SiO2 ($1/m^3$)	O+ ($1/m^3$)	O2+ ($1/m^3$)	Si+ ($1/m^3$)	SiO+ ($1/m^3$)	SiO2+ ($1/m^3$)
100	25	9.7E+15	7.9E+18	2.5E+20	9.4E+15	4.9E+20	7.5E+17	2.2E+14	6E+15	4.2E+14	3.7E+16	1.4E+14
1000	25	1.5E+17	1.3E+19	2.4E+20	2E+17	4.9E+20	7.4E+17	5.5E+15	3.2E+16	4.5E+15	2E+17	7.3E+14
10000	25	1.5E+18	4.9E+19	1.9E+20	5.3E+18	4.6E+20	6.3E+17	2.7E+17	1.5E+17	3.1E+17	8.5E+17	2.2E+15
100	50	3.6E+16	1.7E+19	4.8E+20	2.4E+16	9.6E+20	1.5E+18	6.8E+14	1E+16	3.3E+15	7.5E+16	3.7E+14
1000	50	3.9E+17	4.2E+19	4.5E+20	7.3E+17	9.4E+20	1.4E+18	3.5E+16	6E+16	4.1E+16	3.5E+17	1.4E+15
10000	50	4.8E+18	1.5E+20	3E+20	1.4E+19	8.7E+20	1.1E+18	2E+18	1.4E+17	2E+18	7.2E+17	2.1E+15
100	75	5.4E+16	2.7E+19	7.2E+20	2.9E+16	1.4E+21	2.2E+18	1.1E+15	1.2E+16	9E+15	8.9E+16	5.9E+14
1000	75	5.2E+17	7.8E+19	6.5E+20	8.2E+17	1.4E+21	2.1E+18	7.2E+16	7.4E+16	9.7E+16	3.7E+17	1.8E+15
10000	75	9.5E+18	2.3E+20	4E+20	1.4E+19	1.3E+21	1.6E+18	5.6E+18	8.2E+16	3.5E+18	3.8E+17	1.6E+15

Table A.5: *Species number density Vs Input power @ 1E-6 kg/s input mass flow rate*

Power (W)	Pressure (Pa)	e ($1/m^3$)	O ($1/m^3$)	O2 ($1/m^3$)	Si ($1/m^3$)	SiO ($1/m^3$)	SiO2 ($1/m^3$)	O+ ($1/m^3$)	O2+ ($1/m^3$)	Si+ ($1/m^3$)	SiO+ ($1/m^3$)	SiO2+ ($1/m^3$)
100	25	1.9E+16	1E+19	3.2E+20	1.4E+16	6.3E+20	9.5E+17	3.5E+14	7.4E+15	8.9E+14	5.1E+16	2.1E+14
1000	25	2.4E+17	2E+19	3E+20	4.2E+17	6.2E+20	9.4E+17	1.3E+16	4.3E+16	1.2E+16	2.7E+17	1E+15
10000	25	2.6E+18	8.1E+19	2.3E+20	9.5E+18	5.9E+20	7.9E+17	7.1E+17	1.7E+17	8.5E+17	9.3E+17	2.4E+15
100	50	4E+16	1.9E+19	5.2E+20	2.5E+16	1E+21	1.6E+18	7.6E+14	1E+16	3.9E+15	7.7E+16	4E+14
1000	50	4.1E+17	4.7E+19	4.8E+20	7.7E+17	1E+21	1.5E+18	4.1E+16	6.4E+16	4.9E+16	3.6E+17	1.5E+15
10000	50	5.6E+18	1.6E+20	3.2E+20	1.5E+19	9.4E+20	1.2E+18	2.5E+18	1.3E+17	2.3E+18	6.5E+17	2E+15
100	75	5.5E+16	2.8E+19	7.4E+20	3E+16	1.5E+21	2.3E+18	1.1E+15	1.2E+16	9.5E+15	8.9E+16	6E+14
1000	75	5.3E+17	8.1E+19	6.8E+20	8.1E+17	1.5E+21	2.2E+18	7.5E+16	7.5E+16	1E+17	3.7E+17	1.9E+15
10000	75	1E+19	2.4E+20	4.2E+20	1.4E+19	1.4E+21	1.7E+18	6.1E+18	7.7E+16	3.5E+18	3.5E+17	1.6E+15

Table A.6: *Species number density Vs Input power @ 1E-5 kg/s input mass flow rate*

A.2 Output fluxes

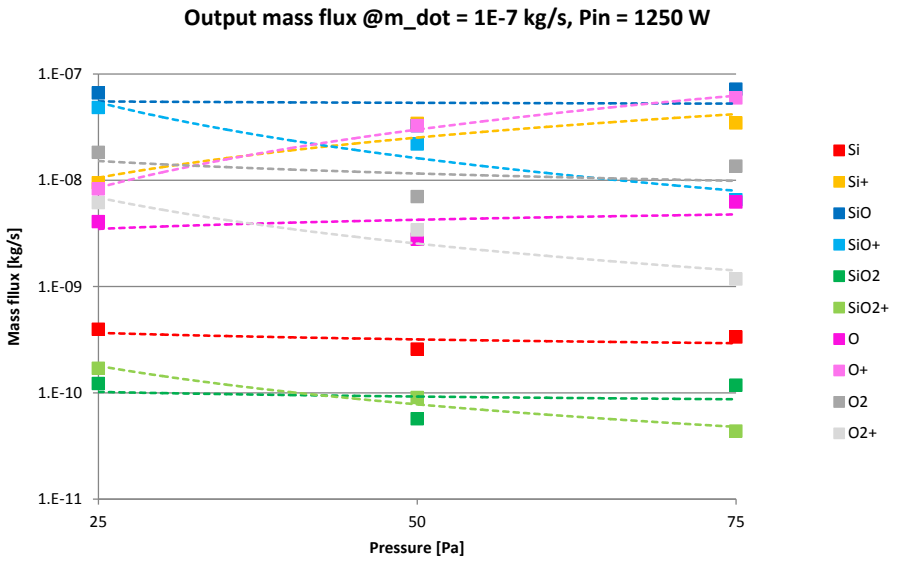

Figure A.1: *Output species mass flow rate Vs Background pressure @ 1E-7 kg/s input mass flow rate*

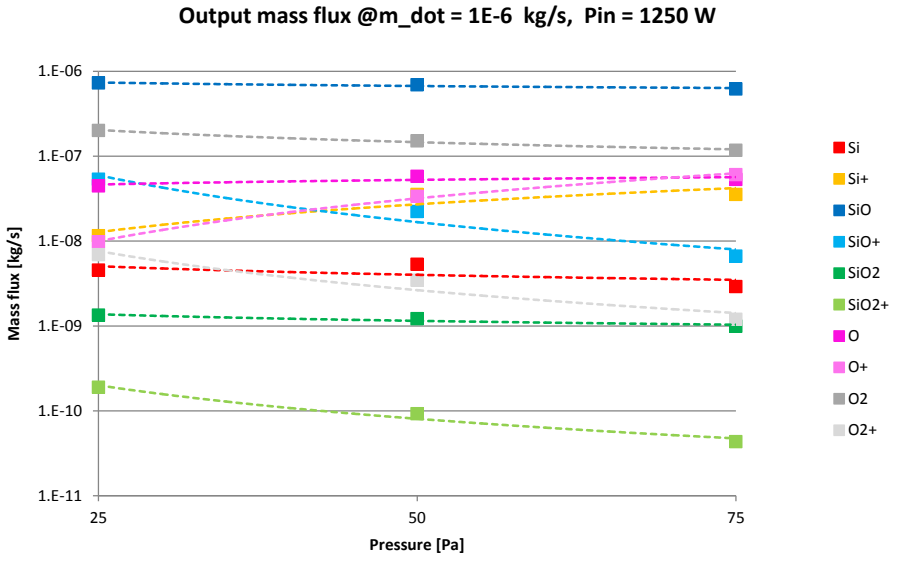

Figure A.2: *Output species mass flow rate Vs Background pressure @ 1E-6 kg/s input mass flow rate*

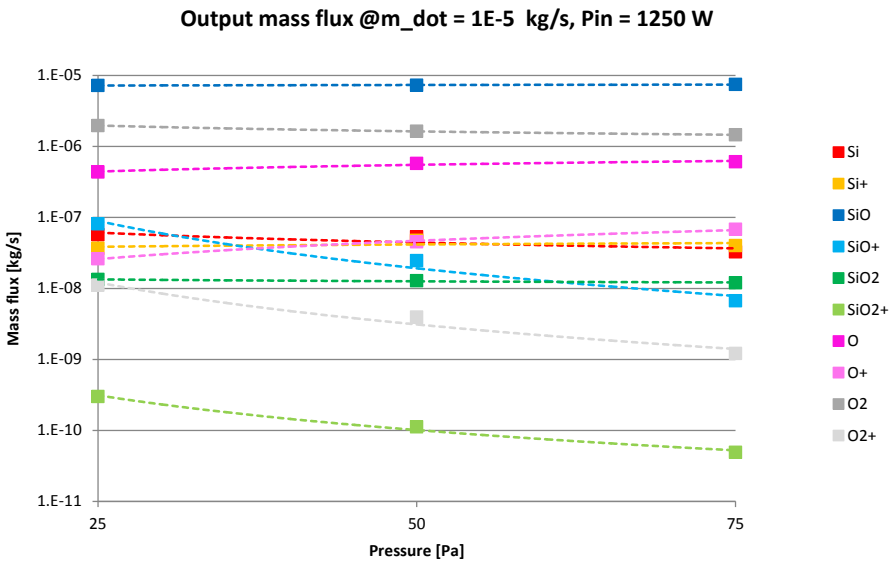

Figure A.3: *Output species mass flow rate Vs Background pressure @ 1E-5 kg/s input mass flow rate*

A.3 Output ion velocities

Pressure (Pa)	Power (W)	O+ velocity (m/s)	Si+ velocity (m/s)	SiO+ velocity (m/s)
25	100	447.6	311.5	276.6
50	100	369.8	257.3	228.4
75	100	293.7	204.3	181.4
25	1000	750.7	522.5	464.0
50	1000	478.3	333.0	295.8
75	1000	372.9	259.6	230.6
25	10000	1123.7	785.4	699.5
50	10000	636.4	445.4	397.2
75	10000	404.8	283.3	252.7

Table A.7: *Output ion velocities Vs Background pressure @ 1E-7 kg/s input mass flow rate*

Pressure (Pa)	Power (W)	O+ velocity (m/s)	Si+ velocity (m/s)	SiO+ velocity (m/s)
25	100	519.9	365.2	325.5
50	100	380.8	266.9	237.7
75	100	297.9	208.7	185.8
25	1000	835.6	585.1	520.8
50	1000	490.0	343.3	305.7
75	1000	377.6	264.4	235.5
25	10000	1237.2	869.0	775.5
50	10000	651.3	458.2	409.4
75	10000	409.3	287.8	257.2

Table A.8: *Output ion velocities Vs Background pressure @ 1E-6 kg/s input mass flow rate*

Pressure (Pa)	Power (W)	O+ velocity (m/s)	Si+ velocity (m/s)	SiO+ velocity (m/s)
25	100	1242.4	906.8	820.6
50	100	495.1	367.4	334.7
75	100	346.7	256.8	233.8
25	1000	1634.7	1180.3	1063.8
50	1000	622.9	456.9	414.4
75	1000	426.0	313.1	284.3
25	10000	2113.8	1521.2	1370.7
50	10000	797.0	583.9	530.0
75	10000	431.7	319.9	291.8

Table A.9: *Output ion velocities Vs Background pressure @ 1E-5 kg/s input mass flow rate*

As can be seen output velocities depend on the input mass flow rate. An explanation to this effect is that a higher mass is introduced with a relatively high enthalpy, due to the boiling temperature at the specific pressure; part of this enthaply obviously is lost exiting the torch, but in general a higher amount of energy is introduced into the system, therefore the energies generated by the dissociations reactions add up to a higher value, increasing the overall ions temperature and then velocity.

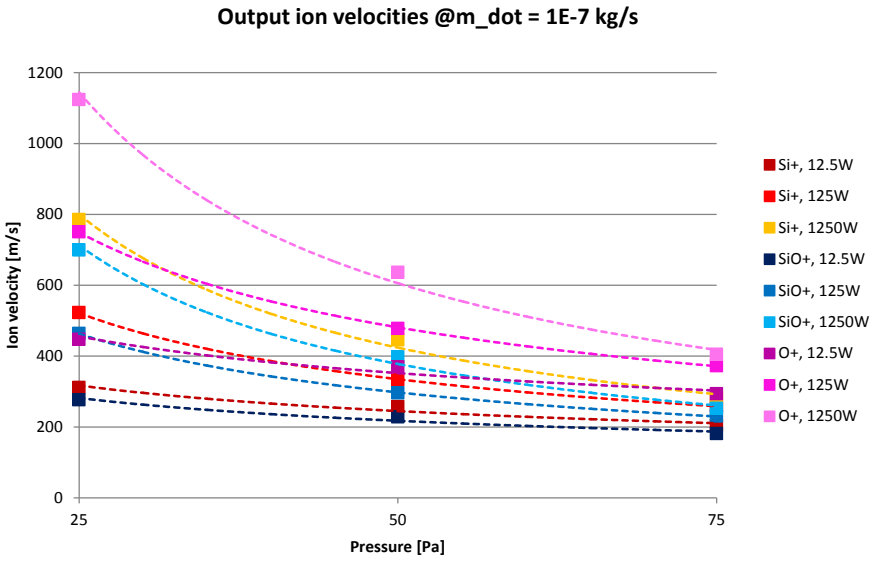

Figure A.4: *Output ion velocities Vs Background pressure @ 1E-7 kg/s input mass flow rate*

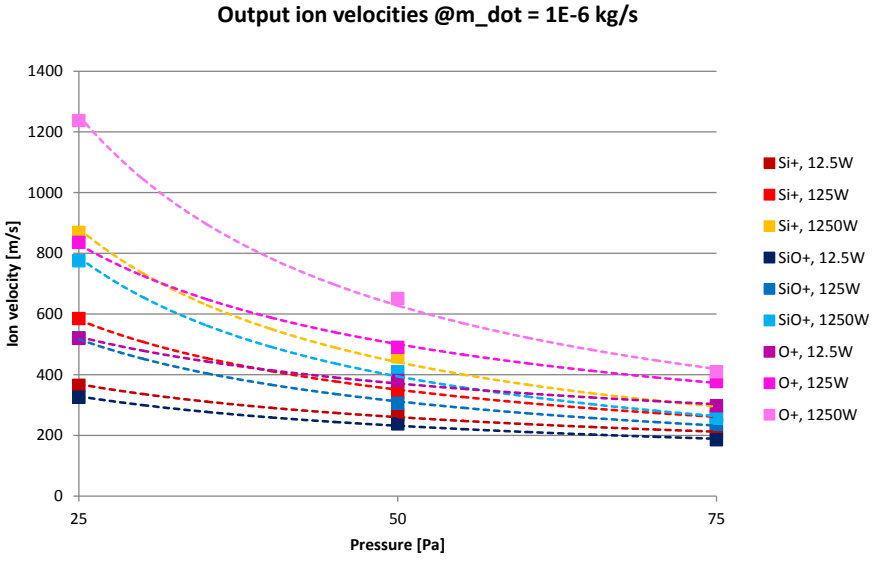

Figure A.5: *Output ion velocities Vs Background pressure @ 1E-6 kg/s input mass flow rate*

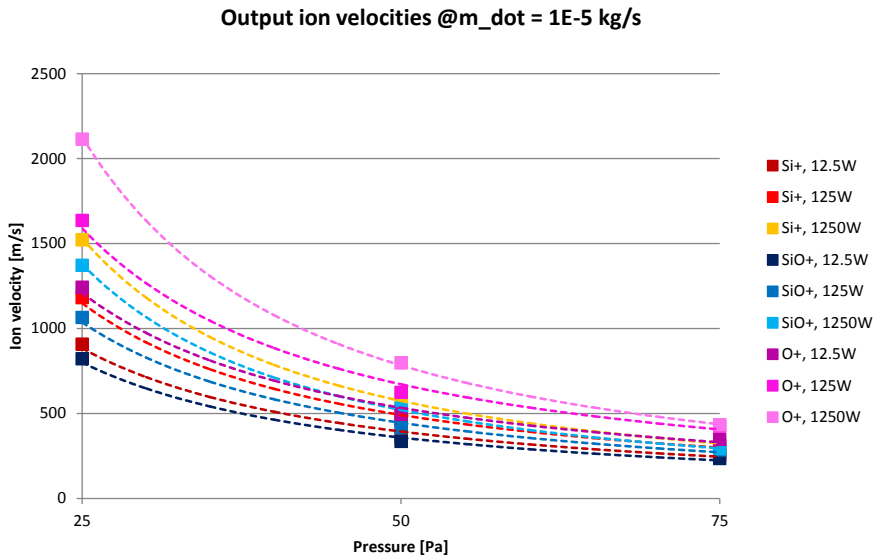

Figure A.6: *Output ion velocities Vs Background pressure @ 1E-5 kg/s input mass flow rate*